EFFECTS OF THE COLLAGEN-DENSE TUMOR MICROENVIRONMENT ON NEUTROPHILS AND MACROPHAGES

By

María Gracia García Mendoza

A dissertation submitted in partial fulfillment of

the requirements for the degree of

Doctor of Philosophy

(Cellular and Molecular Biology)

at the

UNIVERSITY OF WISCONSIN-MADISON

2016

Data of final oral examination: 12/18/2015

The dissertation is approved by the following members of the Final Oral Committee:
Patricia J. Keely Ph.D., Professor and Chair, Cell and Regenerative Biology
Andreas Friedl, M.D., Professor and Chair, Pathology and Laboratory Medicine
Anna Huttenlocher, M.D., Professor, Medical Microbiology & Immunology and Pediatrics
James Shull, Ph.D., Professor, Oncology
Jing Zhang, Ph.D., Associate Professor, Oncology

ACKNOWLEDGEMENTS

I have so many people to be thankful for. Without them, I would not have been able to start, continue, and finish much of this journey. Right now, in case I forget, do not have time, or space to include it in this section, I would like to acknowledge everyone who I crossed paths with while on this journey.

First of all, I want to thank Patti Keely, my advisor. As a PI, you have this magic touch that erases all bad thoughts on bad data. Every time I meet with you and I feel discouraged about my results, you have a way of looking at data that always brings out the positive side. I come out refreshed and ready to keep tackling the problem. As a friend, you have always been there for pillow talk at conferences, and have shared much wisdom about being a woman, a scientist, a mother, a partner, and so much more. You are the one person I would not like to disappoint.

I want to acknowledge my committee for their immense guidance. I assembled a very diverse group that has led me and shaped this project in great ways. Thank you for your time and commitment to this project and my development as a scientist.

I also want to thank my family. I decided to come to UW-Madison to stay close to you, and I truly do not regret that decision. Although it is hard to explain my research in Spanish, I appreciate all the times mis papitos ask about the “celulillas” or the “ratoncitos”. Los quiero mucho a todos y gracias por todo su apoyo. A mis Peruchis también, gracias!

I want to thank my grillito. You came in late to the game, but you delivered. I have not felt happier in my life, and I cannot wait to continue the journey in science and in life with you.

To the Keely gang, the “Keelers”, or whatever we are called these days, thank you so much. I joined this research group because I noticed you were a happy, good and supporting group. You have made it easy and encouraged to come in everyday for more. Even though we goof around a lot, we always get stuff done, troubleshoot, complain, and celebrate together. Jessica in the past and now Suzanne have made huge contributions to my progress. Thank you all for getting me through this. It has been a pleasure to serve as the social committee chair for all these years.

To all my UW friends, thank you. I also accuse you of making me unproductive some times, but I could not have done this without you. Some people say high school friends are for life, some say college friends are for life, but for me: graduate school friends are forever, hands down. I have a couch to sleep on in Durham, NC, Denver, CO, Seattle, WA, Puerto Rico, and soon in other cool places, I cannot wait to visit you.

Finally, to my Loras family, especially Dr. Dave Shealer, thank you. He was my undergraduate advisor and the hardest and best professor I came across. When I was interviewing for graduate school, many P.I.s I interviewed with commented on how good my letters of recommendation were. Thank you for writing so many letters for me, for keeping in touch, for publishing my undergraduate work, and for coming to Madison to watch the Dubuque Saints against the Capitols.

ABSTRACT

The breast tumor microenvironment (TME) is a diverse area where complex interactions between the extracellular matrix (ECM) and multiple cell types (tumor epithelial, endothelial, and inflammatory cells, fibroblasts, and adipocytes) occur resulting in tumor promotion, invasion and metastasis. Differences in breast tissue density have been correlated with a 4-6-fold increased risk for developing breast cancer, and are associated with increased stromal deposition of the ECM protein, collagen I. In a transgenic mouse model of increased collagen ($Col1A1^{Tm1Jae}$), there is a 3-fold increase in mouse mammary tumor virus – polyoma middle T antigen (MMTV-PyMT) tumor formation and lung metastases compared to control, wild type mice. Of the non-malignant cells in the TME, tumor-associated macrophages (TAMs) and tumor-associated neutrophils (TANs) have been shown to alter the TME and ECM, enhance tumor cell migration and invasion, stimulate angiogenesis, and suppress antitumor immunity. The direct interaction of both increased collagen and myeloid cell recruitment leading to increased cancer progression and metastasis has not been characterized. We hypothesized that a collagen-dense TME recruits a population of myeloid cells, which promote tumor progression and metastasis. We show that the collagen-dense TME cytokine cross talk supports neutrophil and monocyte recruitment, as suggested by expression of the cytokine GM-CSF *in vivo*. Depleting neutrophils with anti-Ly6G (1A8) reduces the number of tumors and tumor burden in collagen-dense mice compared to anti-IgG control mice. These effects are not seen in treated wild type mice compared to control mice. Of importance, neutrophil depletion reduces metastasis

in over 80% of treated collagen-dense mice compared to control mice. In contrast, wild type mice show an increase in metastasis with anti-Ly6G treatment. The *in vitro* data presented here focuses on macrophages and demonstrates that macrophage cell lines respond to collagen-dense microenvironments by evading apoptotic signals and increasing proliferation signals. Our study supports the idea that the collagen-dense TME can manipulate other cells in the TME specifically, the pro and anti-tumor functions of Ly6G+ neutrophils in mammary carcinoma.

This work is supported by NIH grants (NIH-CA-114462 and NIH-U54-CA163131) to P.J.K. and NSF Graduate Research Fellowship (2011129283) to M.G.G.M.

TABLE OF CONTENTS

LIST OF FIGURES

CHAPTER 1 - INTRODUCTION

1.1 Breast cancer and mammographic density

According to the American Cancer Society, breast cancer is one of the most common cancers found in American women. About 12% of women in the United States or 1 in 8 will develop invasive breast cancer during their lifetime. Breast cancer deaths are the second leading cause of cancer deaths in America. Advancements in early detection, awareness, and improved treatment are resulting in decreasing death rates [1].

Breast cancer can be distinguished into different types based on the origin of epithelial cells that the cancer is derived from. The most common types are the following: ductal carcinoma *in situ* (DCIS), invasive ductal carcinoma (IDC), and invasive lobular carcinoma (ILC). In DCIS, the cells that line the breast ducts become cancerous, proliferate to fill the luminal space, but have not invaded through the duct walls. IDC is a type of breast cancer in which the cancer cells break through the ductal wall and invade the surrounding fatty tissue. These cells are able to metastasize to other parts of the body via the lymph nodes and the blood stream. Another form of invasive carcinoma is ILC, in this breast cancer the epithelial cells in the milk-producing breast lobules become cancerous and invade into the surrounding tissue [1]. Any of these sub-types of cancer can be diagnosed during pregnancy or within five years from a completed pregnancy; these cases are referred to as pregnancy-associated breast cancer (PABC). The cellular

and molecular research performed in these types of cancer will be discussed in this chapter.

There are several breast cancer risk factors: gender, age, genetics, environmental, etc. As for gender, men can also develop breast cancer, but women are 100 times more likely to develop this disease than men. The risk of developing breast cancer also increases with age, with the most invasive cases found in women age 55 or older. When investigating the genetic components, cancers have a mutation element; only 5-10% of these are germline mutations or inherited from a parent (i.e. BRCA1 and BRCA2, PTEN, etc.). As for race, white women are more likely to develop breast cancer, while African-American women develop more aggressive types of breast cancer with a higher risk of death. The risk of breast cancer is reduced by life style factors including pregnancy, having children at a younger age, and breast-feeding for longer periods of time. In addition, the risk of developing breast cancer is increased by alcohol consumption, obesity, and getting little to no physical exercise [2].

The risk factor studied by the Keely research group is mammographic breast density. The appearance of a mammogram (prognostic x-ray exam of the breast) varies according to the amounts of fat, connective, and epithelial tissue. Fat tissue is radiologically lucent (appears dark), while connective and epithelial tissue is radiologically dense (appears light). Radiologists score breast density based on the variation of the amounts (percentage) of these tissues as they appear in mammograms [3]. Women with high mammographic breast density or with breasts that have 60-70% dense tissue, have a four to six times increased risk of developing breast cancer than

those with low mammographic breast density or with breasts that have under 10% dense tissue [4]. Importantly, pre-invasive breast cancer or DCIS occurs in areas of the breast with the highest percentage of mammographic density [5].

The biological and molecular bases for the increase in breast cancer risk associated with dense mammographic density are still unclear. Many studies aim to characterize the features of dense breast tissue using human tissue sections from benign lesions. High-density tissue is composed of greater areas of stroma, the area composed of connective/structural tissue and other non-epithelial cells, and less fat tissue. These studies correlate mammographically dense tissue with an increased amount of stromal type-I collagen rather than with increased epithelial components [6-8]. Animal studies have been useful in developing a causative link between increased stromal collagen and tumor formation. The study of a spontaneous mammary carcinoma (mouse mammary tumor virus-polyoma middle T antigen, MMTV-PyVT) mouse model with increased collagen density (collagenase resistant, Col1a1^{tm1Jae}) shows a three-fold increase in tumor formation and metastasis when compared to wild-type litter-mates [9, 10]. In addition, the study of another spontaneous mammary carcinoma (MMTV-Neu/HER2) model shows that cancer progression is characterized by stiff tumors that have increased collagen amounts and linearized organization, as well as increased collagen cross-linking driven by lysyl oxidase (LOX) [11]. These studies suggest a functional link between increased collagen and mammary tumor progression.

Research on breast cancer diagnosed up to five years from a completed pregnancy, or pregnancy-associated breast cancer (PABC) also provides a link between

increased stromal components, collagen I, and tumor progression. Following pregnancy, the mammary gland undergoes involution, in which there is extensive programmed cell death (removal of secretory alveolar cells), remodeling of the connective/structural tissue, also called extracellular matrix (ECM), proteolysis of existing matrix and synthesis of new matrix. [12]. Of importance, an involuting gland is characterized by increased deposition of collagen and recruitment of immune cells; specifically, alternatively activated macrophages (M2) [13]. In an involuting mammary gland, fibrillar collagen and cyclooxygenase-2 (COX-2), an enzyme that promotes the production of prostaglandin mediators of inflammation, drive progression of DCIS to invasive breast cancer in mouse models [14]. These studies suggest that inflammation also plays a role in mammary tumor progression when increased collagen is present.

In addition, a recent study of tissue from prophylactic mastectomies correlates regions of high mammographic density with increased collagen I deposition and organization, as well as CD45+/vimentin+ immune cells [15]. This thesis project aims to determine the effects of the collagen-dense microenvironment on immune cell recruitment, and how this contributes to breast cancer progression.

1.2 Cancer and the immune response

In order to understand inflammation and its role in cancer, it is important to understand inflammation in normal processes, such as wound healing. The response to tissue injury involves orchestrated chemical signaling designed to heal the tissue. Platelet activation results in the formation of a fibrin clot and the release of growth factors (transforming growth factor-β, TGF-β, and platelet-derived growth factor, PDGF)

that activate fibroblasts and protease-facilitated ECM remodeling. Leukocytes are recruited to the injury site in response to chemokines via the vascular network. Neutrophils arrive first, followed by monocyte-derived macrophages, which are the major source of cytokines and growth factors, while mast cells also secrete inflammatory mediators. These signals affect endothelial, epithelial, and mesenchymal cells in the normal inflammatory microenvironment. This inflammatory response is self-limiting: initiating pro-inflammatory signals are followed by ceasing anti-inflammatory signals. In chronic inflammation, either the initiating factors persist or, the mechanism to resolve inflammation fails [16-18]. The tumor microenvironment not only hosts malignant epithelial cells, but also non-malignant, CD45+ innate and adaptive immune cells. Several years of research support the idea that the tumor microenvironment is in a chronic state of inflammation. Although they are much more than wounds, tumors engage the wound healing system to generate the stromal or tumor microenvironment that they need to survive and grow [19-21].

While analyzing the role of the immune system, we ask: can immune cells protect the host from tumor development? Research studies with mice lacking certain components of the immune system demonstrate that lymphocytes can prevent tumor development [22]. Shankaran, et al., showed that 129/SvEv mice with a recombination-activating gene-2 (RAG-2) knock-out, lacking mature T and B lymphocytes, formed tumors induced by chemical carcinogen methylcholanthrene (MCA) much more rapidly than wild type tumors with intact immune systems. This same study also utilized mice that lack inflammatory cytokine, interferon-γ (INF-γ) and signaling via IFN-γ receptor,

STAT1, deficiency, which also yielded increased MCA-induced tumor formation compared to wild type mice with intact immune systems [23]. In addition, natural killer, NK, cells also play a role in protection against cancer. Smyth, et al., demonstrated that NK and NKT-cell depletion with antibodies against both cell types (anti-NK1.1) or against NK cells (anti-asilo-GM_1) significantly increased MCA-induced sarcoma formation. NK cell anti-tumor effects are mediated by Interleukin-12 (IL-12) [24]. Hence, T-cells (CD8+ cytotoxic cells, CD4+ helper T cells, γδ T cells, and NKT cells) and NK cells play vital anti-tumor roles. These mainly occur at very early stages before tumor cells are able to evade immune surveillance. This is referred to as the elimination phase of the cancer immunoediting process [22].

Following the elimination phase, the equilibrium phase or latency phase takes over. While the immune system constrains tumor growth, constant changes in the cancer cell genome can give rise to new phenotypes with reduced immunogenicity [22]. This is supported by a report of kidney transplant patients who developed metastatic melanoma two years post-transplant. It was later found that the donor had been treated for melanoma 16 years prior to death, and she was considered tumor-free at the time of transplant. Her tumor cells were in a state of equilibrium with her immune system. In order to accept the kidney, the recipients received immune suppressive medication, suggesting that reduced cancer immune surveillance facilitated the growth of once dormant tumor cells [25].

Finally, in the escape phase of immunoediting, tumor growth occurs unrestrained by the immune system, where the tumor cells have “evolved” into

manipulating the immune system into an immunosuppressive state via secreted cytokines, expression of aberrant surface markers, or stimulation of immunosuppressive T-cells [22]. Of the immune cells that have a role in breast cancer, antibody-producing B-lymphocytes, as well as immunoglobulin (Ig) G+ and IgM+ in the lymph nodes of patients are correlated with advanced breast cancer stages. The predominant lymphocytic population in breast hyperplasia and DCIS are B cells, although the exact mechanisms of how B cells regulate carcinoma development are not clear [26]. During high grade DCIS and invasive breast cancer, the predominant lymphocytic populations are infiltrating T-lymphocytes [27]. CD4+ T-helper cell response can be polarized at primary sites and/or metastatic sites. Th_1-polarized polarized cells secrete pro-inflammatory cytokines (INFγ, tumor necrosis factor-α, TNF-α, TGF-β, and interleukin-2, IL-2), while Th_2-polarized cells induce T-cell unresponsiveness, loss of CD8+ T-cell-mediated cytotoxicity, and express IL-4, IL-5, IL-6, IL-10, and IL-13. Th_1 responses may be anti-tumor, while Th_2 may be pro-tumor [28, 29]. Regulatory T cells (T_{reg}) normally suppress T-cell cytotoxicity to protect tissues from autoimmune disease. Not only are T_{regs} associated with poor breast cancer survival, but also they have the ability to inhibit CD8+ T cells, dendritic cells (DC), NK cells, and B cell activities [30]. These reports suggest that the breast tumor microenvironment recruit different sub-populations of lymphocytes and these have the ability to regulate anti-tumor cytotoxicity.

Innate immune cells are also an important component of the breast tumor microenvironment. Due to their plasticity and ability to secrete several cytokines, chemokines, matrix proteases, growth factors, etc., granulocytes, macrophages, DCs, NK

cells, and mast cells can regulate tissue remodeling, angiogenesis, and enhance tumor cell survival, migration, and metastasis [26, 28]. This thesis project focuses on macrophage and neutrophils because of their abundance in the breast tumor microenvironment and the reports discussed here that support their pro-tumorigenic roles, which may be regulated by the ECM protein, collagen I.

1.3 Macrophages and neutrophils in breast cancer progression

Tumor-Associated Macrophages

Tumor cells rely on non-neoplastic components of the tumor microenvironment in order to thrive. From the array of inflammatory cells attracted to the breast tumor microenvironment, macrophages has been studied and established as one of the most multifunctional [31]. Macrophages are terminally differentiated mononuclear phagocytes originated in the bone marrow as monocytes. Monocytes enter the blood stream and are recruited to tissues, site of inflammation, where they differentiate into macrophages. Macrophages can be activated by hypoxia, changes in pH, lipids, and cytokines (colony stimulating factor 1, CSF-1, TNFα, and INFγ) [16]. Macrophages in tumors are called tumor-associated macrophages (TAMs). There are several chemokines produced by breast cancer cells that attract macrophages. The most studied in breast cancer are monocyte chemoattractant protein-1 (MCP-1), CSF-1, granulocyte/macrophage-colony stimulating factor (GM-CSF), and vascular endothelial growth factor (VEGF). Breast tumors and cell culture studies show that tumor cells express MCP-1 as well as TAMs. High expression of this cytokine has been correlated to a high malignancy phenotype and to poor patient survival [31] . CSF-1 can regulate

macrophage proliferation, differentiation, and survival; and it has been identified as an important factor in mammary tumor progression and metastasis. Studies with the MMTV-PyVT mouse model where CSF-1 is knocked-out show that the transition to carcinoma was preceded by macrophage recruitment because the absence of CSF-1 delays tumor progression [32]. VEGF is widely studied key factor in tumor progression. It is upregulated by hypoxia, and not only induces angiogenesis, but also induces monocyte chemotaxis in cancer [33].

Macrophages have several roles in breast cancer. TAMs have several antitumor activities. They are professional antigen presenting cells that can phagocytize cells, process the tumor antigen, and express it on their surface. CD4+ positive T-helper cells can recognize the antigen and signal to DC-activated CD8+ cytotoxic cells in order to kill the tumor cells [34]. TAMs activated by TNFα, INFγ, and GM-CSF induce tumor cytotoxicity via expression of high levels of reactive oxygen species (ROS). This mechanism involves arginine metabolism via activation of inducible nitric oxide synthase (iNOS); then, nitric oxide (NO) is produced and causes DNA damage. TAMs produce high amounts of pro-inflammatory cytokines and polarize the T-cell response to activate Th_1 cells. Mantovani, et al. classifies these TAMs as M1 or classically activated macrophages, which express high levels of IL-12 and IL-23 [35, 36]. In contrast, M2 or alternatively activated macrophages suppress inflammatory response, scavenge debris, promote angiogenesis and tissue remodeling and repair. They are activated by IL-4, IL-13, and IL-10. Arginine metabolism occurs through the arginase pathway so M2 macrophages are high expressers of arginase. M2 macrophages produce IL-10, IL-1 receptor antagonist

and type II IL-1 decoy receptor [35]. Both types of macrophages can be found in the breast tumor microenvironment, which can influence their polarization. Studies in pregnancy-associated breast cancer (PABC) demonstrate that macrophages are polarized towards an M2 phenotype in the collagen remodeling-rich involuting mammary gland [13]. More studies are needed to determine the mechanism of TAM activation in collagen-dense breast tumor microenvironment.

TAMs have a role in breast cancer cell growth through the secretion of growth factors. They secrete: PDGF, TGF-β, TGF-α, hepatocyte growth factor (HGF), basic fibroblast growth factor (bFGF) and epidermal growth factor (EGF). Macrophages are the main producers of EGF while high expression of EGF receptor in breast cancer is correlated with poor survival and it is used as a prognostic marker. Studies in the MMTV-PyVT model also describe a paracrine loop between macrophage EGF secretion and tumor cell CSF-1 secretion in mammary tumor progression [34, 37]. Macrophages play a causal role in promoting tumor angiogenesis. They secrete potent pro-angiogenic cytokines and growth factors including VEGF, TNFα, IL-8, and bFGF, and other enzymes that modulate angiogenesis including matrix metalloprotease-2 (MMP-2), MMP-7, MMP-9, MMP-12, and COX-2. In PyVT mouse mammary tumors, depleting macrophages slows down the tumor angiogenic switch by reducing vascular density by about 50% [38, 39]. More importantly, the major cause of death in breast cancer is metastatic disease; it is not surprising that macrophages have a role in invasion and metastasis. Breast tumor cell motility *in vivo* and *in vitro* is enhanced by TAMs [40]. Studies in the Condeelis research group suggest tumor cell motility occurs in response to EGF signaling

from TAMs, and tumor cells secrete CSF-1 in response engaging in a paracrine loop that can lead to tumor cell extravasation and metastasis [41]. The Pollard research group showed that depletion of macrophages with L-Clodronate reduced lung metastasis derived from the PyVT model and from human breast cancer line MDA-231 implanted subcutaneously in mice. This metastasis-associated macrophage has a distinct phenotype that expresses CD11b+ (Integrin-α M), Gr-1, CCR2 (CD192), and VEGF receptor [42]. These reports and many more highlight the pro-tumor roles of macrophages. Their interaction with the collagen-rich ECM in breast cancer and how that advances tumors will be discussed in the next section.

Tumor-Associated Neutrophils

Also from the myeloid lineage, neutrophils are immune cells that not only are they much less studied than macrophages, but also they are multifunctional. They play a well-established role in host defense: they originate in the bone marrow, enter circulation, and are first responders to chemotactic cytokines (IL-8 and IL-6) originated at the source of inflammation, for example, damaged tissue. Once they enter tissues, they release activating cytokines (TNFα, IL-1, INFs, etc.), defensins, toxic substances and ROS to phagocytize and kill invading microorganisms. Neutrophils can be activated by *N*-formyl peptides from bacteria and mitochondria that are recognized by membrane proteins from Toll-like receptor family, fibrinopeptides, prostaglandins, and leukotrines [16, 43]. Although neutrophils are the most abundant leukocyte in the human blood, cancers such as melanoma, further increase neutrophil counts and are associated with

poor survival [44]. Neutrophil recruitment is mainly driven by chemokines that bind chemokine (C-X-C motif) receptor 1 (CXCR1) and CXCR2 on its cell surface. CXC ligands (i.e. IL-8, MIP2α) are upregulated in breast cancer; and blocking CXC receptors with antibodies inhibits neutrophil migration in response to conditioned media from MDA-468 human breast cancer cells [45]. Other growth factors are known to have priming, anti-apoptotic effects on neutrophils such as G-CSF and GM-CSF; this not only elongate neutrophil lifespan, but also act as strong chemoattractants [46].

Emerging data describe the roles of neutrophils in several cancers including breast cancer, although not as studies as macrophages. Polymorphonuclear neutrophils (PMNs) from healthy humans with no previous cancer diagnosis are effective killers of transformed cells from mammary, non-small cell lung, cervical, ovarian, and pancreatic carcinoma. Even normal mammary cells, MCF10A, transfected with oncogenes are susceptible to neutrophil killing. This study suggests that the tumor-killing mechanism involves H_2O_2 catalase [47]. Tumor associated neutrophils (TANs) that mediate tumor rejection may also involve G-CSF, IL-2, and TNF-α [46]. Fridlender, et al., has also classified neutrophils in an N1 or N2 polarization based on their studies of lung cell carcinoma-derived tumors and TGF-β blockade. Their research suggests that by blocking TGF-β in tumors, N1 neutrophils have increased tumor cell killing activity via oxidative damage and Fas (stimulates tumor cell apoptosis), can promote CD8+ cytotoxic T-cell recruitment and activation by producing T-cell chemokines (CCL-3) and pro-inflammatory cytokines (IL-12, TNF-α, and GM-CSF). N1 polarization is mediated by interferon-β (IFN-β) [48]. In contrast, N2 neutrophils have a pro-tumor phenotype

driven by TGF-β. They decrease CD8+ T-cell cytotoxicity, produce large amounts of arginase that inactivate T-cell effectors, express CXCR4, VEGF, and MMP-9 [49]. Studies by the same research group suggest that N1 and N2 TANs are part of the tumor microenvironment; N1 neutrophils develop at early state and N2 at later stages in tumor progression [50]. Similar to macrophages, the breast tumor microenvironment: tumor cells, other stromal cells, and the ECM can influence their polarization.

Tumor promoting roles of TANs include: tumor growth and survival, angiogenesis, and metastasis. The Houghton research group showed that neutrophil-secreted neutrophil elastase (NE) enters tumor cells via endosomes and degrade insulin receptor substrate-1 (IRS-1), which binds to the p85 regulatory subunit of phosphoinisitide 3 kinase (PI3K). Upon degradation, PI3K is free to interact with PDGF and activate AKT to induce tumor cell proliferation and survival [51]. Additionally, neutrophils secrete MMP-9, which prevents tumor cell apoptosis in lung cancer [52]. TAN-mediated angiogenesis involves MMP-9 secretion. ECM degradation by MMP-9 releases VEGF and FGF sequestered in the ECM [53, 54]. The role of neutrophils in metastasis is controversial. Kowanetz, et al., showed that treating orthotopic 66c14 mouse mammary tumors with anti-Ly6G (specific antibody that binds and blocks mouse neutrophil recruitment) decreased lung metastasis [55]. Granot, et al., investigated lung metastasis by engrafting MMTV-PyVT tumors in the mammary fat pad of FVB mice and in the 4T1 mouse mammary metastasis model. They showed an increase in lung metastasis with anti-Ly6G treatment [56]. Tabariés, et al recently demonstrated that Ly6G+ granulocytes are recruited to lung and liver metastasis in the 4T1 model. Depleting neutrophils with anti-Ly6G does not affect

lung metastasis, but it does reduce liver metastasis [57]. Coffelt, et al, has recently proposed a mechanism for TAN-induced metastasis in mammary carcinoma. IL-1β from mammary tumor cells stimulates IL-17 expression in γδ T-cells. This results in expansion and polarization of TANs via G-CSF. These TANs suppress CD8+ cytotoxic T-cells, which limit the establishment of metastasis [58]. These studies suggest that more studies need to be done at the metastatic niche to determine the mechanisms by which TANs promote or inhibit metastasis in the breast tumor microenvironment [53].

Several studies suggest that there is a crosstalk between TAMs and TANs. These focus on the results indicating that depletion of macrophages during infection or in cancer models can results in recruitment of neutrophils to compensate for the defects [53]. Results from this thesis project also suggest a crosstalk between the two cells types, as these can physically interact with each other in collagen-dense mouse mammary tumors (Figure 1.1); this crosstalk may be regulated by the collagen-dense tumor microenvironment.

1.4 Macrophages and neutrophils in collagen-dense microenvironments

The information discussed in previous sections describes how immune cells, macrophages, and neutrophils play important roles in tumor progression and metastasis. Are these roles influenced by the collagen-rich microenvironment such as the one found in human patients with increased mammographic density? The chapters in this thesis project will address this question.

The ECM in the collagen-rich microenvironment is made up of structural modules that encode information interpreted by cells through interactions with specific plasma membrane receptor, mostly of the integrin family. The mechanisms of matrix interactions are different from cell type to cell type and influence cell properties and behavior by modifying cytoskeletal organization and activation of protein kinase pathways. The ECM sequesters various factors such as cytokines, growth factors, proteases, and their inhibitors. The normal breast microenvironment has basement membrane matrices and stromal/interstitial matrices. Stromal matrices are primarily composed of fibrillar type-I collagen cross-linked into a stable meshwork and are seen in the majority of the body connective tissue. Once breast cancer occurs, the ECM undergoes changes and remodeling; it is here where TAMs and TANs also play a role [59].

Macrophages and collagen I

In vitro studies of macrophage migration on 3-dimentional (3D) fibrillar collagen I matrices demonstrated that macrophages interact with collagen and adopt an amoeboid migration mode that is protease independent and Rho-associated protein kinase (ROCK) dependent [60]. Collagen fragments induce chemotaxis in alveolar macrophages [61], and in mouse macrophage cell line, J774a.1 [13]. These collagen peptides can activate alveolar macrophages into secreting reactive oxygen intermediates and into becoming cytotoxic towards hepatoma and leukemia cells [61]. *In vivo,* in the mouse mammary tumor model, PyVT, macrophages were visually

associated with collagen I fibers. These fibers surround the tumor mass and facilitate tumor cell migration, which happens ten times faster along collagen fibers [40]. In addition, TAMs secrete several enzymes that degrade the ECM: MMP-2, MMP-9, urokinase-type plasminogen activator (uPA) [62]. Increased uPA activity in breast cancer patients is a strong independent prognostic factor and is correlated to small disease-free intervals [63]. Macrophages have been shown to degrade collagen via endocytosis and routing to the lysosomal compartment; this is enhanced in mannose receptor (MRC1/CD206) expressing, M2 polarized macrophages [64]. Another study reports that macrophage and TNF- α depletion changed collagen microstructure in E0771 mouse mammary adenocarcinoma [65]. All these studies support the idea that interactions between type-I collagen and macrophages occur including macrophage migration and activation and collagen degradation and remodeling. It is unknown whether the collagen-rich tumor microenvironment can recruit and activate macrophages; and in response macrophages can alter the collagen and facilitate tumor progression.

Neutrophils and collagen I

In vitro studies of neutrophil biology have demonstrated the ability of neutrophils to migrate in 3D collagen I matrices [66]. Neutrophils can also adhere and become activated in type I collagen [67]. These neutrophil capabilities, especially neutrophil migration in response to chemoattractants, involve integrin β2, integrin α2, and integrin β1. The two latter integrins mediate cell adhesion to collagen I fibrils [68, 69]. Although rapid leukocyte migration in response to chemokines can be integrin

independent [70], neutrophil chemotaxis in collagen I is also mediated by the collagen receptor, discoidin domain receptor 2 (DDR2). DDR2 regulates neutrophil directionality and persistence by releasing MMPs (MMP-8) that cleave collagen [71]. These studies support the recruitment and activation of neutrophils into collagen-rich microenvironments *in vitro.* TANs express gelatinase B or MMP-9, which displays broad substrate specificity and drives tumor-associated angiogenesis as described in the previous section. Neutrophils also secrete neutrophil collagenase or MMP-8, which cleaves collagen I. In chemically-induced skin cancers, MMP-8 from neutrophils reduced tumor incidence; in melanoma cells, MMP-8 reduced metastasis formation [72]. Expression of MMP-8 in breast cancer correlates with good prognosis and lower incidence of lymph node metastasis [48]. As seen in macrophages, these studies support the idea that interactions between type-I collagen and macrophages occur including neutrophil migration and activation and collagen degradation and remodeling. It is also unknown whether the collagen-rich tumor microenvironment can recruit and activate neutrophils; and in response neutrophils can alter the collagen and facilitate tumor progression.

Motivation for studying the effects of the collagen-dense microenvironment on neutrophils and macrophages in breast cancer

The tumor microenvironment is a diverse community where complex interactions between the extra-cellular matrix (ECM) and cellular elements (tumor epithelial, endothelial, and inflammatory cells, fibroblasts, and adipocytes) occur

resulting in tumor promotion, invasion and metastasis [59]. Changes in this microenvironment, particularly increased type-1 collagen density, which is correlated with increased mammographic density, play a role in the progression of breast cancer. These changes are of great interest because increased mammographic density has been associated with a four- to six-fold increased risk for developing breast cancer [73]. However, the cellular and molecular mechanisms responsible for this increased risk remain largely unknown. Increased deposition of the ECM protein, collagen, in the stroma contributes to mammographic density [6]. The Keely laboratory, has established that not only collagen amounts, but also collagen alignment can be used as a prognostic factor for survival in breast carcinoma. Straight and aligned collagen I fibers oriented perpendicular to the tumor boundary are associated with poor survival [74]. This specific organization of the collagen was first observed in a mouse model with increased collagen deposition (MMTV-PyVT, COL1A1), which has an increase in tumor formation and lung metastases by three-fold in the collagen-dense stroma compared to control mice [10]. The cellular and molecular mechanisms by which the collagen-dense microenvironment enhances tumor progression and metastasis are not entirely clear. *In vitro* collagen-dense 3D matrices create a microenvironment that alters mammary epithelial and cancer cells into an invasive phenotype; this is driven by activation of focal adhesion kinase (FAK), Rho GTPase, and mitogen-activated protein kinase (ERK). The expression of proliferation-signature genes is also upregulated in collagen-dense gels, while cell proliferation denoted by Ki-67 staining is also increased in collagen-dense microenvironments [75].

It remains unclear if a collagen-dense microenvironment directly promotes the recruitment of TAMs and TANs, thus contributing to mammary tumor progression. This thesis project aims to test the hypothesis that the collagen-dense tumor microenvironment induces an altered inflammatory response that recruits and further stimulates TAMs and TANs to promote mammary tumors and metastasis (Figure 1.2)

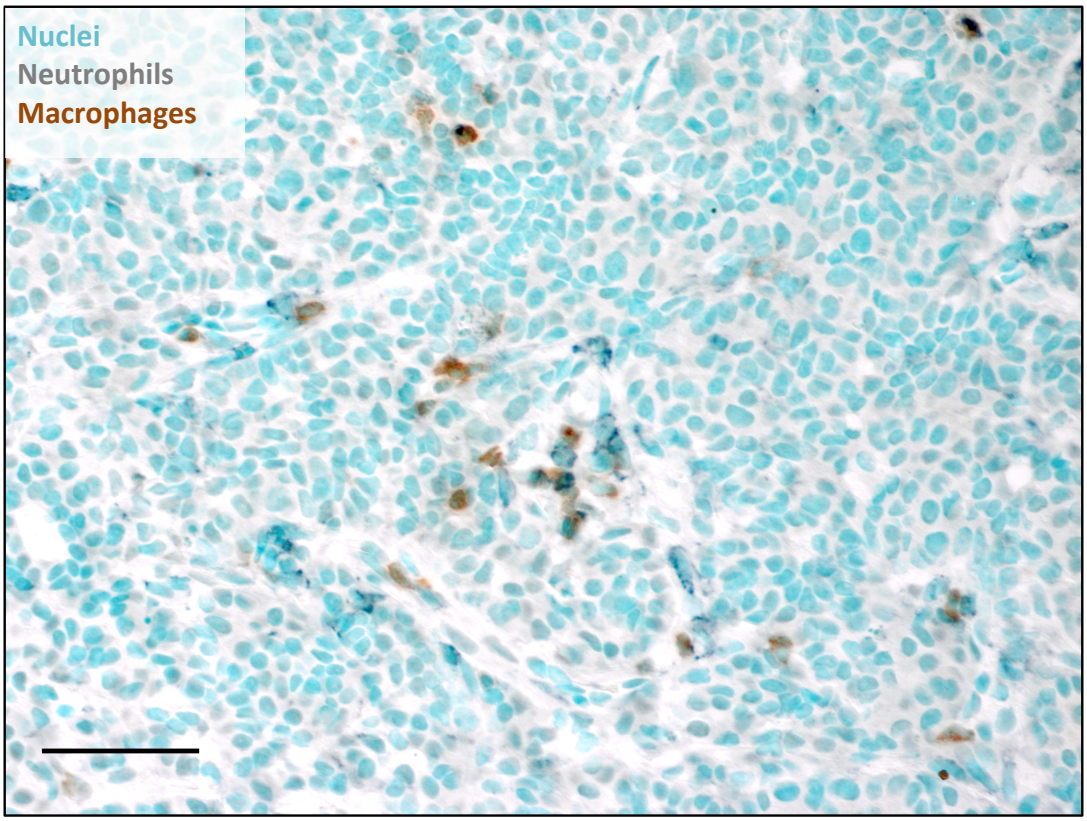

Figure 1-1 Macrophages and neutrophils in PyVT mouse mammary tumors.

Multi-color immunohistochemistry of collagen-dense mouse mammary tumor Col1A1-PyVT collected at late-stage 15 weeks of age. Nuclei were stained with Methyl Green, macrophages with anti-F4/80 and Vector Laboratories NovaRed® (brown), and neutrophils with anti-Ly6G and Vector Laboratories SG® (gray). Scale bar = 50 μm.

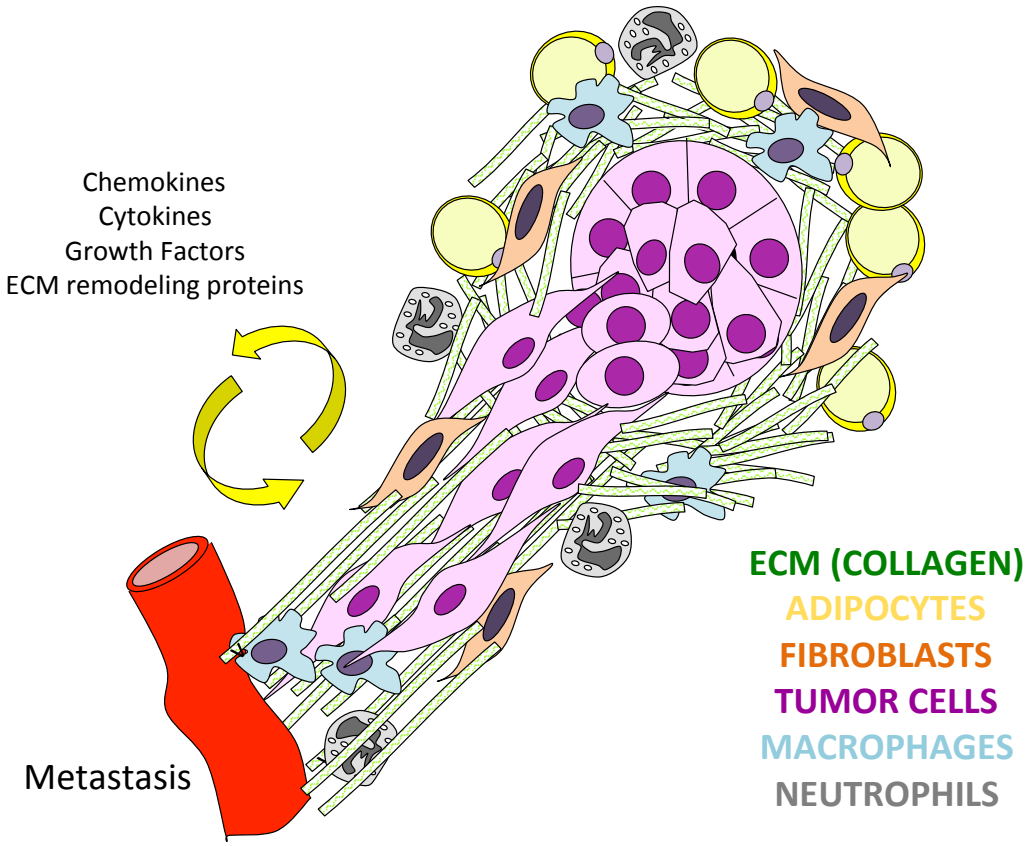

Figure 1-2 The collagen-dense breast tumor microenvironment.

The breast tumor microenvironment is composed of malignant cells, non-malignant cells (adipocytes, fibroblasts, immune cells) and the ECM. The collage-dense tumor microenvironment induces tumor cells invasion and collagen remodeling into aligned highways that lead tumor cells towards blood vessels and increased metastasis. This project discusses neutrophil pro-tumor functions and macrophage biology in the collagen-dense tumor microenvironment.

CHAPTER 2- NEUTROPHILS DRIVE ACCELERATED TUMOR PROGRESSION IN THE COLLAGEN-DENSE MAMMARY TUMOR MICROENVIRONMENT

This chapter is submitted as:

María G. García-Mendoza, David R. Inman, Suzanne M. Ponik, Justin J. Jeffery, Dagna S. Sheerar, Rachel R. Van Doorn, and Patricia J. Keely. *Breast Cancer Research*. 2015, *in review.*

ABSTRACT:

Introduction: High mammographic breast density has been correlated with a 4-6-fold increased risk for developing breast cancer, and is associated with increased stromal deposition of extracellular matrix proteins, including collagen I. The molecular and cellular mechanisms responsible for high breast tissue density are not completely understood.

Methods: We previously described accelerated tumor formation and metastases in a transgenic mouse model of collagen-dense mammary tumors ($Col1A1^{Tm1Jae}$ and MMTV-PyVT) compared to wild type mice. Using ELISA cytokine arrays and multi-color flow cytometry analysis, we studied the signaling crosstalk and the non-malignant, immune cells in the collagen-dense tumor microenvironment that may promote accelerated tumor progression and metastasis.

Results: Collagen-dense tumors did not show any alteration in immune cell populations at late stages. The cytokine crosstalk in the mammary tumor microenvironment was clearly different between wild-type and collagen-dense tumors. Cytokines associated with neutrophil signaling, such as GM-CSF, were increased in collagen-dense tumors.

Depleting neutrophils with anti-Ly6G (1A8) significantly reduced the number of tumors, and blocked metastasis in over 80% of collagen-dense mice, but did not impact tumor growth or metastasis in wild-type mice.

Conclusion: Our study suggests that tumor progression in a collagen-dense microenvironment is mechanistically different, with an increase in activation of neutrophils, compared to a non-dense microenvironment.

1.5 Introduction

Although a significant amount of breast cancer research focuses on the genetic abnormalities seen in cancer cells compared to normal breast epithelial cells, emerging data reveal that components of the extracellular matrix (ECM) and cells in the microenvironment are key regulators of tumor progression and metastasis. Women whose breasts have 75% or greater mammographically dense tissue are four to six times more likely to develop breast carcinoma than women whose breasts have less than 10% mammographically dense tissue [4, 73]. Since the molecular and cellular mechanisms responsible for high breast tissue density are not completely understood, many studies rely on *in vivo* and *in vitro* models of density to discover new preventative, prognostic, and therapeutic targets that will reduce breast cancer risk in patients with high breast tissue density. Much of the *in vitro* work has focused on the response of mammary epithelial cells to collagen-dense matrices in the regulation of proliferation and invasiveness [75, 76].

Mammographic tissue density is largely attributed to increased levels of the ECM protein, type-I collagen [6, 7]. To better understand the role of increased collagen

density, we utilize a mouse model in which the collagen 1a1 gene is mutated to make the molecule resistant to collagenase, resulting in decreased collagen turnover and a net increase in stromal collagen (Col1a1^{tm1Jae}) [10]. These animals are crossed to the mouse mammary tumor virus-polyoma middle T antigen (MMTV-PyVT), which is commonly used because it is comparable with human breast disease, since it progresses from premalignant to malignant to lung metastasis. Not only is the morphology similar to human disease, but also the biomarkers expressed in PyVT tumors are consistent with those associated with poor outcome in humans [77, 78]. PyVT tumors arising in the collagen-dense (COL) Col1a1 background have a three-fold increase in tumor formation and lung metastasis compared to tumors arising in wild-type (WT) mice. The exact mechanism by which increased collagen deposition leads to increased metastasis is not entirely clear. However, we previously noted an increase in the stromal cell populations surrounding tumors within collagen dense environments suggesting activation of the stromal compartment [10].

The breast tumor microenvironment is composed of ECM proteins as well as both malignant and non-malignant cells. Of the non-malignant, CD45+ immune cells, both innate and adaptive cells are present in the tumor microenvironment. T-cells (CD8+ cytotoxic cells, CD4+ helper T cells, γδ T cells) and natural killer (NK) cells play vital anti-tumor roles before tumor cells are able to evade immune surveillance [22, 79]. Myeloid cells, on the other hand, have been shown to often have pro-tumor functions in breast cancer. Tumor cells have the capability to educate and influence macrophages via specific cytokine signaling crosstalk [80] . Tumor associated macrophages (TAMs) can

enhance tumor cell migration and invasion, stimulate angiogenesis, remodel the ECM, and aid breast cancer metastasis [34, 42, 81]. Tissue studies from prophylactic mastectomies show that high mammographic density tissue is characterized by decreased alternatively activated (M2) macrophages in the stroma and $CD45^+$ immune cells in the epithelium [15].

Emerging evidence also suggests neutrophils may be active players in cancer progression. Similar to macrophages, but much less understood, neutrophils are thought to promote tumor growth by reducing pro-inflammatory factors, remodeling the ECM with proteases that also aid in angiogenesis and increasing metastasis [53, 57, 82]. Tumor associated neutrophils (TANs), in addition to TAMs, can reduce cytotoxic T-cell activity that would kill tumor cells, leading to tumor growth [83]. TANs contribute to angiogenesis through matrix metalloprotease 9 (MMP-9) in human fibrosarcoma and prostate cancer cells [84]. Neutrophil involvement in metastasis in different breast cancer models has been uncertain due to conflicting results [85]. In the PyVT model, depleting neutrophils increases lung metastasis [56]. In contrast, depletion of neutrophils in the orthotopic 4T1 mouse mammary carcinoma decreases the number of lung metastases [55].

Here we investigate the non-malignant, immune cells present in the collagen-dense tumor microenvironment that may promote tumor progression and metastasis. In this study, we report that a pro-tumor immune cell and cytokine profile characterize the collagen-dense mouse mammary tumor microenvironment. We find an inherent difference in the cytokine signaling in wild-type versus collagen-dense tumors. These

signals support the recruitment and activation of neutrophils in the collagen-dense tumor microenvironment. Our results suggest that a collagen-dense tumor microenvironment can tip the balance between tumor promoting and tumor suppressing functions of neutrophils. Depleting neutrophils significantly slowed the formation of new tumors, and reduced tumor burden and lung metastasis only in tumors arising in the collagen-dense tumor microenvironment, but not in wild-type MMTV-PyVT mice. These findings suggest that tumor progression in a collagen-dense microenvironment occurs through a distinct subpopulation of immune cell effectors compared to non-dense microenvironments.

1.6 Methods

Mice

Mice were bred and maintained at the University of Madison – Wisconsin under the approval of the University of Wisconsin Animal Care and Use Committee (approved animal protocol number: M01668).

Transgenic male mice expressing the Polyoma Virus middle T antigen under the direction of the mammary mouse tumor virus promoter (MMTV-PyVT) in the FVB background (originated from The Jackson Laboratory, Bar Harbor, ME) were used as a model of breast cancer that develops spontaneous tumors and metastasizes to the lung [78]. These mice were crossed to female mice heterozygote for the $Col1a1^{tmJae}$ mutation in the C57BL/6/129 background (originated from The Jackson Laboratory, Bar Harbor, ME). The Co1A1 mutation renders the alpha 1 chain of collagen I uncleavable by collagenase and increases collagen in the tissue due to decreased remodeling [86]. The

resulting mice were either positive for the MMTV- PyVT (tumor mice) or negative (normal mice), and they were either wild type for the Col1A1 mutation (WT) or heterozygote (COL). Genotyping by polymerase chain reaction (PCR) was performed on DNA extracted from tail biopsies.

Tissue collection:

Female mice were examined for palpable tumors starting at 8 weeks. At 15 weeks of age, matched sibling pairs of WT and COL tumors were anesthetized with 4% isofluorane. Blood was collected via retro orbital procedure into an EDTA (1.3mg/ml of blood) collection tube (Sarstedt, Numbrecht, Germany). Mice were then perfused intracardially with 0.9% Sodium Chloride (Abbott Laboratories, Chicago, IL) supplemented with 1 unit of heparin (Hospira, Lake Forest, IL). Mammary gland tumors and spleens were harvested and placed in high glucose DMEM media (Gibco, Grand Island, NY) supplemented with 10% fetal bovine serum (FBS, Gemini Bio Products, Baltimore, MD) and 1x antibiotic antimycotic solution (Corning, Corning, NY) for ELISA cytokine array and flow cytometry experiments. Tumors from the fourth or fifth (right or left) mammary glands were harvested and fixed in 10% buffered formalin (Thermo Fisher Scientific, Kalamazoo, MI), as well as lungs. Spleens were weighed and cut in half: one half was placed in DMEM with 10% FBS and 1x antibiotic antimitotic for flow cytometry experiments, and the other half was fixed in 10% buffered formalin. Tumors were weighed and approximately 150mg of tumor was used per mice per flow cytometry experiment.

ELISA plate array:

To prepare the cell lysate, 100mg of fresh tumor from WT and COL tumor mice was placed in 1ml of cell lysis buffer (Signosis, Inc., Sunnydale, CA). Tumors were homogenized on ice in a PowerGen 125 homogenizer (Fisherbrand, Pittsburgh, PA) for one minute. Lysates were sonicated at 20% power for 10 seconds three times using a Sonic Dismembrator Model 500 (Fisher Scientific) with a Branson tip Model 102 converter. The samples were centrifuged at 10,000 RPMs for five minutes. The supernatant was then aliquoted and frozen at -80°C until ready to use.

Mouse Cytokine ELISA Plate Array (Chemiluminescence) (Signosis, Inc.) is a 96-well plate divided into four sections, each section has three columns for one sample. Each section has 23 specific cytokine capture antibodies coated on each well and one blank well. Samples were thawed and diluted to 10 μg per 100 μl per well. Briefly, each well was incubated with 100 μl of sample for two hours, followed by biotin-labeled antibody mixture for one hour with gentle shaking then, with strepaviding-HRP conjugate for 30 minutes with gentle shaking, finally, with substrate solution for 2 minutes. The plate was read on a Fluoroskan Ascent™ FL microplate fluorometer using the Ascent™ Software (Thermo Scientific, Waltham, MA).

Single cell isolation:

Single cells were obtained by cutting tumors and spleens into small pieces and digesting tumors with 0.028W/ml of Liberase TM Research Grade (Roche, Mannheim,

Germany), 20μg/ml of DNase I, and 1x antibiotic antimycotic in DMEM with 10% FBS for 1 hour at 37°C with 250 RPM agitation. Digestion was facilitated by pipetting up and down every 15 minutes. The cell suspension was filtered through 70 and 40μm nylon cell strainer (BD Biosciences, Franklin Lakes, NJ). Red blood cells were lysed from tumor and spleen single cell suspensions with lysis buffer (Sigma, St. Louis, MO), and cells were resuspended in wash buffer (3% FBS in PBS, Gibco, Grand Island, NY).

Flow Cytometry:

Cells were resuspended at 10^6 cells per 100μl of wash buffer and blocked with Fc block (anti CD16/CD32, BD Biosciences) for 5 minutes at 4°C. For the myeloid cell flow panel, 10^6 cells were incubated with Alexa Fluor® 488-F4/80 (clone BM8, Invitrogen, Carlsbad, CA), PE-CCR2 (clone 475301, R&D Systems, Minneapolis, MN), PE-Cy™5-CD45 (clone 30-F11), Brilliant Violet 711™-CD3ε (clone 145-2C11), APC-Ly6C (clone, AL-21) from BD Biosciences, Brilliant Violet 421™-Ly6G (clone 1A8, BioLegend, San Diego, CA), Alexa Fluor® 700-CD11b (clone M1/70, eBiosciences, San Diego, CA) for 30 minutes at 4°C in the dark. Other antibodies used include: FITC-CD335 (NKp46) (clone 29A1.4) and APC-CD49b (clone DX5) from BD Biosciences, and PE-F4/80 (clone CI:A3-1, AbD Serotec, Kidlington, UK). For the lymphocyte flow cytometry panel, 10^6 cells were incubated with PE-CD4 (clone GK1.5), PE-Cy™5-CD45 (clone 30-F11), PE-Cy™7-CD25 (clone PC61), Brilliant Violet 711™-CD3ε (clone 145-2C11), APC-CD19 (clone, 1D3) from BD Biosciences, Brilliant Violet 421™-CD8a (clone 53-6.7, BioLegend), Alexa Fluor® 700-CD11b (clone M1/70, eBiosciences, San Diego, CA) for 30 minutes at 4°C. After washing,

cells were stained with 1μl of Fixable Viability Dye eFluor® 780 (eBiosciences) for 30 minutes at 4°C in the dark. Cell samples from the lymphocyte panel were stained with the Foxp3/transcription factor staining buffer set from eBiosciences. Briefly, cells were incubated in 1ml of the Fixation/Permeabilization working solution for 30 minutes at 4°C; cells were washed and left in 1x Permeabilization Buffer overnight at 4°C in the dark. Cells were resuspended in 100μl of 1x Permeabilization Buffer and stained with Alexa Fluor® 488-Foxp3 (clone FJK-16s, eBiosciences) for 30 minutes at room temperature in the dark. After the final wash, all cells were resuspended in 500μl of wash buffer for analysis.

Samples were run on the LSRII and LSR Fortessa (BD Biosciences) benchtop flow cytometers at the University of Wisconsin Carbone Cancer Center (UWCCC) Flow Cytometry Facility. Each experiment was standardized using Sphero™ Rainbow Fluorescent Particles (Mid-Range) (Spherotech Inc., Lake Forest, IL). LSRII and LSR Fortessa sensitivities were optimized during the initial run of the experiment. Rainbow beads were collected at those optimized settings and Median Fluorescent Intensity (MFI) values, target values, were recorded in each channel. For every run, rainbow beads were acquired first. LSRII and LSR Fortessa voltages were adjusted until the bead peaks hit the target value (±10%). The instrument was compensated using UltraComp eBeads (eBiosciences). For each tumor sample 25,000 live, single cell events were collected, and for each spleen sample, 50,000 live, single cell events were collected. Data was analyzed using FlowJo Single Cell Analysis Software (TreeStar, Ashland, OR), and gating was established using Fluorescent Minus One (FMO) controls.

Immunohistochemistry:

Tissues (mammary tumor, mammary gland, spleen, and lungs) were fixed in 10% buffered formalin (Thermo Fisher Scientific) for 48 hours. These were then placed in 70% ethanol and taken to the UWCCC Experimental Pathology Laboratory (EPL) for processing. Tissues were embedded in paraffin and sectioned, and one section was stained with hematoxylin and eosin (H&E) by the EPL. COL and WT tumor sections were deparaffinized by heating at 60°C for 25 minutes. Then, they were placed in xylenes and rehydrated in gradual dilutions of ethanol. Antigen retrieval was done in citrate buffer pH 6.0 in a boiling water bath for 15 minutes. Endogenous horseradish peroxidase (HRP) activity was blocked by incubating sections in 0.3% H_2O_2 in TBS for 20 minutes at room temperature. Sections were blocked with 5% normal serum and 1% BSA in TBS (blocking solution) for 1 hour, and with Avidin/Biotin Block (Vector Laboratories, Burlingame, CA) for 15 minutes each. Sections were incubated with primary rat-anti-mouse Ly6G (1:1000, clone 1A8, Biolegend) for 2 hours, and with affinity purified, mouse absorbed, biotinylated anti-rat secondary IgG (Vector Laboratories) for 45 minutes. All incubations were done at room temperature. Sections were incubated with Vectastain Universal Ready-to-Use ABC reagent (Vector Laboratories) for 30 minutes, stained with 3,3' diaminobenzidine (DAB) and counterstained with hematoxylin (Leica, Nussloch, Germany). Sections were dehydrated in gradual dilutions of ethanol and xylenes before mounting in Richard Allen Scientific mounting medium (Thermo Fisher).

Slides were imaged at the University of Wisconsin - Madison Translational Research Initiatives in Pathology laboratory using the Nuance™ multispectral imaging system (PerkinElmer, Waltham, MA). Eight fields per tumor slide were captured with the 40X objective by the Nuance™ analysis software. Ly6G positive cells were counted manually for each image and averaged per tumor.

Neutrophil depletion:

To deplete neutrophils in COL and WT tumor mice, mice received intra-peritoneal injections of 5.5μg/g of *InVivo*Mab anti mouse Ly6G (clone 1A8, BioXCell, West Lebanon, NH) for the treated group and 5.5μg/g of *InVivo*Mab rat IgG2a (clone 2A3, BioXCell) for the control group. Injections were administered every 3 days for 24 days. Mice were 9 weeks of age at the beginning and 12 weeks of age at the conclusion of the experiment. Systemic neutrophil depletion was evaluated periodically by collecting blood samples from the saphenous vein. Samples were analyzed in a Hemavet 950FS (Drew Scientific, Waterbury, CT) whole blood counter.

Hybrid Positron Emission Tomography (PET) and Computed Tomography (CT) mouse imaging before and at the end of treatment was conducted at the UWCCC Small Animal Imaging Facility. All mice were fasted 12 hours prior to intravenous injection of approximately 8 MBq of 2'-deoxy-2'-[^{18}F]fluoro-D-glucose (^{18}FDG) (IBA-Molecular, Sterling, VA) one hour before imaging. Mice were anesthetized with inhalation gas (2% isoflurane gas mixed with 1L/min of pure oxygen) and kept under a heat lamp during injection until imaging. Mice were imaged on the Siemens Inveon Hybrid micro-PET/CT

(Siemens Medical Solutions, Knoxville, TN) in the prone position. A 10 minute PET scan was acquired and data were plotted as histograms in to one static frame and subsequently reconstructed using ordered-subset expectation maximization (OSEM) of three dimensions followed by the maximum *a posteriori* algorithm (Matrix size = [128,128,159], pixel size = [0.776, 0.776, 0.796] mm, iterations = 18, subsets = 16, and beta smoothing factor = 0.004). Data were not corrected for attenuation or scatter.

Data were analyzed using the Siemens Inveon™ Research Workplace (Siemens Medical Solutions). Source CT 3D images were co-registered with target PET 3D images. Date, time, and dose (Mbq) were entered for each data point (mouse). PET and CT scales were set at specific minimum and maximum percent injection dose per gram (%ID/g) and applied to every data point. Regions of interest (ROIs) were drawn at any mammary gland that had an FDG uptake threshold value between 7.5 and 27%ID/g based on background ROI reading (muscle) and image contrast. ROI data collected included: volume (mm^3), mean %ID/g, minimum %ID/g, and maximum %ID/g. Maximum intensity projections (MIPs) were collected for each hybrid micro-PET/CT mouse 3D image with and without ROIs. The number of ROIs per mouse was counted to generate the number of tumors per mouse; adding the volume of all tumors in each mouse generated tumor burden.

At the end of the experiment, blood, tumors, spleens, and lungs were collected. Tissues were fixed as mentioned before. Neutrophil depletion and changes in tumor and spleen immune cell populations were determined by flow cytometry as explained before. Cell markers used included PE-Cy™5-CD45 (clone 30-F11), Brilliant Violet

711™ CD3ε (clone 145-2C11), APC-CD49b (clone DX5), and FITC-CD335 (NKp46) (clone 29A1.4) from BD Biosciences, Brilliant Violet 421™ -Ly6G (clone 1A8, BioLegend), Alexa Fluor® 700-CD11b (clone M1/70, eBiosciences) and PE-F4/80 (clone CI:A3-1, AbD Serotec).

Lungs were paraffin embedded and sectioned by the UWCCC EPL. Neutrophil counts in tumors and lungs were taken to validate flow cytometry data. Immunohistochemistry was conducted using anti-Ly6G as previously explained. Slides were imaged at the University of Wisconsin - Madison Laboratory of Computational Instrumentation (LOCI) using the Olympus BX53 histology scope (Olympus, Center Valley, PA). Eight fields per tumor slide were captured with the 40X N.A.: 0.75, UPlanFLN, W.D.: 0.51 objective (Olympus) by Olympus cellSens Standard 1.13 software. Ly6G positive cells were counted manually for each image and averaged per tumor.

Lungs were also sectioned through every 100 μm and stained with H&E by the UWCCC EPL. Lung metastatic lesions were imaged at 10X N.A.:0.30, UPlanFLN, W.D.:2.1 objective at University of Wisconsin - Madison LOCI. The area of each lesion in each slide was quantified using the FIJI (Fiji is just ImageJ) [87] (National Institutes of Health, Bethesda, MD) software. The total number of lesions per mouse was counted and the largest area for each metastatic lesion was collected.

Statistical Analysis:

All statistical analysis was conducted using GraphPad Prism 5 (GraphPad Software, La Jolla, CA). For all experiments, unpaired Student's t-tests to compare the

means of the WT versus the COL groups. Differences were considered significant when $p < 0.05$. Data are presented as single data points and mean.

1.7 Results

We previously reported that the number of PyVT mammary tumors and lung metastases in a collagen-dense (COL) background is higher than the number of PyVT tumors and lung metastases in a wild type (WT) collagen background [10]. In order to characterize whether there is a change in the tumor-promoting COL immune microenvironment, we conducted a chemiluminescent ELISA plate assay to analyze the expression levels of 23 cytokines found in lysed whole mammary tumors from 15 week-old mice (Figure 1A and 1B). Interleukin-4 (IL-4), Regulation on activation, normal T cell expressed and secreted (RANTES, CCL5), Macrophage inflammatory protein 1α (MIP-1α, CCL3), and Interferon γ (IFNγ) were expressed at least two-fold higher in WT tumors compared to COL tumors. IL-4, RANTES, and IFNγ, are largely involved in T-cell signaling, recruitment and activation. In contrast, in COL tumors Platelet-derived growth factor subunit B (PDGF-BB), Granulocyte monocyte-colony stimulated factor (GM-CSF), and Interleukin-1α (IL-1α) were all increased by two-fold or more compared to WT tumors (Figure 2B). Of these, GM-CSF is a strong chemoattractant for monocytes and neutrophils, and it enhances production and activation of monocytes and granulocytes. These data suggest that tumors arising in collagen-dense microenvironments secrete distinct cytokines and may recruit distinct subsets of immune cells compared to tumors in WT mice.

T-lymphocyte recruitment is not altered in the collagen-dense tumor microenvironment

The cytokine panel suggested that signaling to T-cells is greater in WT tumors compared to COL tumors. Differences in lymphocyte recruitment into WT and COL tumors at 15 weeks were determined by flow cytometry with a panel of T-cell markers. The percentage of CD45+ leukocytes found in COL tumors did not vary from the percentage found in WT tumors (Fig 2A, 2B). Thus, we do not think that COL tumors were harder to dissociate, as we were able to recover a very similar number of immune cells as we recovered from WT tumors. Moreover, we found no significant difference in the percentage of CD45+CD3+CD11b- T-cells found in WT and COL tumors (Figure 2C, 2D). We also compared CD8 cytotoxic T-cell and CD4 helper T-cell markers in WT and COL tumors (Figure 2E), and found that the percentage of CD45+CD3+CD8+ cytotoxic T-cells (Figure 2F) and CD45+CD3+CD4+ helper T-cells (Figure 3G) did not significantly differ between WT and COL tumors. Recruitment of other lymphocytes such as CD19+ B-cells and NKp46+ natural killer (NK) cells also did not differ in WT versus COL tumors (Supplemental Figure AII-1A and 1B).

We also quantified CD4+CD25+Foxp3+ regulatory T-cells. These cells are characterized by reducing T-cell proliferation and cytotoxicity and by contributing to regulatory T-cell expansion [88]. When comparing CD25 and Foxp3 regulatory T-cell markers (Figure 2H), the percentage of CD45+CD3+CD4+CD25+Foxp3+ regulatory T-cells found in WT and COL tumors was not different (Figure 2I).

The overall myeloid cell populations are not altered in a collagen-dense tumor microenvironment

The cytokine panel suggested that signaling to monocytes and neutrophils is greater in COL tumors compared to WT tumors. We conducted flow cytometry analysis of cells dissociated and isolated from WT and COL tumors at 15 weeks of age. The percentage of CD45+ leukocytes found in COL tumors did not differ from the percentage found in WT tumors (Fig 3A, 3B). When comparing cells expressing Ly6G versus F4/80 in tumors, the percentage of F4/80+ macrophages from the CD45+Ly6G- population did not significantly vary between WT and COL tumors (Figure 3C and 3D). Of cells expressing CD45+CD3-CD11b+, we found no significant difference in the percentage of Ly6G+Ly6C+ neutrophils in COL tumors compared to WT (Figure 3E and 3F). We validated our flow cytometry results by staining formalin fixed paraffin embedded tumor sections from WT and COL tumor mice with anti-Ly6G (1A8) using DAB as the chromogen and hematoxylin as the counterstain (Figure 3G). Figure 3H shows that the average number of Ly6G+ neutrophils found in eight fields of view was not significantly increased in COL tumors.

Some studies denote CD11b+Ly6G+Ly6C+ myeloid cells as granulocytic myeloid derived suppressor cells (MDSCs). Since there was no change in the number of T-cells, specifically regulatory T-cells, in WT versus COL tumors, the Ly6G+ cells we see in the mammary tumors are likely not MDSCs. We, therefore, refer to our population of interest as Ly6G+Ly6C+ neutrophils in the context of this study.

Spleens from collagen-dense tumor mice are enlarged, suggesting an advanced disease state

Splenocytes were isolated to provide controls for flow cytometry experiments. While harvesting the tissue, we observed enlarged spleens in COL tumor mice at 15 weeks of age (Figure 4A). Spleen weight was measured and normalized to the total weight of each mouse. We found a significant increase in the weight of spleens from COL tumor mice compared to WT tumor mice (Figure 4B). Characterization of the immune cell profiles in the spleens demonstrated no significant changes in CD45+ immune cells in COL spleens compared to WT spleens (Fig 4C), whether considering live cells or fixed cells (Figure 4F). Of the cells expressing CD45+CD11b+, the percent of Ly6G+Ly6C+ neutrophils was not significantly increased in COL spleens compared to WT spleens (Figure 4D). The percent of F4/80+ macrophages did not differ between COL and WT spleens (Figure 4E). Using the same lymphocyte flow cytometry cell marker panel as above, we found that the percentage of CD45+CD3+ T-cells and T-cells subsets: CD8+ cytotoxic T-cells, CD4+ helper T-cells, and CD4+CD25+Foxp3 regulatory T-cell did not differ in COL spleens compared to WT spleens (Figure 4H-J). CD19+ B-cells and NKp46+ natural killer (NK) cells also did not differ in spleens from WT versus COL tumor mice (Supplemental Figure AII-1C and 1D). Complete blood counts (Supplemental Figure AII-2A-E), showed a trend towards increased neutrophil to lymphocyte ratio ($p = 0.06$) in COL tumor mice, which is also associated with poor clinical outcome in breast cancer patients [89]. These results suggest that enlarged spleens and changes in neutrophil to lymphocyte ratio are whole-body global effects seen in collagen dense tumor mice.

We did not observe any differences in immune populations due to the Col1A1 transgene in the absence of PyVT tumors in the mammary glands (Supplemental Figure AII-3A-3E). The spleens of normal, non-tumor-bearing COL (not carrying the PyVT transgene) mice were not enlarged (Supplemental Figure AII-4A), their immune cell population recruitment did not differ significantly (Supplemental Figure AII-4B-4F), and there were no significant changes in circulating blood leukocyte counts (Supplemental Figure AII-5A-5E).

Depleting neutrophils with anti-Ly6G reduces tumor burden of collagen-dense mice

The cytokine array results suggest there may be differences in activation of neutrophils in COL mice, even if the number of neutrophils recruited is not significantly different. The function of Ly6G+ neutrophils in tumor progression was studied by blocking the recruitment of neutrophils in COL and WT tumor mice. Mice were treated with anti-Ly6G or anti-IgG for 24 days starting at 9 weeks of age (Figure 5A). In order to dynamically monitor tumor growth in this transgenic (i.e. not luciferase-labeled) model, we made use of hybrid micro PET-CT 3D imaging using the uptake of ^{18}FDG in WT and COL, control and Ly6G-depleted mice. Figure 5B shows a representative maximum intensity projection from each group, where ROIs (regions of interest) are drawn to indicate where the tumor is and its relative size. As expected, on the day before treatment started (d -1), the number of tumors was the same in both control and treatment groups (Figure 5C and 5E). After 21 days, tumor size increased due to disease progression in the PyVT model in both the WT and COL control arms. Antibody-

depletion of Ly6G+ neutrophils significantly slowed down the progression of cancer by reducing the number of COL tumors, but not the number of WT tumors after 21 days (Figure 5C and 5E). The total tumor burden in WT tumor mice increased over time and was not attenuated by treatment with anti-Ly6G (Figure 5D). In contrast, the tumor burden decreased with anti-Ly6G treatment in COL mice at 21 days (Figure 5F). Figures 5G-J display the mean and maximum percent injection dose per gram of each tumor, and demonstrate that ^{18}FDG uptake increases with progression of the disease, but does not change with neutrophil depletion in WT nor COL tumors. PET imaging is a non-invasive imaging modality that utilizes tumor-linked increase in glucose uptake and metabolism to image mammary tumors [90, 91]. Our results show that glucose uptake does not change with treatment or collagen density of tumors, and therefore we conclude that the changes seen in number of tumors and tumor volume is a direct effect of blocking Ly6G+ neutrophils.

Tumors isolated from control and treated groups were analyzed by flow cytometry to understand the effect of depleting neutrophils on immune cell recruitment. Figure 6A and 6G show that the percentage of CD45+ immune cells was similar in all groups of both tumors and spleens. To evaluate depletion of neutrophils, we quantified the percentage of Ly6G+ neutrophils from immune cells that are CD45+CD3-CD11b+ (Figure 6B and 6H). At 12 weeks, anti-Ly6G treatment decreased neutrophil numbers in both WT and COL tumors. Neutrophil depletion was confirmed in spleens of WT and COL tumor mice, demonstrating a significant depletion in Ly6G+ neutrophils with antibody treatment (Figure 6H). Interestingly, treatment with anti-Ly6G significantly increased the

percentage of F4/80+ macrophages in WT tumors, but not in COL tumors, which had variable numbers of F4/80+ macrophages in both control and treatment arms (Figure 6C). Data from spleens also showed the trend of increased F4/80+ macrophages in treated WT spleens. (Figure 6I). Changes in the number of NK cells were not observed in tumors and spleens (Supplemental Figure AII-6A and 6C). No spleen enlargement occurred upon anti-Ly6G treatment at 12 weeks (Supplemental Figure AII-6B). Nor were there other global effects due to anti-Ly6G treatment such as the number of circulating blood cells (Supplemental Figure AII-7A-7E).

Depleting neutrophils with anti-Ly6G reduces the number of lung metastasis in collagen-dense but not wild-type mice

Lungs from WT and COL mice from both control and Ly6G-depleted arms were sectioned and the number of metastatic lesions throughout the whole lung determined. Anti-Ly6G treated COL mice showed an 80% response to treatment; only one out of six mice had lung metastases. In contrast, all Ly6G-depleted WT mice developed metastatic lesions (Fig 7A). In fact, treatment with anti-Ly6G increased the number of WT animals with metastases and the total number of metastases (Figure 7B-F). The number of Ly6G+ neutrophils in the lungs was quantified via immunohistochemistry (Supplemental Figure AII-8A and 8B). There was no correlation between the numbers of Ly6G+ neutrophils found in the lungs versus the number of lung metastatic lesions (Supplemental Figure AII-8C).

1.8 Discussion

Although mammographic density is associated with increased risk of developing breast cancer, the mechanisms underlying this increased risk are poorly understood. Here we use the collagen-dense (COL) MMTV-PyVT model, which has increased collagen deposition, a higher tumor incidence, and more metastases compared to tumors in wild type (WT) animals [10]. Now, we seek to further characterize the mechanisms by which increased stromal collagen enhances tumor progression by identifying immune cell populations present in the COL tumor microenvironment and their effect on tumor progression. The role of leukocyte infiltrates has been shown to promote tumor progression in the MMTV-PyVT mammary tumor model, but not in COL mammary tumors [32, 92, 93]. The upregulation of cytokines, GM-CSF, IL-1α, and PDGF-BB, specifically in tumors from COL mice, while IL-4, MIP-1a, RANTES, and IFNγ were increased specifically in tumors from WT mice. These differences suggest there is an altered host response for tumors arising in collagen-dense microenvironments. Despite differences in cytokine profiles, we do not see a significant change in the recruitment of distinct immune cell populations comparing WT to COL tumors. Rather, there is a functional difference in the role of neutrophils, as depletion of Ly6G+ neutrophils with anti-Ly6G (1A8) antibody diminishes tumor progression specifically in COL mice but has little effect on WT Ly6G depleted tumors. Most importantly, depletion of neutrophils with anti-Ly6G significantly inhibits lung metastasis in COL mice, but does not diminish metastases in WT mice. Thus, we find that neutrophils have a tumor promoting effect

specifically in the context of COL mammary tumors, but do not significantly contribute to progression and metastasis in WT tumors.

Others have also performed similar neutrophil depleting studies using anti-Ly6G (1A8) in orthotopic models [49, 50, 55, 57], but these studies did not investigate the role of collagen density. These studies present conflicting evidence regarding whether neutrophils play a role in breast cancer metastasis. While treating orthotopic 66c14 mouse mammary tumors with anti-Ly6G decreases lung metastasis [55], depletion of neutrophils in orthotopic MMTV-PyVT or 4T1 mouse mammary carcinoma models results in increased lung metastasis [56]. Tabariés, et al. recently demonstrated that Ly6G+ granulocytes are recruited to lung and liver metastasis in the 4T1 model. In their study, depleting neutrophils with anti-Ly6G does not affect lung metastasis, but it does reduce liver metastasis [57]. All of these models rely on cell lines or surgical procedures for the creation of metastasis. An intriguing possibility is that the conflicting results may be due to different wound-healing and fibrotic responses in these different studies, although changes in the extracellular matrix were not determined. Here, we use the MMTV-PyVT model, which develops spontaneous metastasis starting after 10 weeks of age [94] and does not require surgical intervention that may confound the results with variable wound-healing effects. In the current study, anti-Ly6G treatment has no effect on lung metastases in WT mice, but significantly decreases metastases in COL animals.

Our flow cytometry analysis of immune cell types showed an increase in the number of CD11b+F4/80+ macrophages in treated WT tumors. Because TAMs have an established role in tumor progression and metastasis [42, 95], the increase in

macrophages may carry on with invasion and metastasis in the MMTV-PyVT tumors even after depletion of Ly6G+ cells in WT mice. A role for macrophages in metastasis following Ly6G depletion is supported by our observation that the only individual mouse with metastasis in the COL treated group also had the largest recruitment of CD11b+F4/80+ macrophages (data not shown). The COL mouse model has increased collagen I throughout the whole animal. We hypothesized that COL lungs can also recruit Ly6G+ neutrophils, but our results did not support this hypothesis, because the number of lung metastatic lesions did not correlate with the number of Ly6G+ neutrophils found near the lung metastases.

It is not entirely clear why depleting Ly6G+ neutrophils slows tumor growth in COL mice but not WT mice. This finding demonstrates that Ly6G+ neutrophils have an important role in COL tumor progression, but not in WT tumor progression. The Ly6G+ neutrophils in the COL tumors are possibly polarized towards greater pro-tumor activity than the Ly6G+ neutrophils in WT tumors. If Ly6G+ neutrophils in WT tumors are not pro-tumorigenic, depleting them would have little effect, which is what we observe. The idea that there is a fundamental difference in the host response in the COL vs. WT tumors is consistent with our finding that there are differences in the cytokines released within COL compared to WT tumors.

Studies of mesothelioma and lung carcinoma lines injected into the flank of mice have been used to demonstrate the polarization of neutrophils, identifying a tumor-associated neutrophil (TAN) population analogous to TAMs. TANs can have anti-tumorigenic (N1) or pro-tumorigenic (N2) functions, where the predominant N2

phenotype is driven by the presence of TGF- β [49]. These models also show that TANs at early stages of tumor growth are more cytotoxic to tumor cells by either directly killing tumor cells or by secreting reactive oxygen species (ROS), whereas later in tumor development, they acquire a more tumor supportive phenotype [50]. In pancreatic cancer, neutrophils residing within the tumors express MMP-9, which then liberates vascular endothelial growth factor (VEGF) and promotes angiogenesis [54]. Ly6G+ neutrophils are recruited preferentially to liver metastases in the 4T1 model, where they are alternatively polarized towards an N2, pro-tumorigenic phenotype [57]. Thus, our results are consistent with a more general notion that a specific microenvironment milieu is associated with a neutrophil-dependent metastatic process.

In vitro studies of neutrophil biology have demonstrated the ability of neutrophils to migrate in 3D collagen I matrices [66]. Neutrophils can also adhere and become activated in type I collagen [67]. Peptides derived from collagen breakdown are chemotactic for neutrophils *in vivo* and *in vitro* [96]. These neutrophil capabilities, especially neutrophil migration in response to chemoattractants, involve integrins β2, α2, and β1. The two latter integrins mediate cell adhesion to collagen I fibrils [68, 69]. Although rapid leukocyte migration in response to chemokines can be integrin independent [70], neutrophil chemotaxis in collagen I is also mediated by the collagen receptor, discoidin domain receptor 2 (DDR2). DDR2 regulates neutrophil directionality and persistence by releasing MMPs (MMP-8) that cleave collagen [71]. These studies support the recruitment of neutrophils to COL microenvironments *in vitro.*

Our data suggest that tumors arising in a collagen-dense microenvironment are fundamentally different from those arising in a non-dense microenvironment, as there are key differences in cytokine signaling that support tumor progression. All cytokines have specific roles in wound healing or infection, but once the immune system is challenged with cancer, some of these functions are co-opted by the tumor. The presence and function of Ly6G+Ly6C+ neutrophils in COL mammary tumors is likely supported by increased GM-CSF signal compared to WT tumors. This pro-inflammatory cytokine stimulates proliferation and induces maturation of granulocyte and monocyte progenitor cells. GM-CSF has been described as a strong chemoattractant for mouse and human neutrophils [97, 98] that can differentiate monocytes into dendritic cells and polarize T-cells into a Th1 phenotype [99, 100]. GM-CSF can block the angiogenic functions of tumor associated macrophages in FVB mice orthotopically injected with PyVT tumors [101]. Moreover, GM-CSF is associated with aggressive breast cancer subtypes, where GM-CSF secreted by human breast cancer cells primes plasmacytoid predendritic cells (pDC) to polarize the immune microenvironment toward a regulatory Th2 phenotype [102]. Homodimer PDGF-BB is also upregulated in COL tumors. High levels of PDGF-B lead to over-activity of tyrosine kinase PDGF receptor and tumor cell proliferation. This mitogen stimulates growth, survival, and migration of mesenchymal/stromal cells [103]. Breast cancer cell-secreted PDGF targets stromal cells and initiates tumor desmoplasia [104]. *In vitro*, PDGF-BB is a chemoattractant for neutrophils and monocytes, and can activate human neutrophils [105, 106]. Thus, our finding of elevated PDGF-BB in a dense collagen microenvironment is consistent with an

increase in neutrophil activation. Il-1a is not commonly found in circulation except during severe disease. IL-1a can induce matrix degradation and remodeling by breast cancer fibroblasts. Breast cancer cells can secrete IL-6 and IL-8 in response to IL-1a [107]. Although not part of the cytokine array, IL-8 (KC, MIP-2, and LIX homologues in mouse) is a major neutrophil chemoattractant [108, 109]. Our data suggest that all of these contribute to the progression of mammary cancer in the COL tumor microenvironment. It has yet to be determined which cell type contributes to the increased production of these cytokines. Tumor cell cytokine secretion has been widely studied *in vitro*, but new techniques must be developed to answer these questions in a complex, *in vivo* COL tumor microenvironment.

Of the signals downregulated in collagen-dense mammary tumors, CCL5 is the chemokine that shows the greatest differential expression in WT mammary tumors. It is produced by activated T-cells and is a strong T-cell chemoattractant. The role of CCL5 in breast cancer progression and metastasis has been established: this includes upregulation of MMP secretion, pro-tumor effects by generating MDSC in the bone marrow, and a reduction in metastasis when low levels of CCL5 are expressed [110-113]. Also upregulated in WT tumors, IL-4 is one of the most studied Th2 cytokines [114]. Recent studies of IL-4/IL-4R signaling in breast cancer cells *in vitro* and *in vivo* show enhanced cell survival and proliferation via STAT/AKT/MAPK signaling. It is also produced by activated T-cells and promotes differentiation, survival, and proliferation of B and T lymphocytes via IL4 receptor signaling [115]. T-cells (CD3+ T-lymphocytes, especially CD8+ T cells) have also been shown to respond to potent chemo attractant,

CCL3 [116]. CCL3 can recruit and activate monocytes and has been involved in anti-tumor activities as a Th-1 cytokine and increasing NK cell cytotoxicity [117]. On the other hand, CCL3 has been implicated in promoting breast cancer metastasis to the lungs [118]. Also a Th-1 cytokine, IFN-γ works with T-lymphocytes to regulate tumor cell immunogenicity by preventing the development of spontaneous epithelial carcinomas [23]. The presence of these cytokines only in WT tumors leads to the hypothesis that COL tumors have reduced T-cell signaling (recruitment and activation), which may account for their increased tumor incidence and metastasis. We found no major differences in the recruitment of T-cells and subgroups in WT versus COL mammary tumors and spleens. B-cell and NK cell populations also did not differ in recruitment. These results open the doors to studies of lymphocyte activation, proliferation, and cytotoxicity in either 3D *in vitro* collagen gels or in the MMTV-PyVT collagen-dense model.

CONCLUSION:

We find that MMTV-PyVT tumors arising in a dense collagen microenvironment have altered cytokine signaling compared to tumors arising in a non-dense microenvironment. Cytokines involved in neutrophil maturation and recruitment, including GM-CSF, PGDF-BB, and IL-1a, are altered in dense-collagen tumors. Depletion of Ly6G+ neutrophils diminished tumor formation, tumor burden, and lung metastasis, specifically in collagen-dense mammary tumors. Identifying neutrophils as key players in COL mammary tumor progression has important clinical implications for patients with

mammographically dense breast tissue. Although more research is necessary, tumor associated neutrophils may be useful as prognostic markers and possible targets for breast cancer therapy, especially for patients with dense breast tissue.

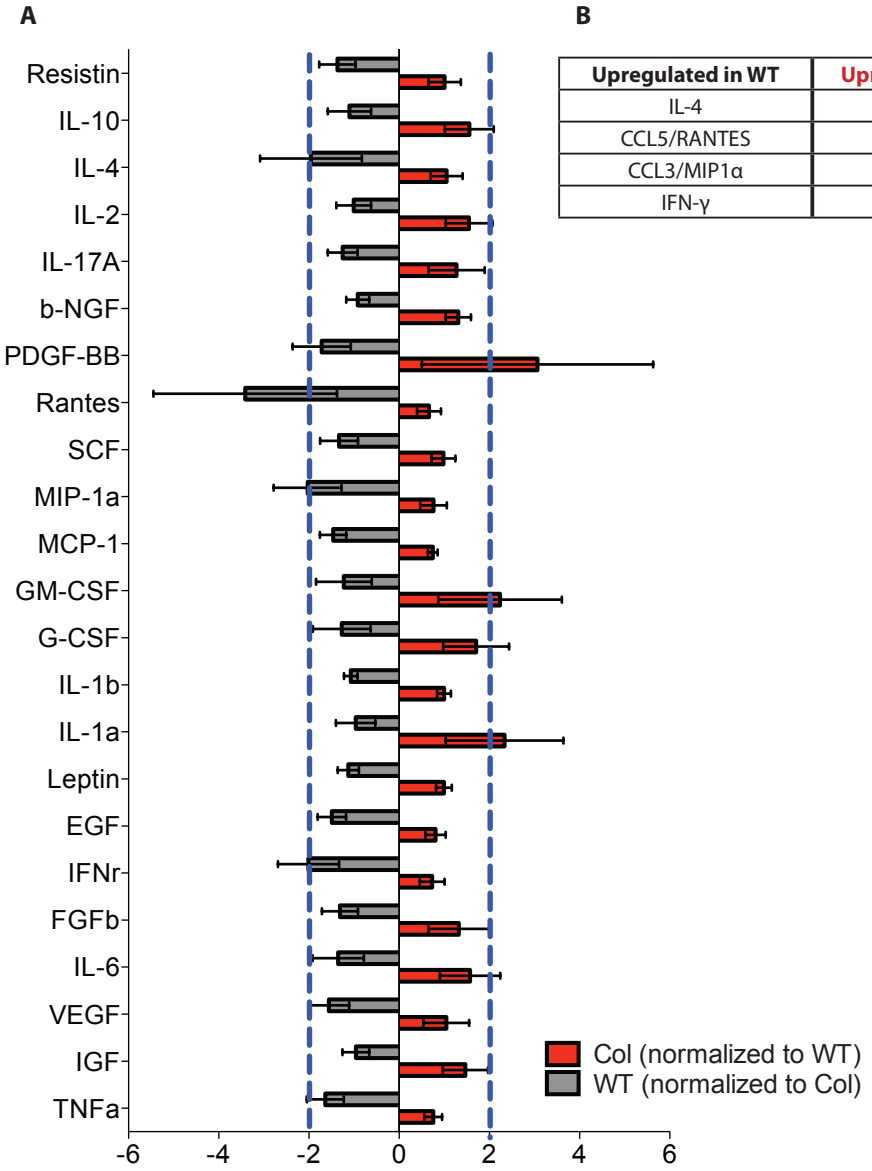

Upregulated in WT	Upregulated in COL
IL-4	PDGF-BB
CCL5/RANTES	GM-CSF
CCL3/MIP1α	IL-1α
IFN-γ	

Figure 2.1 Cytokines in COL and WT tumor microenvironments are inherently distinct. (**A**), cytokine levels from whole WT and COL mammary tumor lysates determined by chemiluminescent Mouse Cytokine ELISA Plate Array. Results are expressed as fold change: WT readings are normalized to COL readings (gray) to show cytokines upregulated in WT tumors, and COL readings are normalized to WT readings (red) to show cytokines upregulated in COL tumors. Blue line denotes a 2-fold increase (n=4 independent tumors). (**B**), table indicates cytokines with a 2-fold increase or greater.

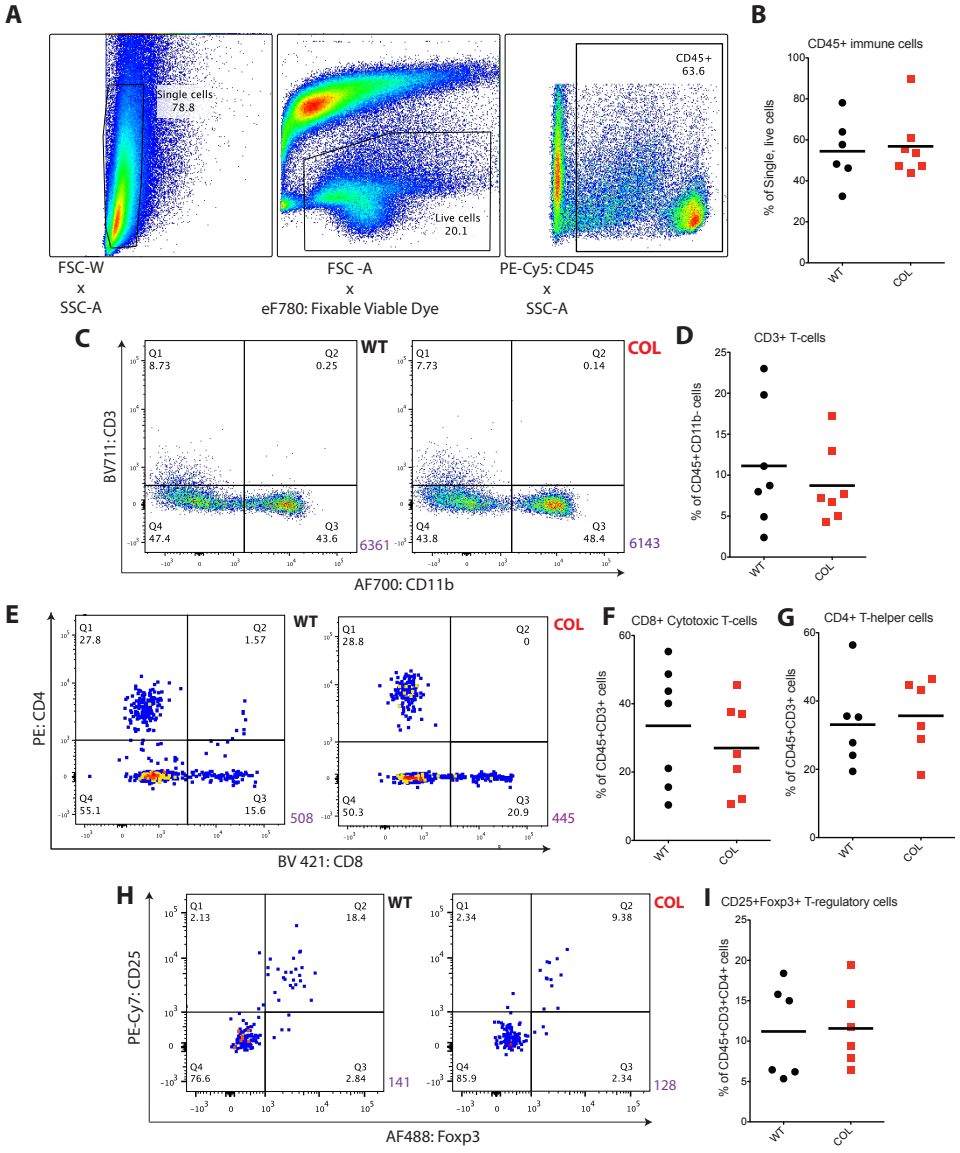
A
Single cells
78.8
Live cells
20.1
CD45+
63.6
FSC-W
x
SSC-A
FSC -A
x
eF780: Fixable Viable Dye
PE-Cy5: CD45
x
SSC-A
B
CD45+ immune cells
% of Single, live cells
WT
COL
C
WT
COL
Q1
8.73
Q2
0.25
Q4
47.4
Q3
43.6
6361
Q1
7.73
Q2
0.14
Q4
43.8
Q3
48.4
6143
BV711: CD3
AF700: CD11b
D
CD3+ T-cells
% of CD45+CD11b- cells
E
WT
COL
Q1
27.8
Q2
1.57
Q4
55.1
Q3
15.6
508
Q1
28.8
Q2
0
Q4
50.3
Q3
20.9
445
PE: CD4
BV 421: CD8
F
CD8+ Cytotoxic T-cells
% of CD45+CD3+ cells
G
CD4+ T-helper cells
% of CD45+CD3+ cells
H
WT
COL
Q1
2.13
Q2
18.4
Q4
76.6
Q3
2.84
141
Q1
2.34
Q2
9.38
Q4
85.9
Q3
2.34
128
PE-Cy7: CD25
AF488: Foxp3
I
CD25+Foxp3+ T-regulatory cells
% of CD45+CD3+CD4+ cells

Figure 2.2 Lymphocyte recruitment is not altered in late-stage collagen-dense tumors. (**A**), flow cytometry gates used to determine lymphocytes. (**B**), percentage of CD45+ immune cells in wild-type (WT) and collagen-dense (COL) mammary tumors (n=6). (**C**), flow cytometry of CD45+ cells comparing CD3 to CD11b in WT (left) and COL (right) mammary tumors, and (**D**) the percentage of CD45+CD3+ T-cells present (n = 7), CD45+CD3+CD8+ cytotoxic T-cells (**E** and **F**), CD45+CD3+CD4+ helper T-cells (**E** and **G**), and CD45+CD3+CD4+CD25+Foxp3+ regulatory T-cells (**H** and **I**) (n = 6). The purple number at lower right represents the number of total events in each graph. These cells were fixed for intracellular staining.

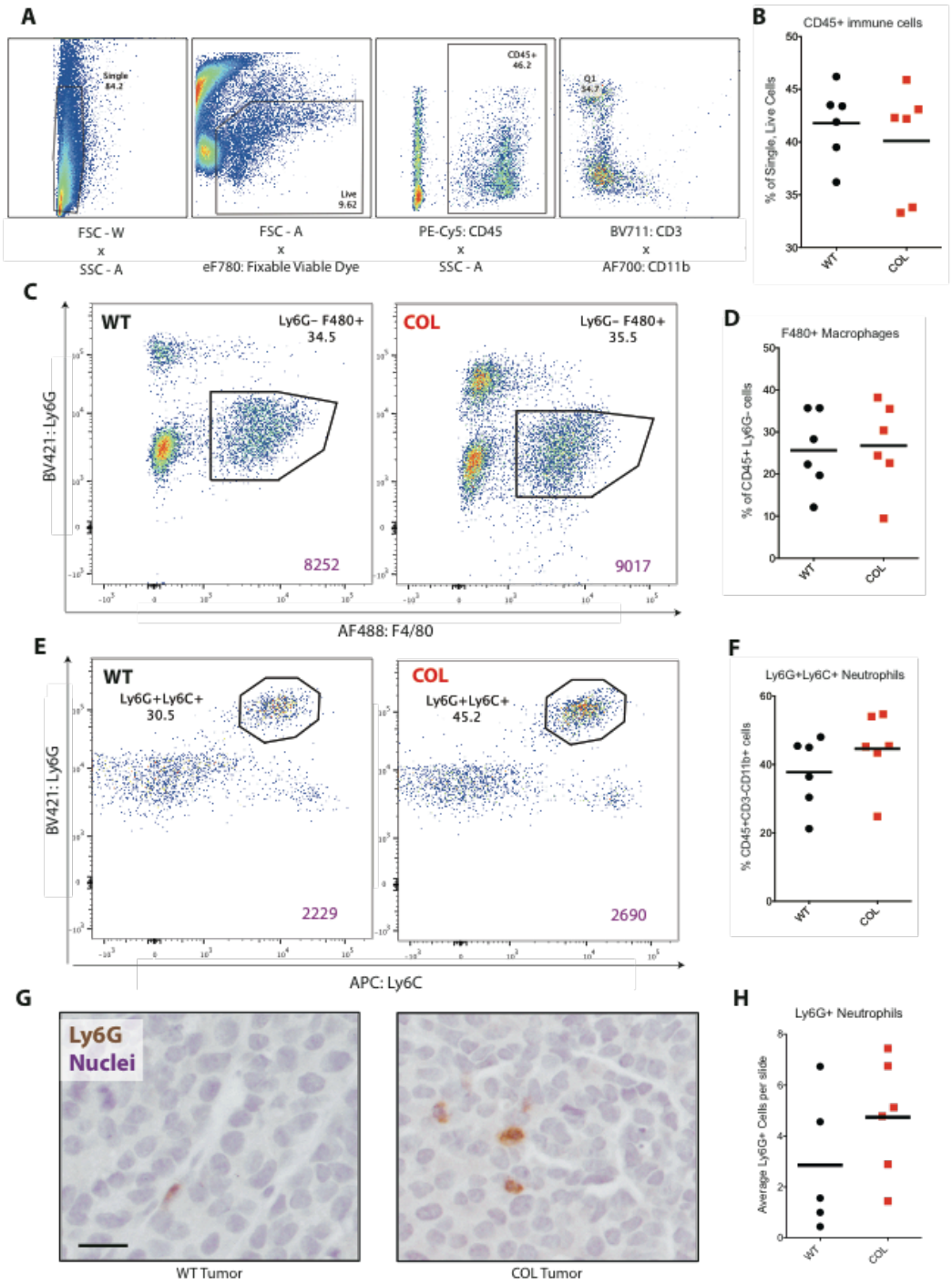
A
Single
84.2
Live
9.62
CD45+
46.2
Q1
54.7
FSC - W
x
SSC - A
FSC - A
x
eF780: Fixable Viable Dye
PE-Cy5: CD45
x
SSC - A
BV711: CD3
x
AF700: CD11b
B
CD45+ immune cells
% of Single, Live Cells
WT
COL
C
WT
Ly6G- F480+
34.5
COL
Ly6G- F480+
35.5
BV421: Ly6G
8252
9017
AF488: F4/80
D
F480+ Macrophages
% of CD45+ Ly6G- cells
WT
COL
E
WT
Ly6G+Ly6C+
30.5
COL
Ly6G+Ly6C+
45.2
BV421: Ly6G
2229
2690
APC: Ly6C
F
Ly6G+Ly6C+ Neutrophils
% CD45+CD3-CD11b+ cells
WT
COL
G
Ly6G
Nuclei
WT Tumor
COL Tumor
H
Ly6G+ Neutrophils
Average Ly6G+ Cells per slide
WT
COL

Figure 2.3 Recruitment of myeloid cells is not altered in late-stage collagen-dense mammary tumors

(**A**), flow cytometry gates used to determine myeloid cells. (**B**), percentage of CD45+ immune cells in wild-type (WT) and collagen-dense (COL) mammary tumors at 15 weeks (n=6, each n is an independent pair of age-matched littermate WT and COL mice). (**C**), flow cytometry of CD45+CD3- cells comparing Ly6G to F4/80 in WT (left) and COL (right) mammary tumors. The purple number represents the number of total events in each graph. (**D**) The percentage of CD45+CD3-CD11b+ cells that are F4/80+ macrophages in WT and COL mice. (**E**), Flow cytometry of CD45+CD11b+CD3- cells comparing Ly6C to Ly6G in WT (left) and COL (right) mammary tumors, and (**F**) the percentage of CD45+CD3-CD11b+Ly6G+Ly6C+ neutrophils present. (**G**), Immunohistochemistry of WT (left) and COL (right) mammary tumors. Tumors were stained with Ly6G (1A8) in DAB and counterstained with hematoxylin. Scare bar = 50 um. (**H**), average number of Ly6G+ cells found in eight fields of view per tumor slide (n = 4).

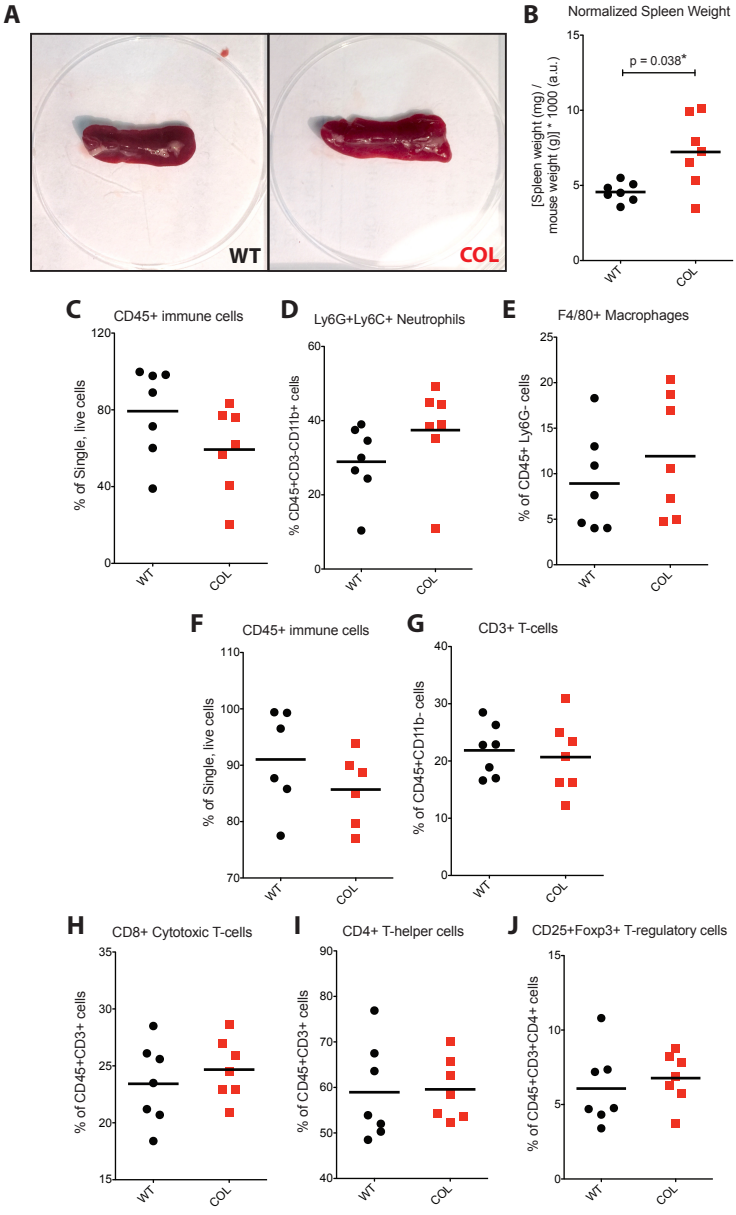
A
WT
COL
B
Normalized Spleen Weight
p = 0.038*
[Spleen weight (mg) / mouse weight (g)] * 1000 (a.u.)
C
CD45+ immune cells
% of Single, live cells
D
Ly6G+Ly6C+ Neutrophils
% CD45+CD3-CD11b+ cells
E
F4/80+ Macrophages
% of CD45+ Ly6G- cells
F
CD45+ immune cells
% of Single, live cells
G
CD3+ T-cells
% of CD45+CD11b- cells
H
CD8+ Cytotoxic T-cells
% of CD45+CD3+ cells
I
CD4+ T-helper cells
% of CD45+CD3+ cells
J
CD25+Foxp3+ T-regulatory cells
% of CD45+CD3+CD4+ cells

Figure 2.4 Spleens from late-stage collagen-dense tumor mice are enlarged relative to WT mice.

(**A**), Representative spleens from WT (left) and COL (right) tumor mice. Note the increased size of the COL spleens. (**B**), spleen weight (mg) normalized to mouse weight (g) from both WT and COL mice (n = 7). (**C**) Percentage of CD45+ immune cells, (**D**) Ly6G+Ly6C+ neutrophils and (**E**) F4/80+ macrophages found in WT and COL spleens, determined by flow cytometry as in Figure 3. Note that there is a trend toward decreased CD45+ immune cells ($p = 0.13$) and increased Ly6G+Ly6C+ neutrophils in COL tumors ($p = 0.18$) (**F**) CD45+ immune cells (lymphoid panel, fixed cells), (**G**) CD3+ T-cells, (**H**) CD8+ cytotoxic T-cells, (**I**) CD4+ T-helper cells, and (**J**) Foxp3+ T-regulatory cells found in WT and COL spleens, determined by flow cytometry as in Figure 2.

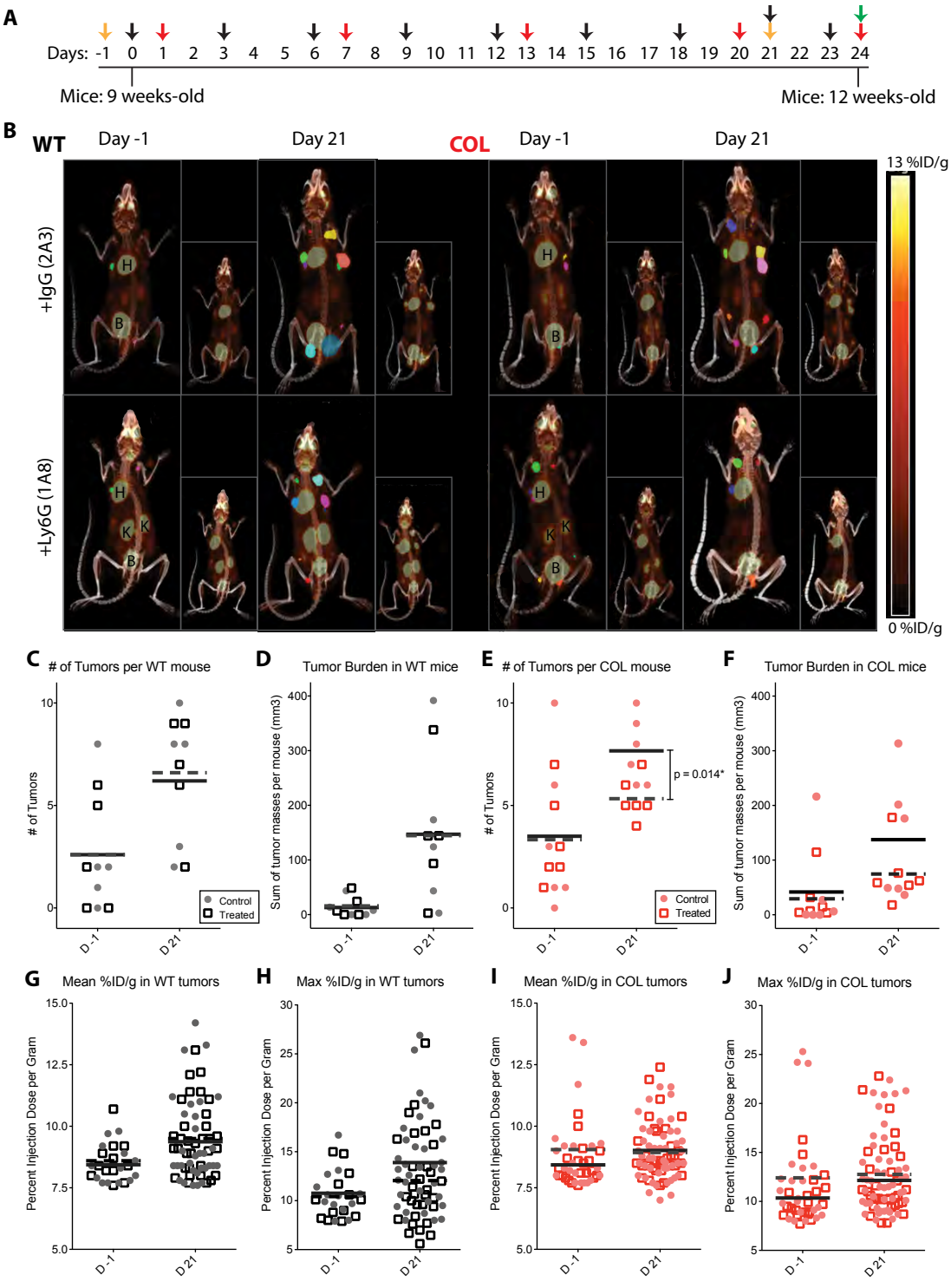
A
Days: -1 0 1 2 3 4 5 6 7 8 9 10 11 12 13 14 15 16 17 18 19 20 21 22 23 24
Mice: 9 weeks-old
Mice: 12 weeks-old
B
WT
Day -1
Day 21
COL
Day -1
Day 21
13 %ID/g
0 %ID/g
+IgG (2A3)
+Ly6G (1A8)
H
K
B
C
# of Tumors per WT mouse
# of Tumors
Control
Treated
D -1
D 21
D
Tumor Burden in WT mice
Sum of tumor masses per mouse (mm3)
E
# of Tumors per COL mouse
p = 0.014*
F
Tumor Burden in COL mice
G
Mean %ID/g in WT tumors
Percent Injection Dose per Gram
H
Max %ID/g in WT tumors
I
Mean %ID/g in COL tumors
J
Max %ID/g in COL tumors

Figure 2.5 Neutrophil depletion with anti-Ly6G antibody reduces collagen-dense tumor formation as measured by ^{18}FDG-PET glucose uptake.

(**A**) Diagram of experimental time line showing timing of injections of 5.5μg/g of control IgG (2A3) or Ly6G (1A8) into the peritoneal cavity of WT and COL tumor mice (n = 5-6 for each group) at 9 weeks of age for 24 days. Yellow arrows indicate day of ^{18}FDG hybrid PET-CT imaging. Black arrows indicate day of treatment. Red arrows indicate day of blood collection. Green arrow indicates day of tissue collection (tumors, spleens, and lungs). (**B**) Detection of mammary tumors by ^{18}FDG-PET/CT. Coronal sections of co-registered ^{18}FDG-PET and CT images of WT and COL tumor mice before treatment at 9 weeks of age (Day -1) and after treatment at 12 weeks of age (Day 21). Regions of interest are drawn and colored at the mouse mammary glands with visible tumors. Physiologic tracer uptake in heart (H), kidneys (K), and bladder (B) is marked. Total number of tumors in (**C**) WT animals and (**E**) COL animals as determined by ^{18}FDG-PET at day -1 and day 21. Sum of the mass (mm^3) of all tumors per (**D**) WT and (**F**) COL mouse at day -1 and day 21 (n = 5 or 6, each data point equals one animal). Note that there is a trend toward decreased tumor burden in anti-Ly6G treated COL tumors ($p = 0.24$). (**G**) Mean glucose uptake (percent injection dose per gram, %ID/g) in WT and COL (**I**) tumors at day -1 and day 21. (**H**) Maximum glucose uptake (%ID/g) in WT and COL (**J**) tumors at day -1 and day 21 (n = 32 to 46, each data point equals one tumor).

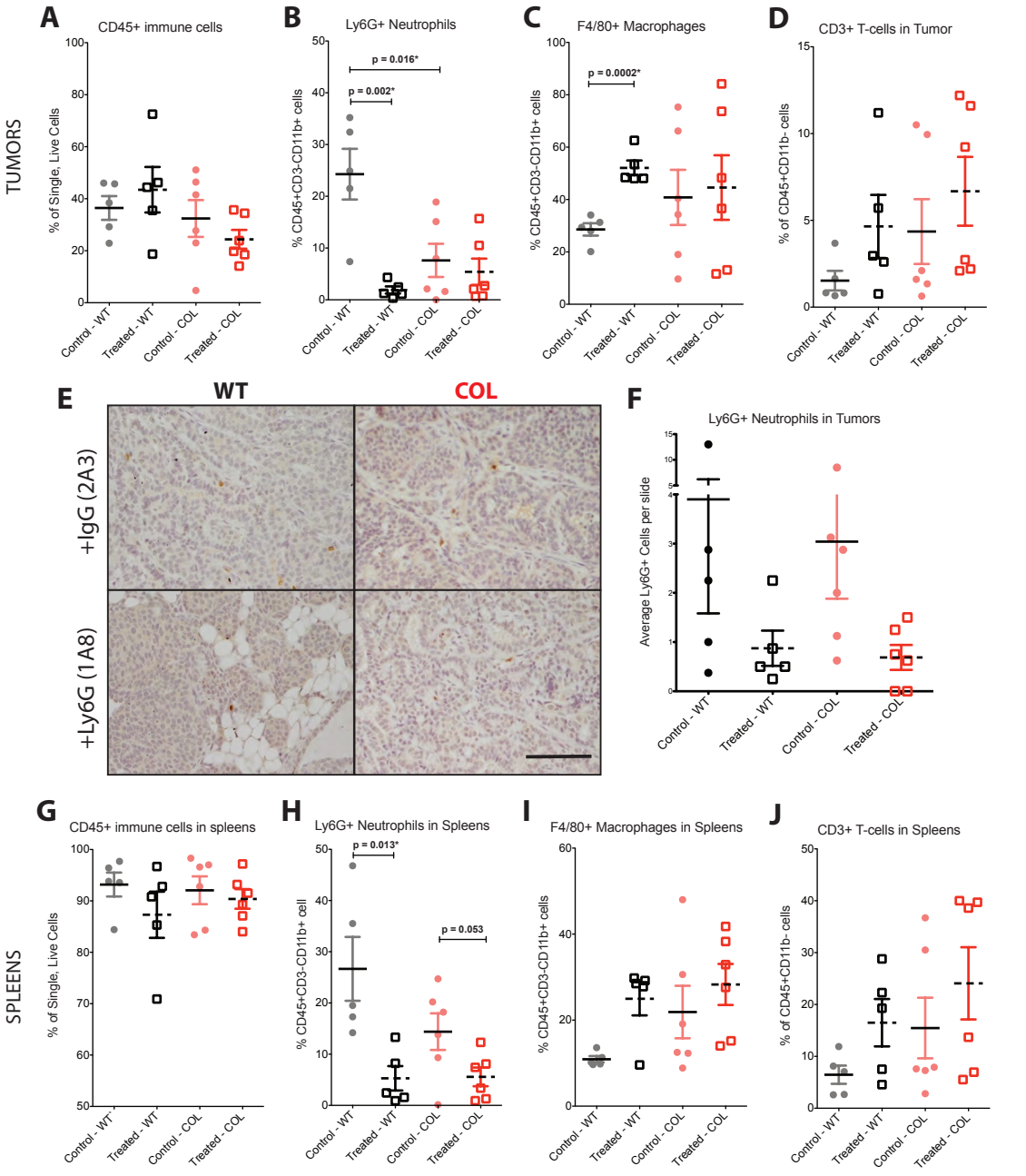
TUMORS
A
CD45+ immune cells
% of Single, Live Cells
B
Ly6G+ Neutrophils
% CD45+CD3-CD11b+ cells
p = 0.016*
p = 0.002*
C
F4/80+ Macrophages
% CD45+CD3-CD11b+ cells
p = 0.0002*
D
CD3+ T-cells in Tumor
% of CD45+CD11b- cells
Control - WT
Treated - WT
Control - COL
Treated - COL
E
WT
COL
+IgG (2A3)
+Ly6G (1A8)
F
Ly6G+ Neutrophils in Tumors
Average Ly6G+ Cells per slide
SPLEENS
G
CD45+ immune cells in spleens
% of Single, Live Cells
H
Ly6G+ Neutrophils in Spleens
% CD45+CD3-CD11b+ cell
p = 0.013*
p = 0.053
I
F4/80+ Macrophages in Spleens
% CD45+CD3-CD11b+ cells
J
CD3+ T-cells in Spleens
% of CD45+CD11b- cells

Figure 2.6 CD45+ immune cell recruitment to tumors and spleens treated with anti-Ly6G. Percentage of CD45+ immune cells (**A**), Ly6G+ neutrophils (**B**), F4/80+ macrophages (**C**), and CD3+ T-cells (**D**) in WT and COL mammary tumors from 12 week old mice treated with control IgG or Ly6G (n = 5-6) obtained by flow cytometry at day 24 of the treatment regimen (described in Figure 5A). Percentage of CD45+ immune cells (**E**), Ly6G+ neutrophils (**F**), F4/80+ macrophages (**G**), and CD3+ T-cells (**H**) in spleens of the same WT and COL animals treated and untreated shown in A-D.

A

	Control WT	Treated WT	Control COL	Treated COL
Mice with metastatic lesions	3/5	5/5	4/6	1/6

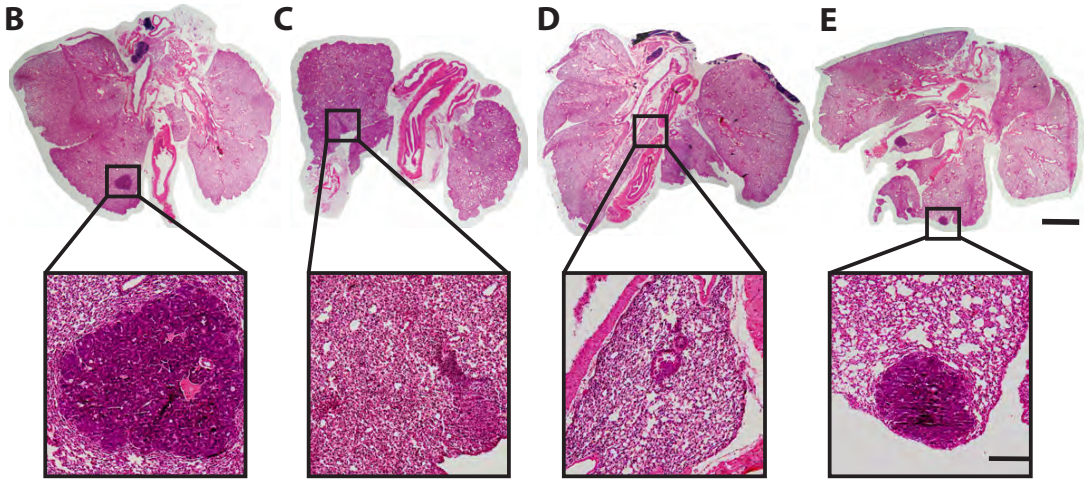

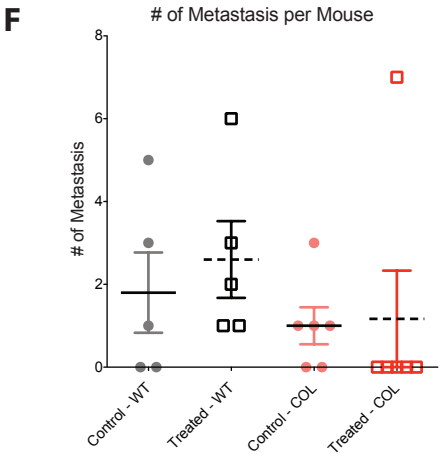

Figure 2.7 Neutrophil depletion with anti-Ly6G antibody reduces the number of dense-collagen metastatic lesions.

(**A**), table describing the number of mice with metastasis per group. Note that all treated WT tumor mice developed metastatic lesions versus one COL tumor mouse ($p < 0.05$). Representative images of lungs with corresponding metastasis in (**B**) WT control group, (**C**) WT anti-Ly6G treated group, (**D**) COL control group, and (**E**) COL anti-Ly6G treated group. Scale bar = 2 mm in whole lung image, and = 250 μm in metastatic lesion image. (**F**), Quantification of the number of metastatic lesions found in each mouse (n = 5-6 per group).

2 CHAPTER 3 – THE COLLAGEN-DENSE MICROENVIRONMENT REGULATES MACROPHAGE PROLIFERATION AND APOPTOSIS

2.1 Introduction

The tumor microenvironment is a diverse community where a complex interplay between the extra-cellular matrix (ECM) and cellular elements (tumor epithelial, endothelial, and inflammatory cells, fibroblasts, and adipocytes) drives tumor promotion, invasion and metastasis [119]. To better understand this interplay and progression, a more in-depth examination of the changes in this microenvironment is required, particularly in the context of increased mammographic density. This is an area of great interest and promise because changes in mammographic density have been associated with a four- to six-fold increased risk for developing breast cancer [120]. However, the cellular and molecular mechanisms responsible for this increased risk remain largely unknown. Several lines of evidence suggest a role for the ECM protein, fibrillar type I collagen. Previously, it has been shown to correlate to mammographic density [6]. In addition, mouse models with increased collagen deposition have a three-fold increase in tumor formation and lung metastases compared to controls[10].

While cancer progression has links to the structural nature of the ECM and the tumor microenvironment, it has also been associated with chronic inflammation by macrophages [18]. Of the many inflammatory cell types in the tumor microenvironment, tumor-associated macrophages (TAMs), have been shown to enhance tumor cell migration and invasion, stimulate angiogenesis, suppress antitumor immunity, and

enhance metastasis [31]. In addition, extensive TAM infiltration into patient breast tissue also correlates with poor prognosis [121]. Conversely, treatments to reduce inflammation show a reduction in breast cancer incidence [122]. Combined this evidence is suggestive of a potential link between the ECM microenvironment and the innate immunity of the body. Other examples of this interplay between the collagen ECM and macrophages exist under more normal developmental conditions, such as, the involuting mammary gland. The involuting microenvironment is characterized by increased collagen deposition, inflammation, and wound healing. Interestingly, the fibrillar type-I collagen found in the involuting mammary gland specifically attracts macrophages [13]. It remains unclear if the increased collagen deposition observed during tumorigenesis directly promotes the recruitment of TAMs, thus, further contributing to tumor progression.

To investigate these questions, this study relies on an *in vitro* 3D collagen matrix model. Previous work has demonstrated that mammary carcinoma cells cultured in stiff matrices (high collagen density) show a proliferative, invasive phenotype caused by increased focal adhesion kinase (FAK) and extracellular signal regulated kinase (ERK) activation, and Rho regulation [75]. Here, we aim to test the hypothesis that the collagen-dense microenvironment recruits and provides a favorable microenvironment for macrophages. This work identifies a trend towards increased amount of F4/80+ macrophages in collagen-dense tumors compared to wild-type tumors. It also finds that macrophage cell lines cultured in collagen-dense matrices exhibit less apoptotic signals and more proliferation compared to cells cultured in low collagen density matrices.

2.2 Methods

Mice

Mice were bred and maintained at the University of Madison – Wisconsin under the approval of the University of Wisconsin Animal Care and Use Committee. Transgenic male mice expressing the Polyoma Virus middle T antigen under the direction of the mammary mouse tumor virus promoter (MMTV-PyVT) in the FVB background (originated from The Jackson Laboratory, Bar Harbor, ME) were used as a model of breast cancer that develops spontaneous tumors and metastasizes to the lung [78]. These mice were crossed to female mice heterozygous for the $Col1a1^{tmJae}$ mutation in the C57BL/6/129 background (originated from The Jackson Laboratory, Bar Harbor, ME). The Co1A1 mutation renders the alpha 1 chain of collagen I uncleavable by collagenase and increases collagen in the tissue due to decreased remodeling [86]. The resulting mice were either positive for the PyVT-MMTV (tumor mice) or negative (normal mice), and they were either wild type for the Col1A1 mutation (WT) or heterozygous (COL). Genotyping by polymerase chain reaction (PCR) was performed on DNA extracted from tail biopsies.

Tissue collection and fluorescence:

Female mice were examined for palpable tumors starting at 8 weeks. At 15 weeks of age, matched sibling pairs of WT and COL tumors were anesthetized with 4% isofluorane. Mammary gland tumors were harvested and fixed in 10% buffered formalin (Thermo Fisher Scientific, Kalamazoo, MI) for 48 hours. These were then placed in 70%

ethanol and taken to the UWCCC Experimental Pathology Laboratory (EPL) for processing. Tissues were embedded in paraffin and sectioned by the EPL. COL and WT tumor sections were deparaffinized by heating at 60°C for 25 minutes. Then, they were placed in xylenes and rehydrated in gradual dilutions of ethanol. Antigen retrieval was done in citrate buffer pH 6.0 in a boiling water bath for 15 minutes. Sections were blocked with 5% normal serum and 1% BSA in TBS (blocking solution) for 1 hour. Sections were incubated with primary rat-anti-mouse F4/80 (1:1000, CI: A3-1 , Biolegend) for 2 hours, and with Alexa Fluor® 488 (1:1000) for 45 minutes. All incubations were done at room temperature. Tissues were counterstained with bisbenzamide at 1:15,000 for 5 minutes at room temperature. After washing, sections were dehydrated in gradual dilutions of ethanol and xylenes before mounting in Richard Allen Scientific mounting medium (Thermo Fisher).

Slides were imaged at the University of Wisconsin – Laboratory of Optical and Computational Imaging. These were imaged via second harmonic generation (SHG), a technique that employs multiphoton microscopy to allow visualization of non-centrosymmetric molecules independent of fluorescence. Acquisition was conducted on WiscSan software and a Nikon 20x Plan Apo VC (numerical aperture, N.A. 0.75 and working distance, W.D. 1.0) was used to visualize the collagen matrix.

Flow Cytometry:

Mammary gland tumors and spleens were harvested and placed in high glucose DMEM media (Gibco, Grand Island, NY) supplemented with 10% fetal bovine serum (FBS,

Gemini Bio Products, Baltimore, MD) and 1x antibiotic antimitotic solution (Corning, Corning, NY) for flow cytometry experiments. Tumors were weighed and approximately 150mg of tumor was used per mice per flow cytometry experiment. Single cells were obtained by cutting tumors and spleens into small pieces and digesting tumors with 0.028W/ml of Liberase TM Research Grade (Roche, Mannheim, Germany), 20μg/ml of DNase I, and 1x antibiotic antimitotic in DMEM with 10% FBS for 1 hour at 37°C with 250 RPM agitation. Digestion was facilitated by pipetting up and down every 15 minutes. The cell suspension was filtered through 70 and 40μm nylon cell strainer (BD Biosciences, Franklin Lakes, NJ). Red blood cells were lysed from tumor and spleen single cell suspensions with lysis buffer (Sigma, St. Louis, MO), and cells were resuspended in wash buffer (3% FBS in PBS, Gibco, Grand Island, NY). Cells were resuspended at 10^6 cells per 100μl of wash buffer. 10^6 cells were incubated with Alexa Fluor® 488-F4/80 (clone BM8, Invitrogen, Carlsbad, CA), PE-CD326 (Ep-CAM) (clone G8.8, BioLegend, San Diego, CA), APC-CD45 (clone 30-F11, Biolegend), PE-Cy™7-CD31 (clone 390), and DAPI (4',6-diamidino-2-phenylindole, Invitrogen) for 30 minutes at 4°C in the dark. After the final wash, all cells were resuspended in 500μl of wash buffer for analysis.

Samples were run on the LSRII (BD Biosciences) benchtop flow cytometer at the University of Wisconsin Carbone Cancer Center (UWCCC) Flow Cytometry Facility. The instrument was compensated using UltraComp eBeads (eBiosciences). For each tumor sample, 500,000 events were collected. Data was analyzed using FlowJo Single Cell Analysis Software (TreeStar, Ashland, OR).

Cell Lines:

Mouse macrophage cell lines J774A.1 (TIB-67™) and Raw 264.7 (TIB-71™) were obtained from American Type Culture Collection (ATCC). They were maintained in high glucose DMEM media supplemented with 10% Fetal Bovine Serum. These cells were cultured in non-tissue culture treated petri dishes to keep them in floating conditions. Cells were passaged every three days.

3D collagen gels:

Preparation of collagen gels has been previously described here [123]. Briefly, cells were cultured in low density (LD) or high density (HD) collagen gels. Low density gels were 2 mg/ml of rat collagen (BD Biosciences) neutralized with 100 mM HEPES (Sigma) solution and 2.5 x 10^4 cells/ml. The densities of the collagen were determined as described here [60]. For all experiments unless indicated, macrophage cell lines in collagen gels were cultured for seven days. Media was replenished on the third and sixth day of culture.

Western Blotting:

Western immunoblotting followed procedures explained here [123]. Macrophages in LD and HD gels were washed with PBS, and lysed in RIPA buffer using the mechanical force of a syringe and 18G needle. The collagen was pelleted and the supernatant collected. Supernatant was boiled in Laemmli buffer, and gel

electrophoresis was performed. SDS-PAGE gels were transferred to Immobilon protein membranes (Millipore, Bedford, MA). Membranes were incubated in 3% bovine serum albumin (BSA) plus 0.3% Tween-20 in tris-buffered saline (TBS, TBS-T) or 5% milk depending on instructions from antibody manufacturers. Antibodies used were anti-mouse: Caspase 3, Caspase 8 (clone D35G2), AKT, phosphorylated AKT (Thr308) (clone C31E5E), Bcl-xL, and phosphorylated Pyk2 (Tyr402) from Cell Signaling Technologies (Davers, MA), NFκB p65 RelA (clone C-20) and IκB-α (clone C-21) from Santa Cruz Biotechnology (Santa Cruz, CA), p190B (clone 54/P190-B, BD Biosciences), FAK (clone 4.47, Millipore), phosphorylated FAK (Tyr397) (44-624G, Life Technologies, Rockford, IL), ERK 1/2 and ACTIVE® MAPK (Promega, Madison, WI). Protein signals were visualized using chemiluminescence with Femto (Thermo Fisher, Waltham, MA) as the substrate, and imaged and quantified in Licor Odyssey FS (Licor, Lincoln, NE, USA). All protein signals were normalized to loading control, p190B, or in the case of phosphorylated or cleaved proteins, to total protein.

Immunofluorescence:

Immunofluorescence was performed as described here [123]. Macrophages were cultured in 3D LD and HD collagen gels at 2 x 10^3 cell/ml. After 7 days, gels were washed in PBS and fixed in 4% paraformaldehyde (PFA) (Sigma) and permeabilized in Triton-X (Sigma). Gels were blocked with 1% fatty acid-free BSA and 1% donkey serum (Jackson Laboratories, Bar Harbor, ME) in PBS overnight. Gels were stained with anti-mouse Ki67 (Abcam, Cambridge, MA) primary antibody, Alexa Fluor® 488 (Invitrogen)

secondary antibody, TRITC phalloidin to label F-actin (Sigma), and bis-benzimide to label nuclei (Sigma). Fluorescence microscopy was carried out using an Olympus Fluoview FV1000 confocal microscope (Olympus, Center Valley, PA) with a 60x/1.42NA oil immersion objective. FIJI ImageJ (FIJI Consortium, National Institutes of Health, Bethesda, MD) was used for linear adjustments of brightness and contrast. Eight fields of view per gel were taken and cells expressing Ki67 were counted as positive over the total number of cells with nuclei (positive for bisbenzimide). Data was displayed as the average of eight fields of view per experiment (n = 3).

For immunofluorescence of macrophages in 2D glass dishes, macrophages were cultured in glass bottom dishes (MatTek Corporation, Ashland, MA) for 24 hours. Cells were fixed, stained and imaged as previously explained. Gels were stained with anti-mouse CD29, integrin β1 (clone HM β1-1) primary antibody, Alexa Fluor® 488 (Invitrogen) secondary antibody, TRITC phalloidin to label F-actin (Sigma), and bis-benzimide to label nuclei (Sigma). Cells were imaged in the same way as 3D collagen gels.

Pharmacological inhibitor and antibody blocking studies:

Macrophages were cultured in 3D LD and HD collagen gels at 1.25 x 10^5 cells/ml for four days. Gels were treated with 1μM of MK-2206 dihydrochloride (Selleck Chemicals, Houston, TX) to block AKT activity. Control cells were treated with DMSO. Treatments occurred on the first and third day. On the fourth day, cells were lysed and western blotting was performed.

Integrin β1 activation was blocked by treatment with function blocking purified no azide/low endotoxin (NA/LE) anti-mouse CD29 (clone HM β1-1, BD Bioscience). One million cells were suspended in DMEM (Gibco) and incubated with 10 μg per ml of anti-CD29 and control purified no azide/low endotoxin (NA/LE) Hamster IgG2, λ1 isotype control (clone Ha4/8, BD Biosciences) for 30 minutes. Integrin signaling was stimulated with 100 μg per ml of collagen I (BD Biosciences) for one hour. Cells were lysed as explained above and western blotting was performed.

2.3 Results

F4/80 macrophages are part of the collagen-dense tumor microenvironment. We previously reported that mice with the PyVT transgene in a collagen-dense (COL) background have a higher tumor incidence and more metastases than mice with the PyVT transgene in a wild type (WT) background. In order to determine if this aggressive phenotype is associated with tumor-associated macrophages recruitment in the COL microenvironment, we isolated cells via flow cytometry from whole WT and COL late-stage tumors at 15 weeks. These cells were analyzed using CD45, pan-immune cell marker, and the F4/80 mature mouse macrophage marker. We did not observe a significant increase in the percentage of CD45+F4/80+ cells in COL tumors compared to WT tumors (Figure 1B and C). Next, we aimed to establish whether there were any differences in distribution or compartmentalization of macrophages within the WT and COL tumors. Imaging of formalin-fixed paraffin-embedded tumor sections stained by immunofluorescence showed that, in WT tumors, F4/80+ macrophages (*) are found within the expected tumor niche (dense area composed of tumor, vascular, immune,

and other components) and along blood vessels. In COL tumors, F4/80+ macrophages are more concentrated along the collagen-dense stromal compartment and along blood vessels (Figure 1A). Consistent with our flow cytometry data, the number of F4/80+ macrophages was similar in COL tumors compared to WT tumors. The data suggest collagen may not play a role in macrophage recruitment.

To garner a greater understanding of the interplay between the collagen-dense microenvironments and macrophages at the cellular level, we simplified the study model and cultured macrophage cell lines in collagen matrices of different densities. We used J774a.1 cells, which were isolated from murine reticulum cell sarcoma ascites [124], and Raw264.7 cells, which were isolated from ascites from murine tumors induced with Abelson leukemia virus[125]. The two macrophage-like cell lines have macrophage characteristics, such as activation when exposed to lipopolysaccharide (LPS), synthesis and secretion of lysozyme, and phagocytosis [124, 125]. For these reasons, they will be called macrophages for the purpose of this study.

Before using the *in vitro* 3D model of collagen density, we first wanted to validate whether these cells express integrins known to facilitate cellular interactions with the matrix. Fibrillar type I collagen-cell interactions are mostly mediated through $\alpha 2$ and $\beta 1$ integrins [126]. Immunofluorescence staining of $\beta 1$ integrin showed that macrophages actively express the machinery necessary to interact with collagen fibrils (Figure 2A). We then transitioned to the 3D collagen density model and validated that these cells can be easily cultured and imaged in 3D (Figure 2B and 2C).

Macrophages are versatile cells that can undergo changes in phenotype in response to their environment. The different responses to their physical environment are discussed by McWhorter et al. [127], but they do not explore biological processes such as cell survival and proliferation. In normal wound healing and inflammation, macrophages are recruited to the inflammatory site, they secrete inflammatory signals, a cascade of events activates other cells in the environment to heal the wound, and finally, anti-inflammatory signals would clear these macrophages from the tissue by egression or by apoptosis. In chronic inflammation and in the tumor microenvironment, resolution of inflammation does not occur, and accumulation of macrophages and the inflammatory milieu is promoted by the inhibition of apoptosis [128]. We investigated whether macrophages in the collagen-dense microenvironment evade apoptosis, and whether this microenvironment stimulates signals that lead to proliferation.

The collagen-tumor microenvironment is a permissive microenvironment for macrophages that inhibits apoptosis

Caspase 3 is a major downstream target of apoptotic initiation and is activated by proteolytic cleavage. The activated catalytic product then carries out the rest of the apoptotic process [129]. After 7 days in high-density (HD) collagen matrices, J774a.1 macrophages had lower levels of apoptosis. Western blots for caspase 3 in J774a.1 showed a cleavage band only in LD matrices and not in HD matrices (Figure 3A). The activation of caspase 3 in LD occurred in a timely manner starting at 48 hours for J774a.1 cells, observed again at 72 hours, and finally at 7 days (Figure 3C). Time point

analysis of upstream caspase 8 cleavage revealed only the p30 subunit, but not the active enzyme subunit p18, suggesting caspase 8 activation preceding caspase 3 activation is not a process that occurs in J774a.1 apoptosis in response to collagen.

Caspase 3 activation analysis in Raw264.7 macrophages, however, did not show a difference in the level of the cleaved catalytic band (Figure 3B) after 7 days in culture. The activation of caspase 3 in LD occurred starting at 72 hours (Figure 3C and 3D) until 5 days. This reveals a clear difference in the response to collagen matrices in Raw264.7 versus J774a.1 macrophages. Only Raw264.7 macrophages showed caspase 8 cleavage product, active catalytic subunit p18, when cultured in LD matrices (Figure 3C and 3D) suggesting Raw264.7 apoptosis is through the extrinsic (FAS/TNF-α) pathway; this is not seen in J774a.1.

Western blotting analysis was used to determine whether pro-survival signals are upregulated in HD matrices and whether they are responsible for the reduction of cell apoptosis in J774a.1 macrophages. NfκB and IκB protein levels showed no significant difference in expression in macrophages cultured in LD or HD matrices (Figure 4A). Pro-survival Bcl-2 family protein, Bcl-XL, was also not upregulated in macrophages cultured in HD matrices (Figure 4B). Analysis of cell survival related protein kinase B (PKB) or Akt also showed no statistically significant difference in AKT activation in J774a.1 macrophages cultured in LD versus HD matrices. There is however, a trend towards a reduction in AKT activation when macrophages are in HD matrices ($p = 0.06$). Hence, we further analyzed the role of AKT in J774a.1 macrophage survival by using allosteric AKT inhibitor, MK-2206. Blocking did not affect apoptosis, assayed by

cleavage of caspase 3. These results suggest that collagen-mediated survival in HD matrices does not involve changes in AKT activation.

The collagen-tumor microenvironment is a permissive microenvironment for macrophage cell line proliferation

Fibrillar type I collagen can signal to cells via integrins that activate focal adhesions and start downstream signaling cascades that can lead to cell proliferation [130]. Cell proliferation was studied using proliferation marker Ki-67. J774a.1 and Raw 264.7 macrophages were cultured in LD and HD collagen matrices for 7 days. Only Raw264.7 cells showed a trend of increased proliferation in HD matrices ($p = 0.06$) (Figure 5A and 5B). The mechanisms for this increase were analyzed by western blotting of protein tyrosine kinases known to be activated by collagen I signaling. These western blotting experiments were done after 2 hours of culture in 3D collagen matrices because these signals are known to occur rapidly. First, focal adhesion kinase (FAK) activation was analyzed by western blot and showed no difference in its phosphorylation in macrophages cultured in LD and HD matrices for 2 hours (Figure 6A). We proceeded to investigate proline-rich tyrosine kinase 2 (Pyk2), which is a FAK related kinase that is restrictively expressed in hematopoietic cells, hence, it could be activated downstream integrin signals in Raw264.7 macrophages. Pyk2 activation was not different in macrophages cultured in LD compared to HD matrices for 2 hours (Figure 6B). Finally, downstream of both FAK and PyK2, extracellular signal-regulated kinase (ERK) is activated and can stimulate the transcription of genes important in the cell cycle [131]

ERK activation was not altered in macrophages cultured in LD compared to HD collagen matrices for 2 hours (Figure 6C).

Since β1 integrin is responsible for adherence to fibrillar collagen I in most cells and transducers of physical signals from the ECM to the cell, the role of this integrin in downstream ERK phosphorylation was examined in Raw264.7 macrophages. Macrophages were cultured with blocking antibodies to β1 integrin and allowed to interact with 100 μg/ml of collagen 1. ERK was activated in a similar way in both the IgG control and anti-β1 treatment groups. These results suggest that activation of FAK/PyK2 and downstream ERK signals are not regulated by β1 integrin or by collagen density in macrophage cell lines. The mechanisms that lead to increased proliferation in Raw264.7 macrophages are still unclear.

2.4 Discussion

The collagen-dense (COL) mouse mammary tumor model (Col1A1-PyVT) provides a good model to investigate how increased stromal collagen enhances tumor progression. The mice in this model have a higher tumor incidence and more metastases than wild type PyVT mice [10]. In addition, the tumor cells in this model display increased migration and proliferation, as well as changes in the collagen organization during disease progression *in vivo* [132]. Moreover, the characterized phenotypic and genotypic changes in mammary epithelial cells cultured in increased collagen density show consistent invasive phenotypes with increased FAK, Rho, ERK signaling, and expression of proliferation signature-genes *in vitro* [75]. Now, we seek to extend our understanding of these mechanisms by studying another potentially significant

component of the collagen-dense tumor microenvironment: the innate immune system and inflammation. Macrophages have already been largely implicated in tumor progression [95], and here we use the COL mouse model and *in vitro* assays to quantify and understand how macrophages respond to the collagen-rich tumor microenvironment.

Our results showed that the collagen-dense tumor microenvironment recruits F4/80+ macrophages *in vivo* at similar amounts as the WT tumor microenvironment. Although the data quantifying the number of macrophages in the tumors were variable and not statistically significant, the location of macrophages in the collagen-dense microenvironment suggested this environment is inherently different from normal microenvironments; not only in the ECM components (collagen I), but also in the inflammatory cell components (macrophages). It is important to note that most macrophage studies reported *in vitro* depend on macrophage activation/differentiation in response to lipopolysaccharide (LPS), tumor necrosis factor α (TNF-α) or with phorbol myristate acetate (PMA). We aimed to isolate the sole effects of collagen I on these macrophages. Hence, J774a.1 and Raw264.7 macrophages were cultured in collagen matrices with low collagen density (LD) and high collagen density (HD). Our results suggested fibrillar collagen alone could produce quantifiable effects on macrophage cell death and proliferation. We found that both cell types respond differently when cultured in HD collagen matrices: J774a.1 cells were resistant to apoptosis, while Raw264.7 cells were more proliferative.

We began to investigate macrophage apoptosis by analyzing caspase protein expression, which is essential for apoptosis. Caspase 3 is an obvious candidate as when it has been activated or cleaved, the catalytic products are in charge of cleaving most apoptotic substrates. This is the point where the cell is committed to undergo apoptosis [133]. In HD, J774a.1 macrophages failed to activate effector caspase 3, while the catalytic subunit is clearly present in LD matrices. Time course experiments show the absence of cleaved caspase 3 starting at 48 hours and even after 7 days in culture. The other cell line studied in this project, Raw264.7 macrophages, were cultured in HD matrices and also avoided apoptotic signaling via cleavage of caspase 3, but this occurred after 72 hours and only until 5 days in culture in comparison to J774a.1. Time course experiments also suggested that activation or cleavage of upstream initiator, caspase 8, occurs prior to caspase 3 activation, which is part of the extrinsic caspase activation pathway (Figure 7). The extrinsic pathway involves binding of extracellular ligands, such as TNF-α or Fas ligand (FasL), to death receptors on the cell membrane. Then, a complex of adaptor proteins and several caspase 8 molecules are recruited and aggregate, promoting caspase 8 activation [134]. Cleavage of caspase 8 into active catalytic subunit p18 was not observed in J774a.1 macrophages, suggesting a different mechanism for both cell types. The intrinsic pathway that involves the release of cytochrome c is a good candidate to study in macrophages cultured in collagen matrices.

Macrophage fate in inflammation is determined by a balanced network of cell death and cell survival proteins. One of the signaling pathways involved in cell death and survival is nuclear factor κB (NFκB) signaling, which also has a central role in

inflammatory reactions [128]. Upon activation, phosphorylation events in the canonical NFκB module lead to proteolytic degradation of inhibitor IκB. The nuclear factor, RelA (p65), then forms a heterodimer with p50 and translocates to the nucleus where it can stimulate transcription of anti-apoptotic target genes [131]. Western blots comparing HD to LD revealed no difference between RelA p65, p50, or IκB protein levels. As there were no differences in proteins levels, we will seek to investigate whether the levels of activation change in response to matrix density by performing more sophisticated experiments, such as electrophoretic mobility shift assays (EMSA), to rule out collagen density regulation of NFκB/DNA binding activity.

Another player involved in cell death are the BCL-2 family proteins. The anti-apoptotic B-cell lymphoma 2 (BCL-2) family protein, Bcl-xL, prevents the oligomerization of pro-apoptotic BAK and/or BAX in the outer membrane of the mitochondria, which leads to the release of cytochrome c into the cytoplasm. These are part of the intrinsic apoptosis pathway [134]. Bcl-xL protein expression analysis in macrophages cultured in HD matrices showed no difference when compared to LD matrices. Another BCL-2-family protein is BAD (BCL-2 antagonist of cell death). This protein is regulated by an important player in cell survival, protein kinase B (PKB), or AKT. AKT is activated by phosphoinositide 3-kinase, PI3K, which phosphorylates AKT at Thr 308. During survival signaling, activated AKT inactivates BAD by phosphorylation, and leads to its sequestration by 14-3-3 proteins [134]. We analyzed AKT activation and observed a trend towards decreased AKT phosphorylation at Thr308 in J774a.1 macrophages cultured in HD. These results suggested that macrophages in the process of undergoing

apoptosis in LD matrices exhibit a compensatory activation of the AKT survival pathway. Further analysis by treatment with allosteric AKT inhibitor, MK2206, showed no difference in cleaved caspase 3 in treated compared to untreated cells suggesting AKT may not contribute to macrophage cell death. Studies of J774a.1 macrophage necroptotic cell death (programed form of necrosis induced by inhibition of caspase 8) demonstrates an increase in AKT Thr308 phosphorylation in necroptotic macrophages, but also showed that inhibition of AKT did not protect the cells from death [135]. It is still unknown whether macrophages forgo apoptosis and undergo necrosis in HD matrices. Additional experiments are required to dissect the specific mechanisms driving J774a.1 apoptotic signals and balancing survival signals in HD collagen matrices.

The second cell process we investigated was cell proliferation in collagen matrices. Upregulation of cell proliferation was previously shown in NMuMG mouse mammary cells cultured in HD matrices, which involves collagen mechano-signaling via integrins that activate focal adhesion kinase (FAK) and downstream signaling to mitogen-activated protein kinase, MAPK/ERK, leading to transcription of cell cycle and proliferation genes [75]. In our studies, Raw264.7 macrophages cultured in HD matrices showed a proliferative phenotype, with a trend towards increased Ki67 staining after 7 days in culture. Ki67 staining is a clinically relevant proliferation signature that predicts patient outcome [75]. We then explored the mechanisms of this observation by analyzing FAK-ERK activation. Unexpectedly, in Raw264.7 macrophages, the activation of FAK and ERK signaling was not increased in HD matrices after two hours. FAK is activated upon cell adhesion to ECM proteins and growth factors [136], but in

hematopoietic cells, proline-rich tyrosine kinase 2 (PyK2) is highly expressed and activated by β2 integrin [137]. As an alternative, we analyzed PyK2 activation by phosphorylation and found no significant difference in Pyk2 activation in cells cultured in LD compared to HD matrices for 2 hours. Other studies barely detect Pyk2 phosphorylation by collagen I, and indicate the process is very fast starting at 1 minute and plateau starting at 20 minutes [137]. Cell adhesion, which facilitates transduction of signals from the ECM to the cell, to fibrillar collagen I is thought to be mediated by β1 and β2 integrins in macrophages [127]. Raw264.7 macrophages, though, poorly adhere to fibrillar collagen, but mainly adhere to denatured collagen I [138]. We also investigated whether activation of ERK pathways in collagen matrices is mediated by adhesion to β1 integrin. Blocking the function of β1 with an antibody did not reduce ERK activation suggesting that other macrophage receptors are responsible for adhesion to collagen I and transduction of matrix signals that lead to ERK activation. Another collagen receptor, discoidin domain receptor 1 (DDR1), is expressed by macrophages (J774a.1 was reported) and has been shown to activate ERK, NFκB, p38, and c-Jun N-terminal kinase (JNK) [139]. In addition, a study by Gowen, et al., showed that adhesion to denatured collagen I in Raw264.7 macrophages was modulated by class A macrophage scavenger receptor (SR-A) [138].

Although most of the previous studies discussed above stimulate macrophages with very small amounts of collagen I (nano versus micro grams), they suggest other receptors and pathways may be regulated by culturing macrophages in low and high density collagen. In the current study, we found that macrophage cell lines, without any

added chemical stimuli, respond to collagen I at high density by evading apoptosis and increasing proliferation. The diagram in Figure 7 shows the signaling pathways that lead to and regulate cell survival, apoptosis, and proliferation, which were partly explored by culturing macrophage cell lines in collagen matrices. We report that in high-density collagen matrices, J774a.1 macrophages evade cleavage of caspase 3, and this does not involve Bcl-xL anti-apoptotic regulation nor AKT survival signal activation. Raw 264.7 macrophages are more proliferative in high-density matrices, and this process does not involve signaling via β1-integrin-FAK/Pyk2-ERK kinases.

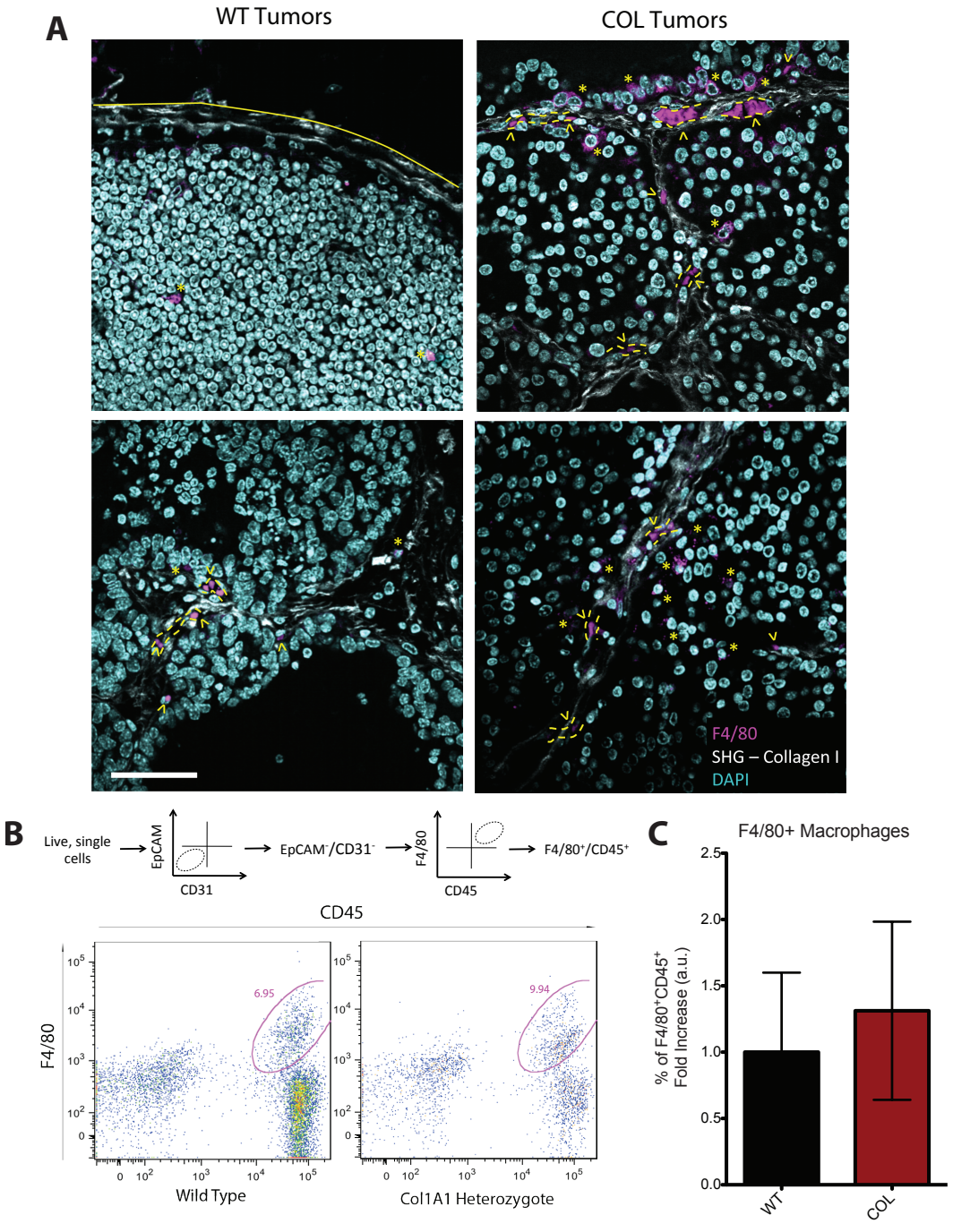
A
WT Tumors
COL Tumors
F4/80
SHG – Collagen I
DAPI
B
Live, single cells
EpCAM
CD31
EpCAM⁻/CD31⁻
F4/80
CD45
F4/80⁺/CD45⁺
CD45
F4/80
6.95
9.94
Wild Type
Col1A1 Heterozygote
C
F4/80+ Macrophages
% of F4/80⁺CD45⁺ Fold Increase (a.u.)
2.5
2.0
1.5
1.0
0.5
0.0
WT
COL

Figure 3-1 F4/80+ macrophages in collagen-dense mammary tumors.

(**A**) Immunofluorescence of formalin-fixed paraffin-embedded tumor sections from WT and COL mouse mammary tumors at 15 weeks of age. Macrophages were stained with F4/80+ (magenta), nuclei was stained with bisbenzimide (cyan), fibrillar collagen was imaged by second harmonic generation (SHG, white), scale bar = 50 μm. The tumor boundary was denoted by a solid line —, blood vessels by dashed line ---, F4/80+ macrophages by *, and autofluorescent red blood cells by ^. (**B**), flow cytometry gates used to determine CD45+F4/80+ macrophages. (**C**), percentage of CD45+F4/80+ immune cells in WT versus COL mammary tumors at 15 weeks displayed as a fold increased (n=4, each n is an independent pair of age-matched littermate WT and COL mice).

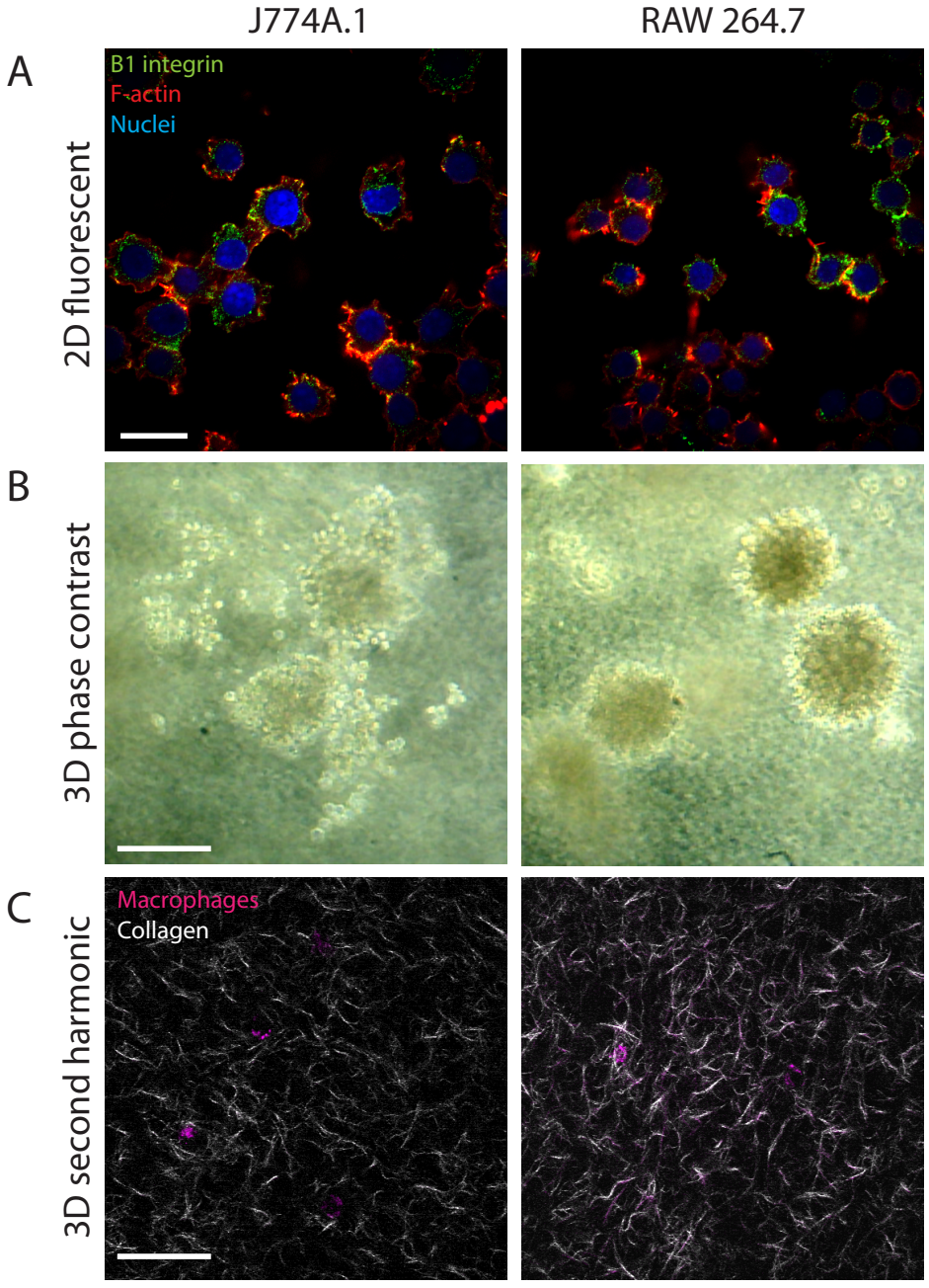
J774A.1
RAW 264.7
A
2D fluorescent
B1 integrin
F-actin
Nuclei
B
3D phase contrast
C
3D second harmonic
Macrophages
Collagen

Figure 3-2 Macrophage-like cell lines are easily cultured in 3D collagen matrices.

(**A**) J774a.1 and Raw264.7 cultured in 2D glass dishes for 2 hours were stained with β1 integrin (green), which mediates adhesion to collagen 1, phalloidin (red), which labels F-actin, and bisnezimide (blue), which labels the nuclei. Scale bar = 25μm (**B**) Phase-contrast image of macrophages in 3D collagen matrices cultured for 7 days. Scale bar = 100μm. (**C**) Second harmonic images of macrophage cell lines cultured in 3D collagen matrices for 2 hours. Cell endogenous fluorescence (autofluorescence) is in magenta, and fibrillar collagen I in white. Scale = 50 μm.

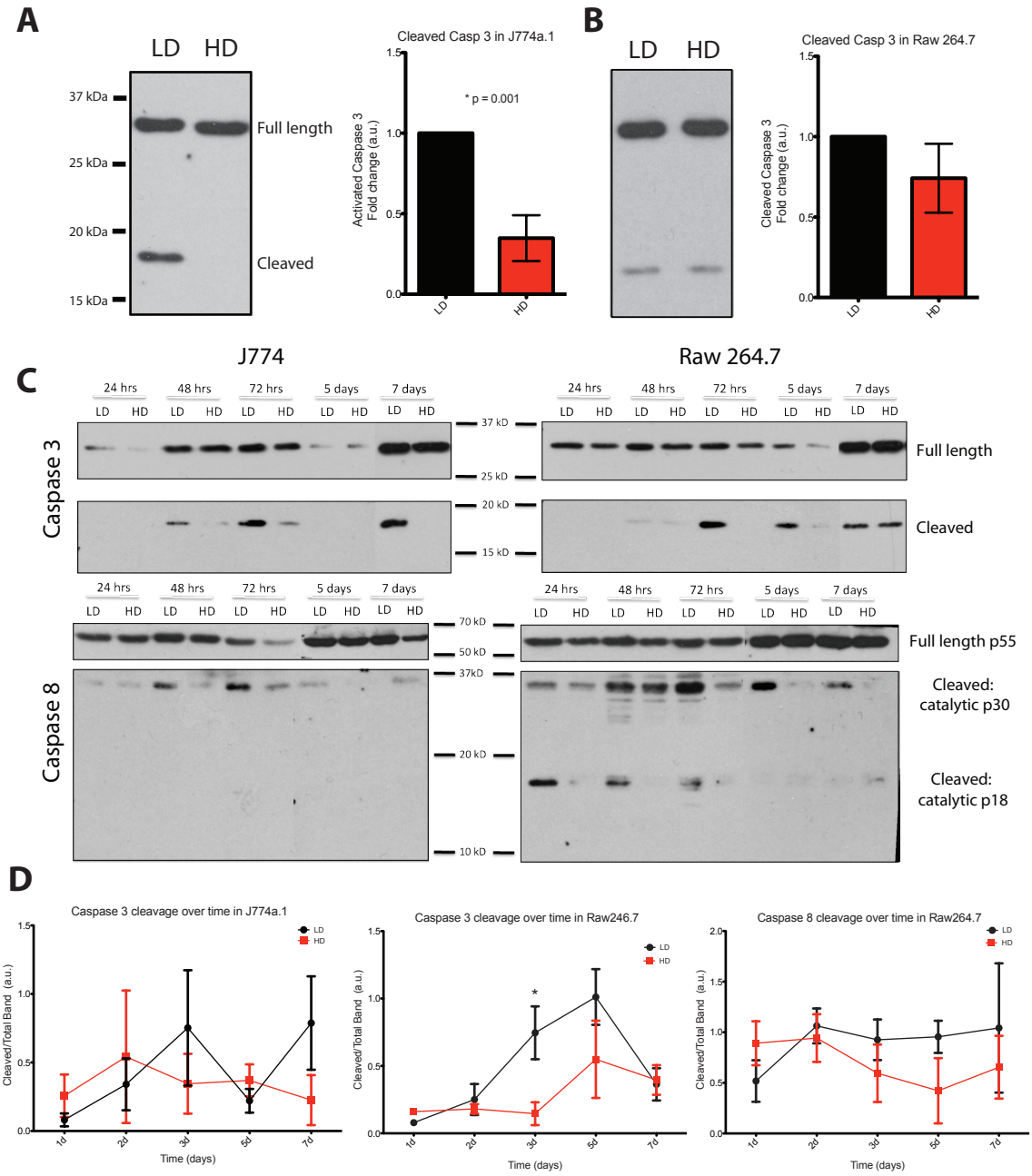
A
LD HD
37 kDa
25 kDa
20 kDa
15 kDa
Full length
Cleaved
Cleaved Casp 3 in J774a.1
* p = 0.001
Activated Caspase 3
Fold change (a.u.)
B
LD HD
Cleaved Casp 3 in Raw 264.7
Cleaved Caspase 3
Fold change (a.u.)
C
J774
Raw 264.7
24 hrs
48 hrs
72 hrs
5 days
7 days
LD HD
Caspase 3
37 kD
25 kD
20 kD
15 kD
Full length
Cleaved
Caspase 8
70 kD
50 kD
37kD
20 kD
10 kD
Full length p55
Cleaved:
catalytic p30
Cleaved:
catalytic p18
D
Caspase 3 cleavage over time in J774a.1
Caspase 3 cleavage over time in Raw246.7
Caspase 8 cleavage over time in Raw264.7
Cleaved/Total Band (a.u.)
Time (days)
1d
2d
3d
5d
7d

Figure 3-3 Macrophages resist apoptosis when cultured in collagen-dense matrices.

Quantitative western blotting analysis of Caspase 3 and its activated cleavage product (p17) in J774a.1 (**A**) and Raw 264.7 (**B**) macrophage cell lines cultures in low-density collagen matrices (LD) or in high-density collagen matrices (HD) for 7 days. 40 μg of protein were loaded in each gel. Cleaved caspase 3 bands were normalized to full-length bands and displayed as fold changes from expression in LD (n = 3). (**C**, **D**), Quantitative western blot analysis of Caspase 3 and its cleavage product, and upstream effector Caspase 8 and its activated cleavage products (p30 and p18) at different time-points: 24 hours, 48 hours, 72 hours, 5 days, and 7 days (n = 3).

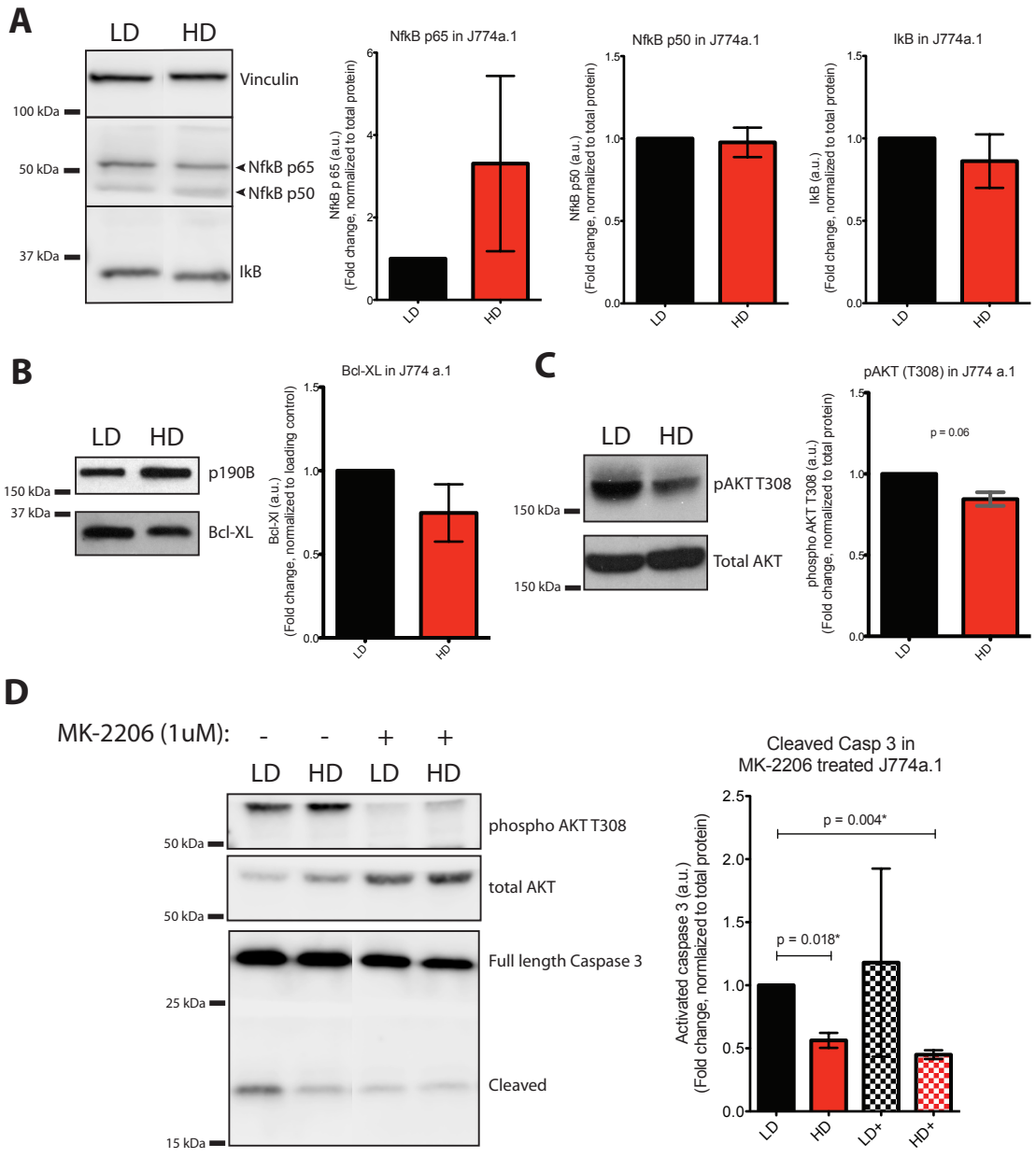
A
LD
HD
Vinculin
100 kDa
50 kDa
NfkB p65
NfkB p50
37 kDa
IkB
NfkB p65 in J774a.1
NfkB p 65 (a.u.)
(Fold change, normalized to total protein)
NfkB p50 in J774a.1
NfkB p50 (a.u.)
(Fold change, normalized to total protein)
IkB in J774a.1
IkB (a.u.)
(Fold change, normalized to total protein)
B
LD
HD
150 kDa
37 kDa
p190B
Bcl-XL
Bcl-Xl in J774 a.1
Bcl-Xl (a.u.)
(Fold change, normalized to loading control)
C
LD
HD
150 kDa
150 kDa
pAKT T308
Total AKT
pAKT (T308) in J774 a.1
phospho AKT T308 (a.u.)
(Fold change, normalized to total protein)
p = 0.06
D
MK-2206 (1uM): - - + +
LD
HD
LD
HD
50 kDa
50 kDa
25 kDa
15 kDa
phospho AKT T308
total AKT
Full length Caspase 3
Cleaved
Cleaved Casp 3 in
MK-2206 treated J774a.1
Activated caspase 3 (a.u.)
(Fold change, normalized to total protein)
p = 0.004*
p = 0.018*
LD
HD
LD+
HD+

Figure 3.4 Protein analysis of pro-survival pathways in J774a.1 macrophages.

(**A**), Quantitative western blotting of NfκB and IκB expressed in J774a.1 cultured in LD and HD collagen matrices for 4 days. Vinculin was used as a loading control. Bands were normalized to loading control and displayed as a fold changes from expression in LD (n = 3). (**B**), Quantitative western blotting of pro-survival protein, Bcl-xl, in J774a.1 cultured in LD and HD collagen matrices for 4 days. P190B RhoGAP was used as a loading control. Bands were normalized to loading control and displayed as a fold change from expression in LD (n = 3). (**C**), Quantitative western blotting of pro-survival signal phosphorylated AKT (Thr308), in J774a.1 cultured in LD and HD collagen matrices for 4 days. Bands were normalized to total AKT protein and displayed as fold changes from expression in LD (n = 3). (**D**), Analysis of AKT involvement in activation of downstream effector, caspase 3. Quantitative western blotting of J774a.1 cultured in LD and HD collagen matrices were treated with AKT inhibitor, MK2206 (1μM), for 4 days. Cleaved caspase 3 bands were normalized to full-length bands and displayed as fold changes from expression in LD (n = 3).

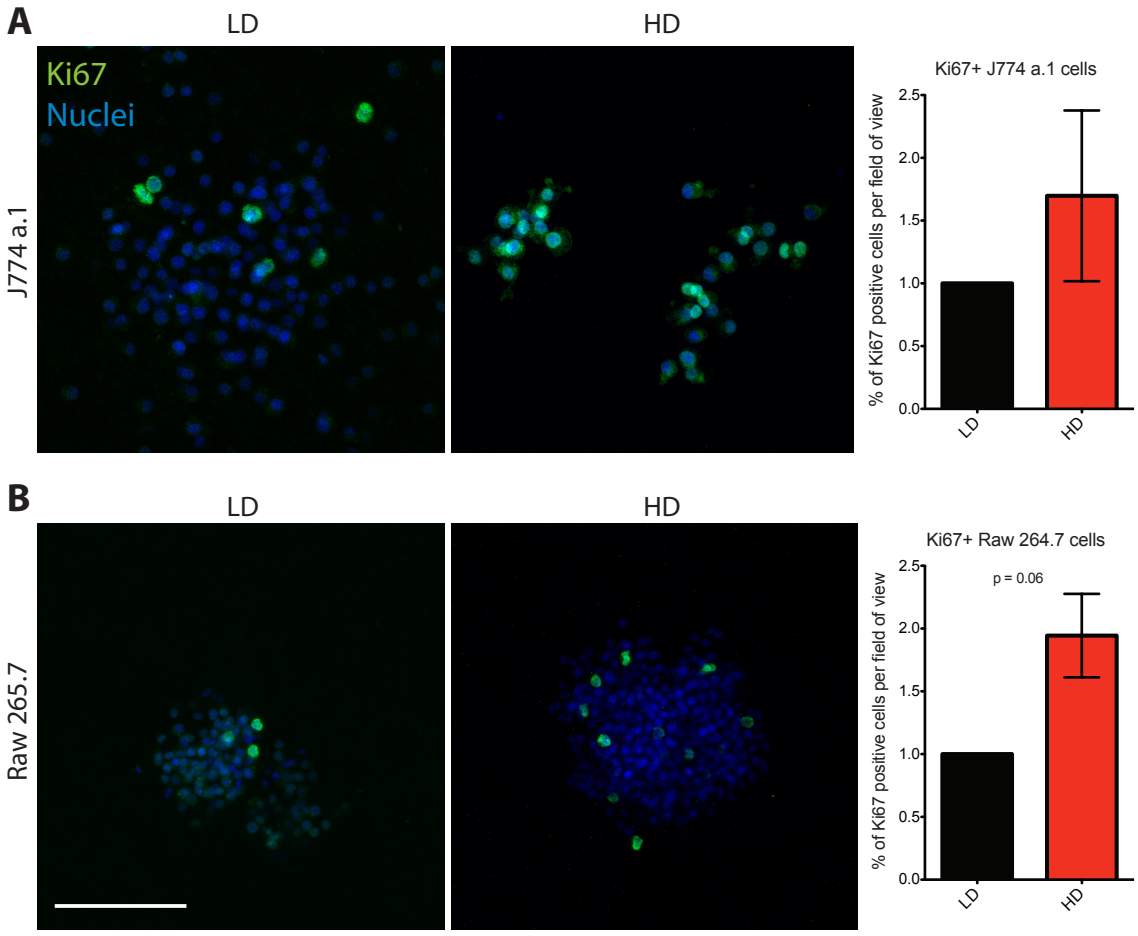

Figure 3.5 Collagen-dense matrices (HD) induce proliferation of macrophages

Immunofluorescence of J774a.1 (**A**) and Raw264.7 (**B**) macrophages cultured in LD and HD. Cells were stained with proliferation marker, Ki67 (green), and nuclei was stained with bisbenzimide. The number of Ki67 positive cells were counted and normalized to the total number of cells in images from 8 fields of view per experiment (n = 3), scale = 50 μm.

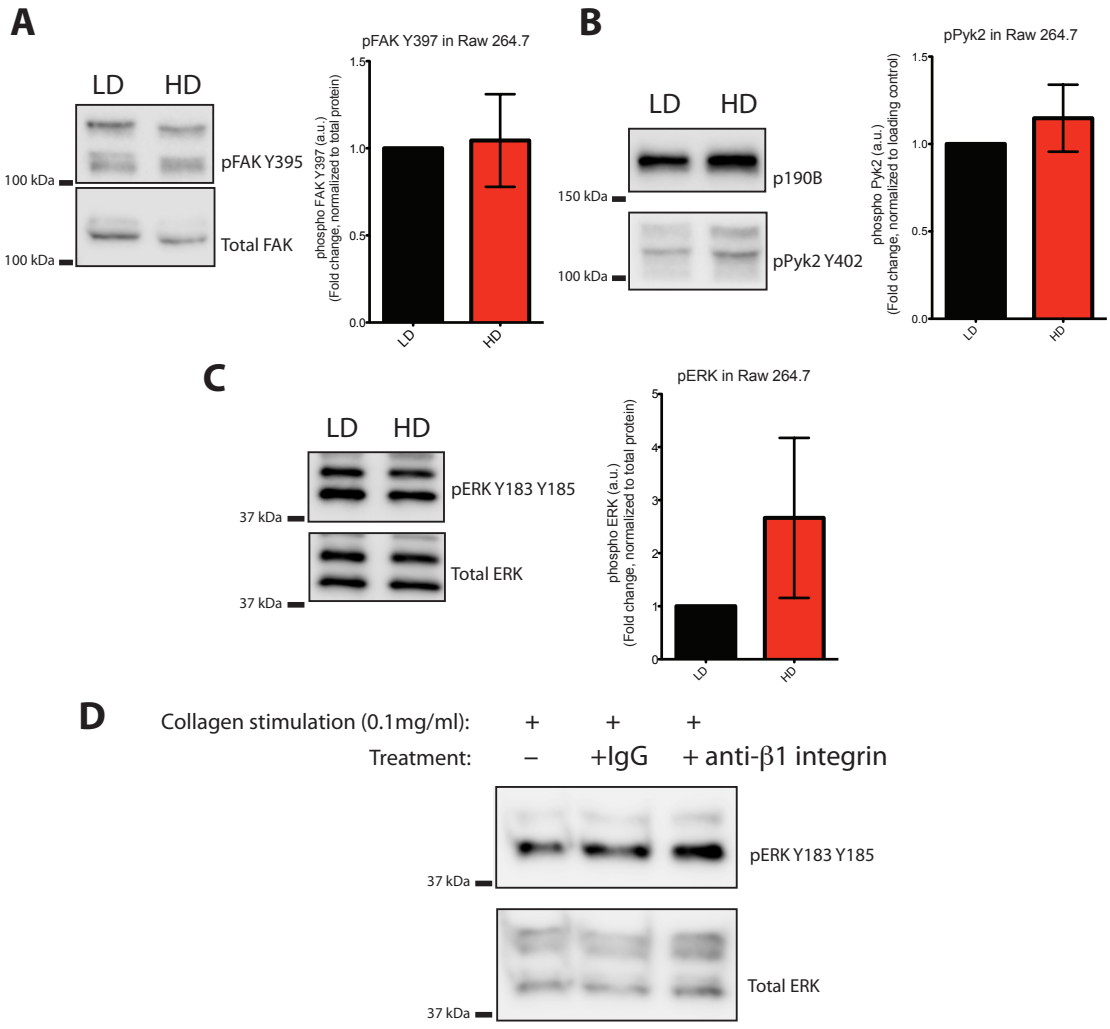
A
LD
HD
100 kDa
pFAK Y395
100 kDa
Total FAK
pFAK Y397 in Raw 264.7
phospho FAK Y397 (a.u.)
(Fold change, normalized to total protein)
1.5
1.0
0.5
0.0
LD
HD
B
LD
HD
150 kDa
p190B
100 kDa
pPyk2 Y402
pPyk2 in Raw 264.7
phospho Pyk2 (a.u.)
(Fold change, normalized to loading control)
1.5
1.0
0.5
0.0
LD
HD
C
LD
HD
37 kDa
pERK Y183 Y185
37 kDa
Total ERK
pERK in Raw 264.7
phospho ERK (a.u.)
(Fold change, normalized to total protein)
5
4
3
2
1
0
LD
HD
D
Collagen stimulation (0.1mg/ml): + + +
Treatment: – +IgG + anti-β1 integrin
37 kDa
pERK Y183 Y185
37 kDa
Total ERK

Figure 3-6 Increase in macrophage proliferation is not due to increased β-1 integrin signaling. (**A**), Quantitative western blotting of activated FAK (Tyr 395) expressed in Raw 264.7 cultured in LD and HD collagen matrices. Bands were normalized to total FAK protein expression and displayed as a fold changes from expression in LD (n = 3). (**B**), Quantitative western blotting of activated Pyk2 (Tyr 402) expressed in Raw 264.7 cultured in LD and HD collagen matrices. P190B RhoGAP was used as a loading control. Bands were normalized to loading control and displayed as a fold change from expression in LD (n = 3). (**C**), Quantitative western blotting of activated ERK (Tyr 183 and 185) in Raw264.7 cultured in LD and HD collagen matrices. Bands were normalized to total ERK protein and displayed as fold changes from expression in LD (n = 3). (**D**), Function blocking antibody against β1 integrin was used to block integrin activation by collagen 1 (0.1 mg/ml). Activation was assayed by western blotting of downstream effector ERK (n = 3).

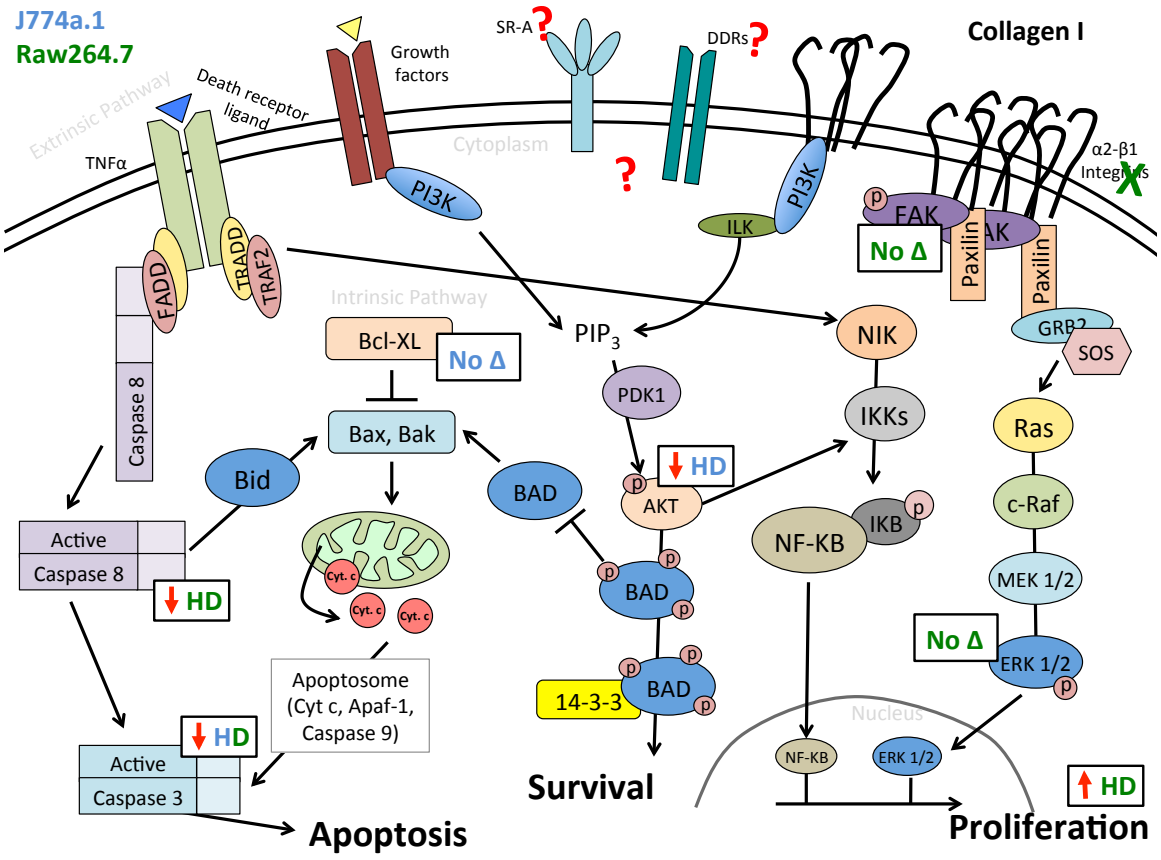

Figure 3-7 . Diagram of pathways involved in macrophage cell line signaling in collagen-dense matrices.

Signals observed in J774a.1 macrophages are in blue and signals observed in Raw264.7 macrophages are in green. Arrow pointing upwards = upregulated in HD. Arrow pointing downwards = downregulated in HD. No Δ = no change.

CONCLUSIONS AND FUTURE DIRECTIONS

The main goal of this thesis project was to determine if the collagen-dense tumor microenvironment induces an altered inflammatory response, which recruits and further stimulates tumor-associated neutrophils (TANs) and tumor-associated macrophages (TAMs) to promote mammary tumors and metastasis. This is important because it can further our understanding of the cellular and molecular mechanisms involved with the increased risk of breast cancer in women with high mammographic density, which is correlated with increased collagen deposition.

The data presented in Chapter 2 describe the role of TANs in collagen-dense mammary tumors. We find that mammary tumors arising in the collagen-dense microenvironment have altered cytokine and growth factor signaling compared to tumors arising in a non-dense microenvironment. The cytokines altered in dense-collagen tumors include GM-CSF, PGDF-BB, and IL-1; these are involved in neutrophil maturation and recruitment.

Of the cytokines upregulated in collagen-dense tumors, PDGF-BB was expressed at the highest level. Several studies have shown that this cytokine is secreted by tumor cells and stromal cells, while fibroblast in particular, express the PDGF receptor [103]. The paracrine interactions between tumors cells and myofibroblasts involve PDGF signaling and lead to desmoplasia in breast cancer [104]. It will be beneficial to investigate other stromal cells, such as carcinoma-associated fibroblasts (CAFs), and how they may be activated in the collagen-dense tumor microenvironment. CAFs have also been implicated in tumor inflammation in breast and ovarian cancer via secretion

of inflammatory cytokines (IL-6, COX-2 and CXCL1) [140, 141]. Future experiments are needed to determine whether the collagen-dense tumor microenvironment stimulates CAF secretion of inflammatory cytokines. With this knowledge, the connections between collagen density, inflammation, myeloid cell activation, and fibroblast activation in breast cancer can be used to better identify or improve therapeutic targets.

The most important finding of this project is that collagen-dense tumors have the ability to functionally alter neutrophil recruitment and activation. We observed this by blocking Ly6G+ neutrophil recruitment into mammary tumors. Although blocking Ly6G+ neutrophils diminished tumor formation, and tumor burden, the mechanisms for the reduction in tumor progression are still unclear. Neutrophils can be alternatively activated to promote tumors. This is most likely the case for neutrophils found in the collagen-dense mammary tumor microenvironment. It would be, then, appropriate to look for markers of tumor-promoting neutrophils such as MMP-9, NE, CXCR4, VEGF and arginase [50] in collagen-dense tumors. These experiments may be better performed *in vivo*, since neutrophils are short lived, but they could be transferred to the 3D collagen matrix density model as a start.

In addition to blocking tumor progression, blocking TANs decreased lung metastasis, specifically in collagen-dense mammary tumors. We are interested in the collagen-dense metastatic niche as well. Blocking of neutrophils was systemic as was the collagen mutation in the COL mouse model. Hence, the lungs also show changes in the amounts of collagen present. Although neutrophil numbers in the metastatic lungs did not correlate to number of metastasis found, it will be necessary to investigate the

immune cell recruitment, as well as the cytokine crosstalk in the lungs, and how these are affected by the collagen-dense microenvironment.

An interesting finding of the blocking studies came from blocking Ly6G+ neutrophils in wild type tumors, which increased the recruitment of macrophages in the primary mammary tumors. Tumors in treated WT mice did not have delayed development and metastasized. This brings up the question: in the absence of neutrophils, do macrophages become more involved in tumor progression and metastasis? If so, there is another interesting area of study: tumor-associated macrophages. Macrophages can also be polarized into pro-tumor macrophages, and now in the absence of neutrophils, they are the first responders to the cytokines secreted by tumor cells. The functional role of tumor-associated macrophages in collagen-dense tumors has not yet been determined.

Chapter 3 describes our efforts in understanding if collagen-dense microenvironments have a functional effect on macrophage biology. We utilize macrophage cell lines and observed a change in apoptosis and in proliferation in response to altered collagen matrix density. J774a.2 macrophages in high-density (HD) matrices showed a decrease in apoptotic signal by caspase 3 cleavage. Several pathways, including PI3-K/AKT, were assessed to determine the mechanisms for decreased apoptosis in high-density matrices, however these pathways do not appear to play a role. We would like to explore the possibility that macrophages cultured in HD matrices induce caspase-independent necroptosis or necrosis. The other cell line studied, Raw264.7 macrophages, in HD matrices showed a decrease in caspase 8 cleavage

followed by a decrease in caspase 3 cleavage, which suggests that Raw264.7 cells follow the TNFα/FasL pathway of apoptotic signaling in low-density (LD) matrices. Future experiments are planned using pharmacological inhibitors to block TNFα/FasL receptors to determine if this is the mechanism used by Raw264.7 macrophages. In addition, analyzing macrophage secreted factors in 3D collagen matrices, such as TNFα, FasL, and cleaved caspases, will determine if these cytokines are involved in density-induced apoptotic signaling, or breast cancer-induced inflammation and tumor progression.

Furthermore, we investigated how Raw264.7 macrophages express increased amounts of proliferation marker Ki-67 in HD matrices. We tried to replicate the effects of a collagen-dense microenvironment seen in mammary epithelial cell lines, with the hope that collagen alone can activate the macrophage population. This does not seem to be the case, and there is still a question whether proliferation is an effect of immortalized immune-like cell lines. We also are not sure of the exact mechanisms these cells communicate with collagen. Previous studies suggest the exploration of other non-integrin collagen receptors such as discoidin domain receptors (DDRs) and macrophages scavenger receptors (SR-A) [138, 139], and how HD collagen matrices may affect their expression and further downstream signaling in response to density.

In conclusion, identifying neutrophils as key players in COL mammary tumor progression has important clinical implications for patients with mammographically dense breast tissue. Our results suggest that TANs may be useful prognostic markers for women with increased mammographic density. We must determine what specific molecular events induced by collagen-dense microenvironments turn neutrophils from

anti-tumor cells into tumor promoting cells, and subsequently target those events for therapy in women with density associated breast cancer.

APPENDIX I

Neutrophils drive accelerated tumor progression in the collagen-dense mammary tumor microenvironment

These supplemental figures are submitted as:

María G. García-Mendoza, David R. Inman, Suzanne M. Ponik, Justin J. Jeffery, Dagna S. Sheerar, Rachel R. Van Doorn, and Patricia J. Keely. *Breast Cancer Research*. 2015, *in review.*

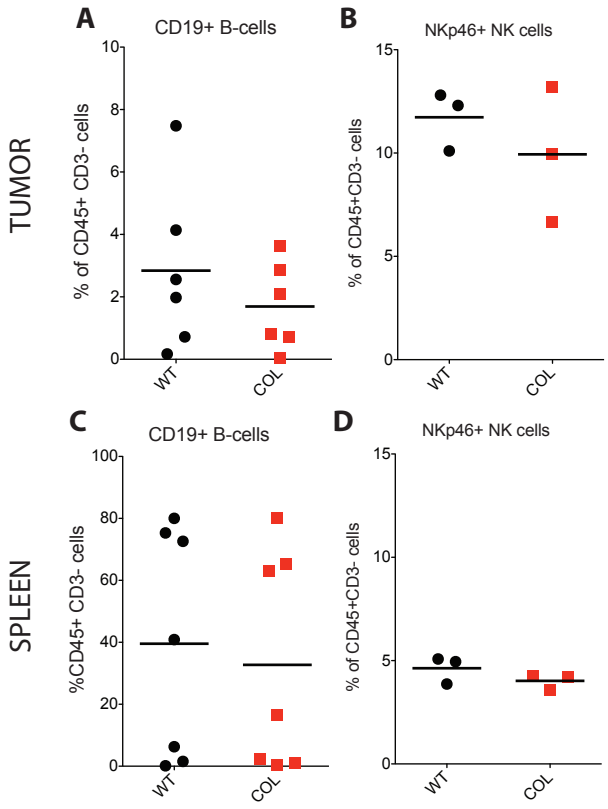

Figure AI-1 Quantification of B-cell and NK cells found in late-stage mammary tumors.

(**A**) The percentage of CD45+CD3- cells that are CD19+ B-cells in WT and COL tumors and (**C**) spleens at 15 weeks. (**B**) The percentage of CD45+CD3- cells that are Nkp46+ NK cells in WT and COL tumors and (**D**) spleens at 15 weeks.

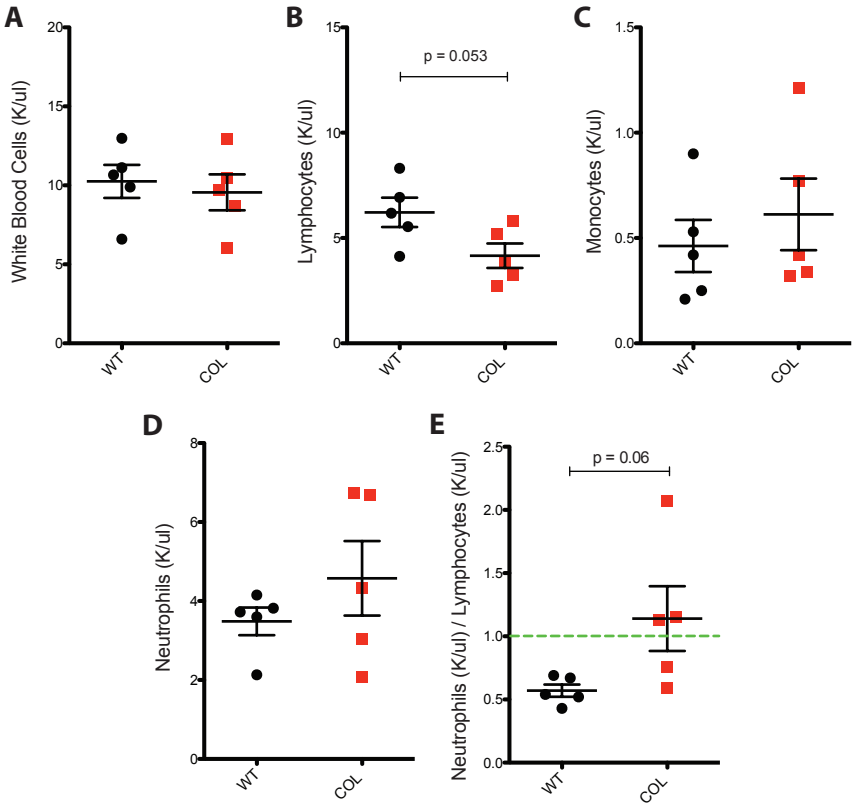

Figure AI-2 Tumor mice complete blood counts at late tumor stages.

White blood cell, (**B**) lymphocyte, (**C**) monocyte, and (**D**) neutrophil counts in 10^3 per μl of blood from WT and COL tumor mice at 15 weeks. Blood was obtained by retro-orbital bleeding procedure and counted on Hemavet 950FS hematology system. **(E)** Neutrophil to lymphocyte ratio (NLR) a.u. Green dash line denotes no change (NLR = 1) (n = 5).

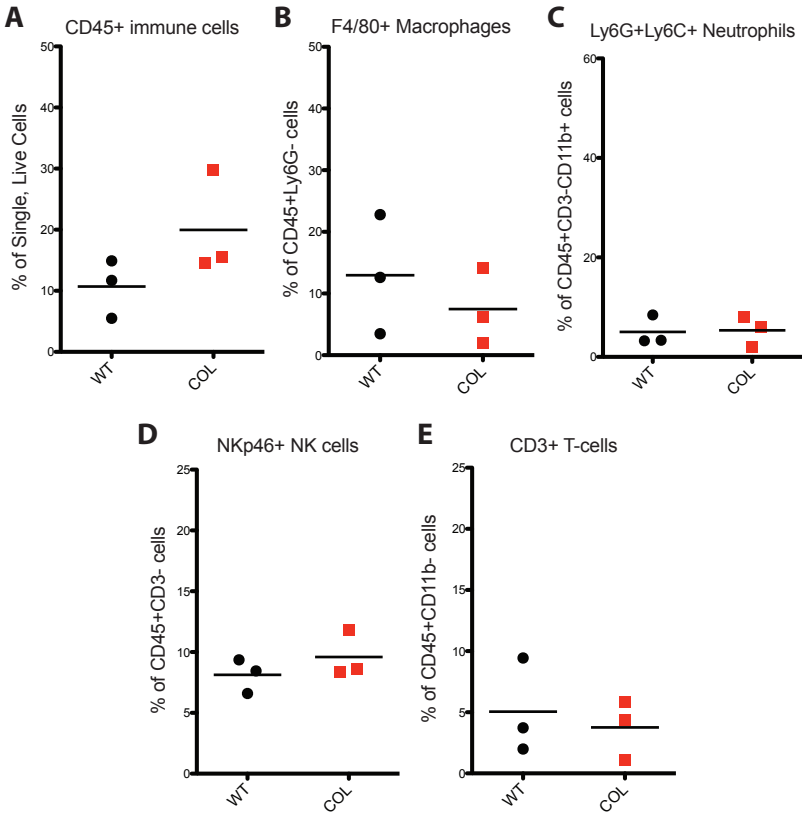

Figure AI-3 Quantification of immune cells in wild type and collagen-dense non-tumor mammary glands.

(**A**) Percentage of CD45+ immune cells in WT and COL mammary glands at 15 weeks (n=3, each n is an independent pair of age-matched littermate WT and COL non-tumor mice). (**B**) Percentage of CD45+CD3-CD11b+ cells that are F4/80+ macrophages in mammary glands. (**C**) Percentage of CD45+CD3-CD11b+ cells that are Ly6G+Ly6C+ neutrophils. (**D**) Percentage of CD45+CD3- cells that are Nkp46+ NK cells. (**E**) Percentage of CD45+CD3+ T-cells in mammary glands, determined by flow cytometry as in Figure 1.

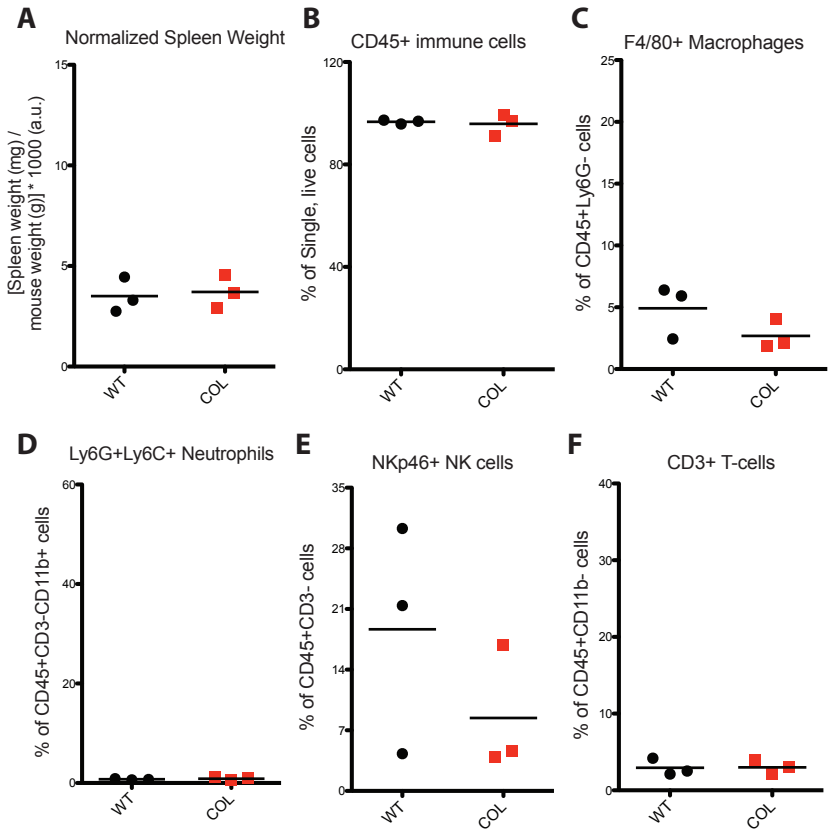

Figure AI-4 Quantification of immune cells in spleens from wild type and collagen-dense non-tumor mice.

(A) Spleen weight (mg) normalized to mouse weight (g) from both WT and COL mice (n = 3). (**B**) Percentage of CD45+ immune cells, (**C**) CD45+CD3-CD11b+ cells that are F4/80+, (**D**) CD45+CD3-CD11b+ cells that are Ly6G+Ly6C+ neutrophils, (**E**) CD45+CD3-CD11b+ cells that are Nkp46+ NK cells, and (**F**) CD45+CD3+ T-cells found in WT and COL spleens from non-tumor mice at 15 weeks, determined by flow cytometry as in Supplemental Figure 3.

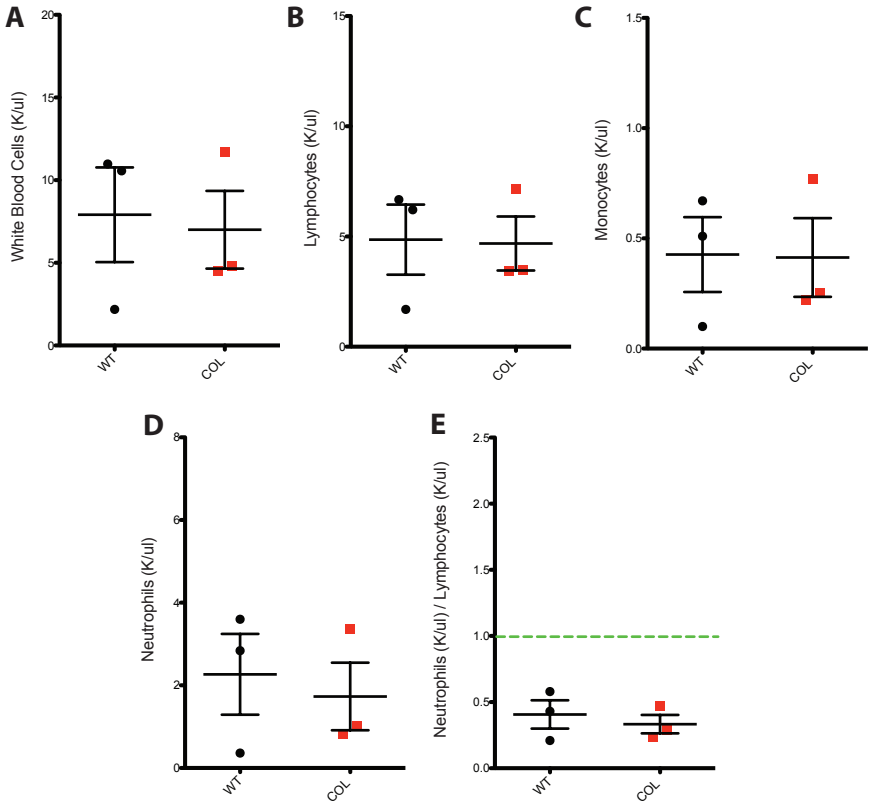

Figure AI-5 Non-tumor mice complete blood counts at 15 weeks of age.

(**A**) White blood cell, (**B**) lymphocyte, (**C**) monocyte, and (**D**) neutrophil counts in 10^3 per μl of blood from WT and COL non-tumor. Blood was obtained as in Supplemental Figure 2. **(E)** Neutrophil to lymphocyte ratio (NLR) a.u. Green dash line denotes no change (NLR = 1) (n = 3).

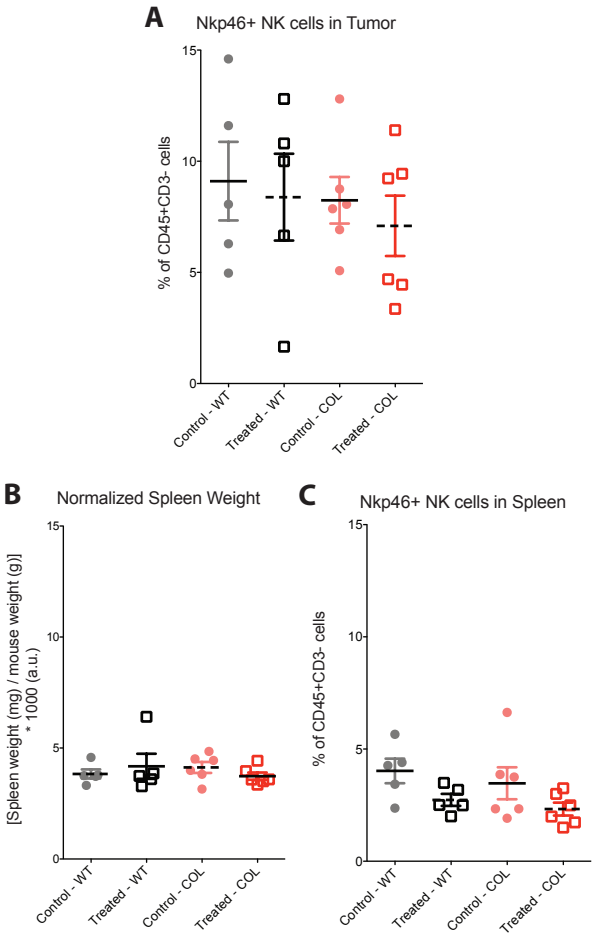

Figure AI-6 Recruitment NK cells in neutrophil depleted tissues.

(**A**) The percentage of CD45+CD3- cells that are Nkp46+ NK cells in anti-Ly6G treated or IgG control WT and COL tumors at 12 weeks. (**B**) Spleen weight (mg) normalized to mouse weight (g) from anti-Ly6G treated and IgG control WT and COL tumor mice. (**C**) The percentage of CD45+CD3- cells that are Nkp46+ NK cells in anti-Ly6G treated or IgG control WT and COL spleens at 12 weeks.

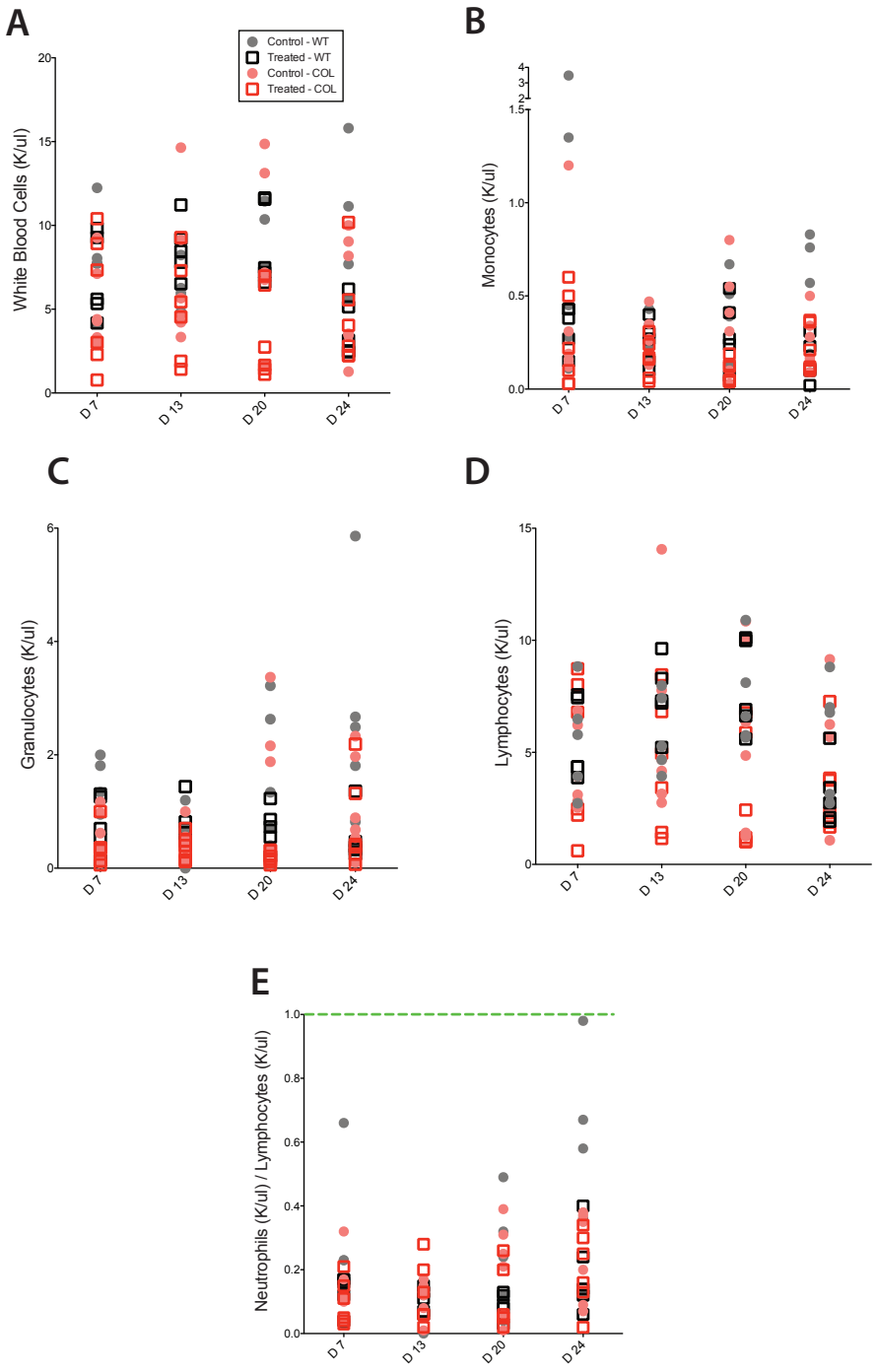
A
Control - WT
Treated - WT
Control - COL
Treated - COL
White Blood Cells (K/ul)
0
5
10
15
20
D 7
D 13
D 20
D 24
B
Monocytes (K/ul)
0.0
0.5
1.0
1.5
2
3
4
C
Granulocytes (K/ul)
0
2
4
6
D
Lymphocytes (K/ul)
0
5
10
15
E
Neutrophils (K/ul) / Lymphocytes (K/ul)
0.0
0.2
0.4
0.6
0.8
1.0

Figure AI-7 Complete blood counts at different time points during neutrophil depleting study.

(**A**) White blood cell, (**B**) monocyte, (**C**) granulocyte, and (**D**) lymphocyte count in 10^3 per μl from treated and control WT and COL mice obtained by saphenous vein bleeding procedure. Counted on Hemavet 950FS hematology system. (**E**) Neutrophil to lymphocyte ratio (NLR) a.u. (n =5 or 6).

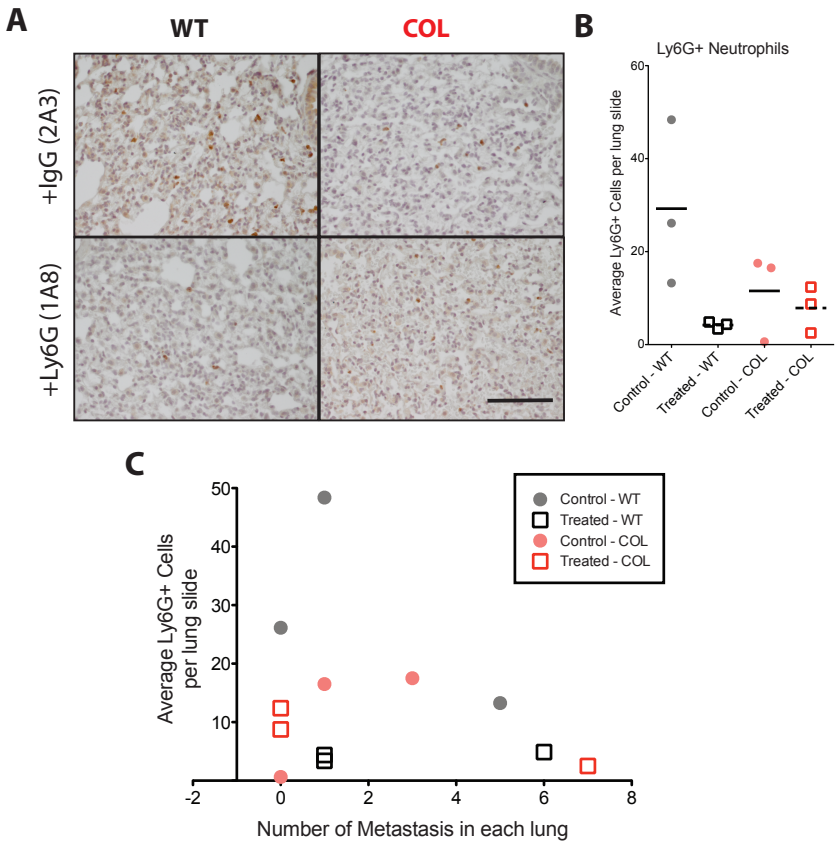

Figure AI-8 Neutrophil counts in metastatic lungs do not correlate with number of metastases in depletion study.

(**A**) Immunohistochemistry of lungs from the four treatment groups. Tumors were stained with Ly6G (1A8) in DAB and counterstained with hematoxylin. Scare bar = 100 um. (**B**), average number of Ly6G+ cells found in eight fields of view per tumor slide (n = 3). (**C**), average number of Ly6G+ cells per lung versus the number of metastatic lesions per lungs.

APPENDIX II

The collagenase-deficient mammary tumor mouse model (Col1a1-MMTV-PyVT) results in net increased collagen deposition associated with a three-fold increase in tumor formation [10]. Collagen in these tumors is organized into characteristic patterns, termed tumor associated collagen signatures (TACS). During the progression from a normal mammary duct to invasive carcinoma tissue, the collagen is remodeled from a non-aligned, random structure (TACS-1) to radially aligned fibers (TACS-3) [132]. This alignment is functionally significant as carcinoma cells migrate out from the tumor along these aligned fibers. Collagen fibers can enhance carcinoma cell intravasation because some of these fibers converge on blood vessels. Hence, aligned fibers serve as highways that guide invasive cells to vessels [142]. Collagen remodeling facilitates local invasion and can predict metastasis. In the collagen dense mouse, this alignment was augmented and correlates to three-fold increase in lung metastasis [10]. Of importance, collagen organization into radially aligned fibers (TACS-3 positive) is associated with poor outcome in breast cancer patients, making it a prognostic signature for disease-free survival in human breast cancer [74].

The mechanisms that drive the reorganization into TACS-3 are not well understood. Of the components in the tumor microenvironment, macrophages have been found to play a role in collagen I fibrillogenesis by promoting collagen assembly into long, organized fibers during mammary development [143]. This interplay between macrophages and collagen may be significant as clinically, in human patients, high macrophage recruitment into breast tumors is associated with poor survival [121].

Tumor associated macrophages (TAMs) are known to secrete matrix metalloprotease-2 (MMP-2), MMP-7, MMP-9, and MMP-12, which can be responsible for collagen remodeling [39]. Although it is also unclear if TACS-3 collagen reorganization involves proteases secreted by macrophages, these data beg the following questions: are macrophages involved in TACS-3 reorganization? Can both collagen alignment and macrophage infiltration predict breast cancer survival?

Tumor tissue cores from 207 breast cancer patients were assembled into a tissue microarray (TMA) in collaboration with Dr. Andreas Friedl [74] and were analyzed for collagen alignment. In brief, 196 qualified cases were used following institutional review board approval. Surgery on all of the patients had been performed by one surgeon between 1981 and 1995. The tissue array was assembled with a manual MTA-1 instrument (Beecher Instruments) equipped with a 1.0 mm punch needle. After assembly, paraffin embedded tissue samples were sectioned at 4 μm thickness. This TMA had previously been characterized with respect to patient age, tumor size, histologic subtype, tumor grade, lymph node status, estrogen (ER) and progesterone receptor (PR) expression, HER-2 overexpression, and Ki67 proliferation index. The median follow-up time was 6.2 years with a range between 1 month and 18.6 years [144]. The relative concentration of collagen and the orientation of fibers with respect to the tumor boundary were assessed by second harmonic generation (SHG) using a multi-photon microscope at the UW-Madison Laboratory for Optical and Computational Instrumentation (LOCI). The SHG image was overlaid with an array of 14 regions of interest and shared amongst a panel of three independent reviewers who were blind to

the patient outcome. The reviewers scored “yes” or “no” TACS-3, where bundles of straightened, aligned collagen fibers oriented perpendicular to the tumor boundary were defined as being TACS-3 positive, and a normalized TACS-3 manual score was generated. A Cox proportional hazard model was used to evaluate whether the presence of TACS-3 predicts survival. The results indicate a strong statistical evidence for poor survival in patients with TACS-3 and that collagen alignment is an independent biomarker for survival [74].

This tissue microarray was stained by immunohistochemistry by the UW-Madison Translational Research Initiatives in Pathology (TRIP) laboratory. Anti-CD68 was used as a macrophage marker stained with 3,3’-diaminobenzidine (DAB) as the chromogen, and counterstained with hematoxylin. The TMA containing 195 tumor cores was imaged by Vectra® automated quantitative pathology imaging system with a 20X objective lens. The images (two per tumor core) were analyzed using the inForm® advanced image analysis software, images were segmented into tumor niche (epithelial, immune, adipose, and mesenchymal cells that make up the tumor mass), tumor stroma, and other/blank components; then, the number of positive CD68 cells in each core was counted and a percentage was calculated from all the cells in each core (Figure 1).

We proceeded to correlate the macrophage counts to the manual TACS-3 scores to test if an increase in macrophage recruitment corresponds to a high TACS-3 score. The Spearman’s Rank Correlation showed no significant correlation between TACS-3 scores and macrophage infiltration either in the tumor niche or in the stroma (Figure 2A). A Cox proportional hazard analysis was done to determine if macrophage

infiltration can predict disease-specific survival (DSS) or time from date of diagnosis to death caused by breast cancer or last follow-up evaluation, and disease-free survival (DFS) or time from date of diagnosis until date of first cancer recurrence. The analysis showed that macrophage infiltration either to the tumor niche or to the stroma does not have prognostic significance and cannot predict DSS or DFS in this cohort (Figure 2B). Lastly, Kaplan-Meier curves were generated to analyze DSS and DFS, and the LogRank test determined whether survival curves were different among all the scores (0, 1, or 2) in the tumor niche and the stroma. The LogRank test showed that neither tumor niche nor stromal macrophage infiltration scores differ from each other with regards to cancer reoccurrence in patients (Figure 2C) or patient survival (Figure 2D) over time.

This TMA analysis suggests that macrophage recruitment is not correlated to tumor areas with highly aligned collagen. Although collagen alignment can predict survival in this patient cohort, macrophage infiltration cannot. It is not out of the question that, even though the number of macrophages recruited to tumor areas with aligned collagen is not significant, the activation of macrophages may be altered. Macrophages in tumors have been reported to secrete growth factors and cytokines that promote tumor progression; further analysis of secreted factor or markers of macrophage alternative activation would answer those questions. Interestingly, the only factor positively correlated with TACS-3 was the expression of stromal syndecan-1 [74]. The connection between macrophages and syndecan-1 was mainly established in atherosclerosis research, which demonstrated that syndecan-1 expression in macrophages is associated with anti-inflammatory M2-polarization, and with increased

motility of murine and human macrophages. These results suggested a role of syndecan-1 in resolution and rapid clearance of inflammatory macrophages [145]. It is unknown whether the syndecan-1 found in the aligned collagen tumor microenvironment is secreted by anti-inflammatory tumor-associated macrophages, and this allows for rapid macrophage emigration.

These results also suggest that other components of the tumor microenvironment may play bigger roles in aligning collagen into TACS-3. Cancer-associated fibroblasts are candidates because they secrete collagen, as well as cell-surface proteoglycans such as syndecans, which are associated with poor patient outcome [144, 146]. Based on the research reported in this thesis project, tumor-associated neutrophils are involved in promoting cancer in a collagen-dense tumor microenvironment; however, their role in collagen alignment has not yet been studied. Understanding the mechanisms of collagen alignment in breast cancer will aid in developing new therapies to slow or block tumor progression.

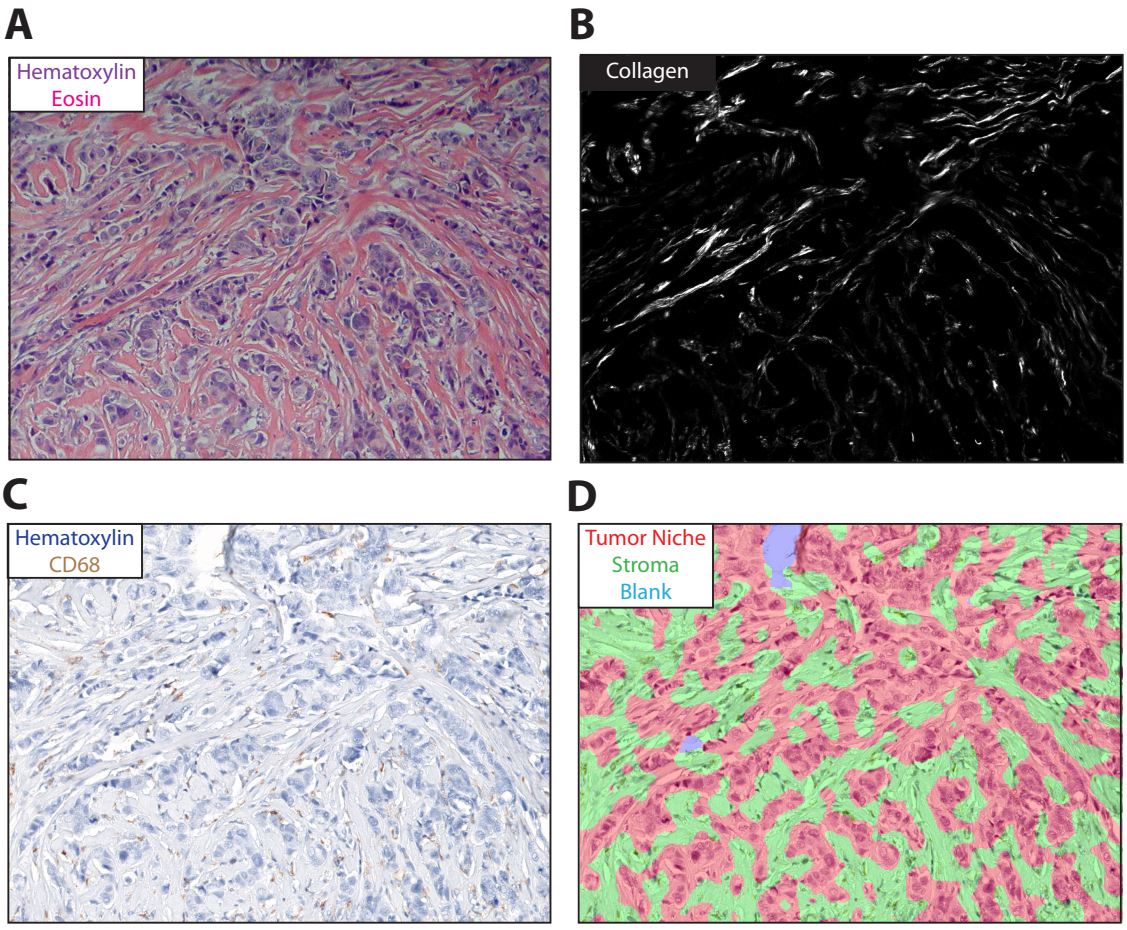

E

CD68+ cell scoring	
Tumor Niche	Stroma
0 = 0%	0 = 0 - 4.99%
1 = 0.11 - 0.49%	1 = 5 - 14.99%
2 = 0.5 - max (6.04%)	2 = 15 - max (38.1%)

Figure AII-1 Tissue microarray imaging and scoring

(**A**)The tissue microarray (TMA) was stained with hematoxylin (purple) and eosin (pink). (**B**) Each tumor core was imaged by second harmonic generation to quantify fibrillar collagen (white) alignment [74] (**C**), TMA core approximately 25 μm away from the section in **A** was stained with macrophage marker anti-CD68 in DAB (brown) (n = 195). (**D**) Images of the TMA were segmented into tumor niche and stroma areas and analyzed using inForm® advanced image analysis software. CD68 positive cell counts were performed by the inForm® software in the tumor niche (epithelial, immune, adipose, and mesenchymal cells that make up the tumor mass) and in the stroma. (**E**) The percentage of CD68 positive cells in a tissue core was collected and the data from all the cores were classified into three scores (0, 1 or 2) based on the median percentage.

A

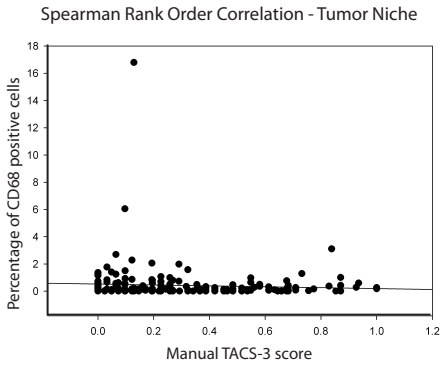

Correlation coeff.	P value	# of samples
- 0.06	0.41	195

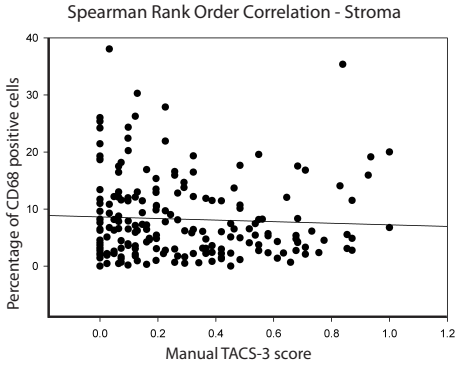

Correlation coeff.	P value	# of samples
- 0.01	0.88	195

B

Disease-Free Survival (DFS)				Disease-Specific Survival (DSS)			
Covariate	Hazard Ratio	P value	# of events	Covariate	Hazard Ratio	P value	# of events
% of CD68+ Tumor Niche	1.006	0.741	57	% of CD68+ Tumor Niche	1.001	0.972	51
% of CD68+ Stroma	1.124	0.104	57	% of CD68+ Stroma	1.189	0.009*	51

C

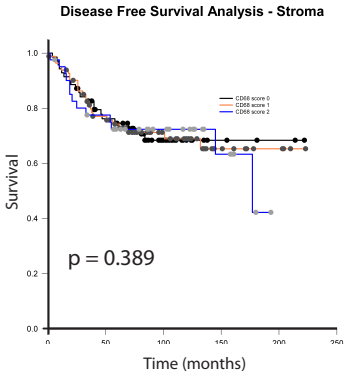

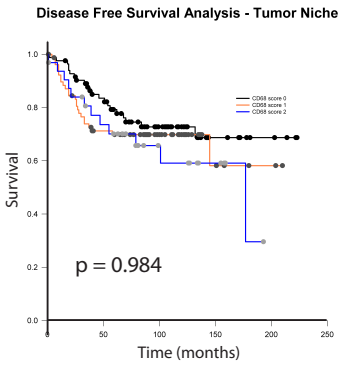

D

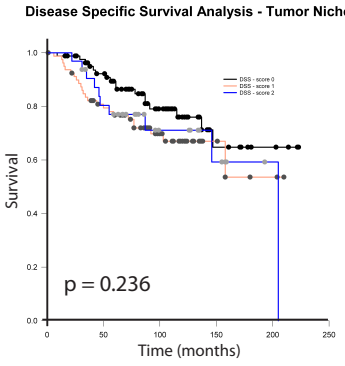

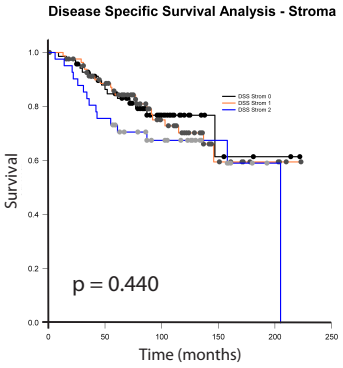

Figure AII-2 Statistical analysis of the TMA

(**A**), Spearman rank order correlation analysis of the percent of CD68 positive cells in the tumor niche and the stroma compared to their manual TACS-3 score. (**B**), Cox regression proportional hazards model was fitted to evaluate the association between the percent of CD68 positive cells (tumor niche and stroma) and disease-free and disease-specific survival. The p-values were calculated from covariate analysis; * indicates that the hazard rate was significantly affected by the percent of CD68 positive cells in the stroma. (**C**), Kaplan-Meier curves for disease-free and disease-specific survival rates and all three macrophage infiltration scores. P-values were provided by the LogRank test (**D**).

APPENDIX III

Microtubules regulate GEF-H1 in response to extracellular matrix stiffness

This appendix is published as:

Jessica N. Heck, Suzanne M. Ponik, Maria G. Garcia-Mendoza, Carolyn A. Pehlke, David R. Inman, Kevin W. Eliceiri, and Patricia J. Keely. *Mol. Biol Cell*. 2012 Jul 1; 23: 2583-92. PMID: 22593214.

Abstract:

Breast epithelial cells sense the stiffness of the extracellular matrix through Rho-mediated contractility. In turn, matrix stiffness regulates RhoA activity. However, the upstream signaling mechanisms are poorly defined. Here we demonstrate that the Rho exchange factor GEF-H1 mediates RhoA activation in response to extracellular matrix stiffness. We demonstrate the novel finding that microtubule stability is diminished by a stiff three-dimensional (3D) extracellular matrix, which leads to the activation of GEF-H1. Surprisingly, activation of the mitogen-activated protein kinase kinase/extracellular signal-regulated kinase pathway did not contribute to stiffness-induced GEF-H1 activation. Loss of GEF-H1 decreases cell contraction of and invasion through 3D matrices. These data support a model in which matrix stiffness regulates RhoA through microtubule destabilization and the subsequent release and activation of GEF-H1.

REFERENCES

1. **American Cancer Society Breast Cancer Detailed Guide** [http://www.cancer.org/cancer/breastcancer/detailedguide/index]
2. **Factors That Affect Breast Cancer Risk** [http://ww5.komen.org/AboutBreastCancer/RiskFactors/FactorsAffectingBreastCancerRisk/FactorsAffectingBreastCancerRisk.html]
3. Boyd NF, Byng JW, Jong RA, Fishell EK, Little LE, Miller AB, Lockwood GA, Tritchler DL, Yaffe MJ: **Quantitative classification of mammographic densities and breast cancer risk: results from the Canadian National Breast Screening Study**. *Journal of the National Cancer Institute* 1995, **87**(9):670-675.
4. Boyd NF, Lockwood GA, Byng JW, Tritchler DL: **Mammographic densities and breast cancer risk**. *Cancer Epidemiology, Biomarkers & Prevention* 1998, **7**:1133-1144.
5. Ursin G, Hovanessian-Larsen L, Parisky YR, Pike MC, Wu AH: **Greatly increased occurrence of breast cancers in areas of mammographically dense tissue**. *Breast cancer research : BCR* 2005.
6. Guo YP, Martin LJ, Hanna W, Banerjee D, Miller N: **Growth factors and stromal matrix proteins associated with mammographic densities**. *Cancer Epidemiology, Biomarkers & Prevention* 2001, **10**:243-248.
7. Alowami S, Troup S, Al-Haddad S, Kirkpatrick I, Watson PH: **Mammographic density is related to stroma and stromal proteoglycan expression**. *Breast cancer research* 2003, **5**:R129-R135.
8. Li T, Sun L, Miller N, Nicklee T, Woo J, Hulse-Smith L, Tsao M-SS, Khokha R, Martin L, Boyd N: **The association of measured breast tissue characteristics with mammographic density and other risk factors for breast cancer**. *Cancer epidemiology, biomarkers & prevention : a publication of the American Association for Cancer Research, cosponsored by the American Society of Preventive Oncology* 2005, **14**(2):343-349.
9. Conklin MW, Keely PJ: **Why the stroma matters in breast cancer: insights into breast cancer patient outcomes through the examination of stromal biomarkers**. *Cell adhesion & migration* 2012, **6**(3):249-260.
10. Provenzano PP, Inman DR, Eliceiri KW, Knittel JG, Yan L, Rueden CT, White JG, Keely PJ: **Collagen density promotes mammary tumor initiation and progression**. *BMC medicine* 2008, **6**:11.
11. Levental KR, Yu H, Kass L, Lakins JN, Egeblad M, Erler JT, Fong SFT, Csiszar K, Giaccia A, Weninger W *et al*: **Matrix crosslinking forces tumor progression by enhancing integrin signaling**. *Cell* 2009, **139**:891-906.
12. Schedin P, O'Brien J, Rudolph M, Stein T: **Microenvironment of the involuting mammary gland mediates mammary cancer progression**. *Journal of Mammary gland biology neoplasia* 2007, **12**:71-82.
13. O'Brien J, Lyons T, Monks J, Lucia MS, Wilson RS, Hines L, Man Y-g, Borges V, Schedin P: **Alternatively Activated Macrophages and Collagen Remodeling**

Characterize the Postpartum Involuting Mammary Gland across Species. *The American Journal of Pathology* 2010, **176**(3):1241-1255.

14. Lyons TR, O'Brien J, Borges VF, Conklin MW, Keely PJ, Eliceiri KW, Marusyk A, Tan A-CC, Schedin P: **Postpartum mammary gland involution drives progression of ductal carcinoma in situ through collagen and COX-2**. *Nature medicine* 2011, **17**(9):1109-1115.
15. Huo CW, Chew G, Hill P, Huang D, Ingman W, Hodson L, Brown KA, Magenau A, Allam AH, McGhee E *et al*: **High mammographic density is associated with an increase in stromal collagen and immune cells within the mammary epithelium**. *Breast cancer research : BCR* 2015, **17**:79.
16. Thomas J. Kindt RAG, Barbara A. Osborne: **Kuby Immunology**, Sixth edn. New York, NY: W. H. Freeman and Company; 2007.
17. Brigati C, Noonan DM, Albini A, Benelli R: **Tumors and inflammatory infiltrates: friends or foes?** *Clinical & Experimental Metastasis* 2002, **19**:247-258.
18. Coussens LM, Werb Z: **Inflammation and cancer**. *Nature* 2002, **420**(6917):860-867.
19. Bissell MJ, Hines WC: **Why don't we get more cancer? A proposed role of the microenvironment in restraining cancer progression**. *Nature medicine* 2011, **17**(3):320-329.
20. Dvorak HF: **Tumors: wounds that do not heal. Similarities between tumor stroma generation and wound healing**. *The New England journal of medicine* 1986, **315**(26):1650-1659.
21. Dvorak HF: **Tumors: Wounds That Do Not Heal—Redux**. *Cancer Immunology Research* 2015, **3**(1):1-11.
22. Dunn GP, Old LJ, Schreiber RD: **The immunobiology of cancer immunosurveillance and immunoediting**. *Immunity* 2004, **21**(2):137-148.
23. Shankaran V, Ikeda H, Bruce AT, White JM, Swanson PE, Old LJ, Schreiber RD: **IFNgamma and lymphocytes prevent primary tumour development and shape tumour immunogenicity**. *Nature* 2001, **410**(6832):1107-1111.
24. Smyth MJ, Crowe NY, Godfrey DI: **NK cells and NKT cells collaborate in host protection from methylcholanthrene-induced fibrosarcoma**. *International immunology* 2001, **13**(4):459-463.
25. MacKie RM, Reid R, Junor B: **Fatal melanoma transferred in a donated kidney 16 years after melanoma surgery**. *New England Journal of Medicine* 2003, **348**(6):567-568.
26. DeNardo DG, Coussens LM: **Balancing immune response: crosstalk between adaptive and innate immune cells during breast cancer progression**. *Breast Cancer Res* 2007.
27. Ruffell B, Au A, Rugo HS, Esserman LJ, Hwang ES, Coussens LM: **Leukocyte composition of human breast cancer**. *Proceedings of the National Academy of Sciences* 2011, **109**(8):27962801.
28. DeNardo DG, Andreu P, Coussens LM: **Interactions between lymphocytes and myeloid cells regulate pro- versus anti-tumor immunity**. *Cancer metastasis reviews* 2010, **29**:309-316.

29. Ostrand-Rosenberg S, Grusby MJ: **Cutting edge: STAT6-deficient mice have enhanced tumor immunity to primary and metastatic mammary carcinoma**. *The Journal of Immunology* 2000, **165**:6015-6019.
30. Merlo A, Casalini P, Carcangiu ML, Malventano C, Triulzi T, Mènard S, Tagliabue E, Balsari A: **FOXP3 expression and overall survival in breast cancer**. *Journal of clinical oncology : official journal of the American Society of Clinical Oncology* 2009, **27**(11):1746-1752.
31. Leek RD, Harris AL: **Tumor-associated macrophages in breast cancer**. *J Mammary Gland Biol Neoplasia* 2002, **7**(2):177-189.
32. Lin EY, Nguyen AV, Russell RG, Pollard JW: **Colony-stimulating factor 1 promotes progression of mammary tumors to malignancy**. *The Journal of experimental medicine* 2001, **193**(6):727-740.
33. Clauss M, Gerlach M, Gerlach H, Brett J, Wang F, Familletti PC, Pan Y-CE, Olander JV, Connolly DT, Stern D: **Vascular permeability factor: a tumor-derived polypeptide that induces endothelial cell and monocyte procoagulant activity, and promotes monocyte migration**. *The Journal of Experimental Medicine* 1990, **172**:1535-1545.
34. Russell DL, Adrian LH: **Tumor-associated macrophages in breast cancer**. *Journal of mammary gland biology and neoplasia* 2002, **7**(2):177-189.
35. Mantovani A, Sozzani S, Locati M, Allavena P, Sica A: **Macrophage polarization: tumor-associated macrophages as a paradigm for polarized M2 mononuclear phagocytes**. *Trends in Immunology* 2002, **23**(11).
36. Solinas G, Germano G, Mantovani A, Allavena P: **Tumor-associated macrophages (TAM) as major players of the cancer-related inflammation**. *Journal of Leukocyte Biology* 2009, **86**(1065-1073).
37. Wyckoff J, Wang W, Lin E, Wang Y, Pixley F, Stanley ER, Graf T, Pollard JW, Segall J, Condeelis J: **A paracrine loop between tumor cells and macrophages is required for tumor cell migration in mammary tumors**. *Cancer research* 2004, **64**:7022-7029.
38. Lin EY, Li J-F, Gnatovskig L, Deng Y, Zhu L, Grzesik DA, Qian H, Xue X, Pollard JW: **Macrophages regulate the angiogenic switch in a mouse model of breast cancer**. *Cancer research* 2006, **66**(23):11238-11246.
39. Lewis CE, Pollard JW: **Distinct Role of Macrophages in Different Tumor Microenvironments**. *Cancer Research* 2006, **66**(2):605-612.
40. Wyckoff JB, Wang Y, Lin E, Li J-F, Goswami S, Stanley ER, Segall JE, Pollard JW, Condeelis J: **Direct visualization of macrophage-assisted tumor cell intravasation in mammary tumors**. *Cancer research* 2007, **67**(6):2649-2656.
41. Goswami S, Sahai E, Wyckoff JB, Cammer M, Cox D, Pixley FJ, Stanley R, Segall JE, Condeelis JS: **Macrophages Promote the Invasion of Breast Carcinoma Cells via a Colony-Stimulating Factor-1/Epidermal Growth Factor Paracrine Loop**. *Cancer Research* 2005, **65**(12):5278-5283.
42. Binzhi Q, Yan D, Jae Hong I, Ruth JM, Yiyu Z, Jiufeng L, Richard AL, Jeffrey WP: **A distinct macrophage population mediates metastatic breast cancer cell extravasation, establishment and growth**. *PloS one* 2009.

43. Mantovani A, Cassatella MA, Costantini C, Jaillon S: **Neutrophils in the activation and regulation of innate and adaptive immunity**. *Nature reviews Immunology* 2011, **11**(8):519-531.
44. Schmidt H, Bastholt L, Geertsen P, Christensen IJ, Larsen S, Gehl J, von der Maase H: **Elevated neutrophil and monocyte counts in peripheral blood are associated with poor survival in patients with metastatic melanoma: a prognostic model**. *British journal of cancer* 2005, **93**(3):273-278.
45. Strell C, Lang K, Niggemann B, Zaenker KS, Entschladen F: **Neutrophil granulocytes promote the migratory activity of MDA-MB-468 human breast carcinoma cells via ICAM-1**. *Experimental cell research* 2010, **316**(1):138-148.
46. Fridlender ZG, Albelda SM: **Tumor-associated neutrophils: friend or foe?** *Carcinogenesis* 2012, **33**(5):949-955.
47. Yan J, Kloecker G, Fleming C, Bousamra M, Hansen R, Hu X, Ding C, Cai Y, Xiang D, Donninger H *et al*: **Human polymorphonuclear neutrophils specifically recognize and kill cancerous cells**. *Oncoimmunology* 2014, **3**(7).
48. Piccard H, Muschel RJ, Opdenakker G: **On the dual roles and polarized phenotypes of neutrophils in tumor development and progression**. *Critical reviews in oncology/hematology* 2012, **82**(3):296-309.
49. Fridlender ZG, Sun J, Kim S, Kapoor V, Cheng G, Ling L, Worthen GS, Albelda SM: **Polarization of tumor-associated neutrophil phenotype by TGF-beta: "N1" versus "N2" TAN**. *Cancer cell* 2009, **16**(3):183-194.
50. Mishalian I, Bayuh R, Levy L, Zolotarov L, Michaeli J, Fridlender ZG: **Tumor-associated neutrophils (TAN) develop pro-tumorigenic properties during tumor progression**. *Cancer immunology, immunotherapy : CII* 2013, **62**(11):1745-1756.
51. Houghton AMG, Rzymkiewicz DM, Ji H, Gregory AD, E. EE, Metz HE, Donna BS, Land S, Marconcini LA, Kliment CR *et al*: **Neutrophil elastase-mediated degradation of IRS-1 accelerates lung tumor growth**. *Nature medicine* 2010, **16**(2):219-224.
52. Acuff HB, Carter KJ, Fingleton B, Gorden DL, Matrisian LM: **Matrix metalloproteinase-9 from bone marrow–derived cells contributes to survival but not growth of tumor cells in the lung microenvironment**. *Cancer Research* 2006, **66**(1):259-266.
53. Swierczak A, Mouchemore KA, Hamilton JA, Anderson RL: **Neutrophils: important contributors to tumor progression and metastasis**. *Cancer metastasis reviews* 2015.
54. Nozawa H, Chiu C, Hanahan D: **Infiltrating neutrophils mediate the initial angiogenic switch in a mouse model of multistage carcinogenesis**. *Proceedings of the National Academy of Sciences* 2006, **103**(33):12493-12498.
55. Kowanetz M, Wu X, Lee J, Tan M: **Granulocyte-colony stimulating factor promotes lung metastasis through mobilization of Ly6G+ Ly6C+ granulocytes**. *Proceedings of the National Academy of Sciences* 2010, **107**(50):21248-21255.
56. Granot Z, Henke E, Comen EA, King TA, Norton L, Benezra R: **Tumor entrained neutrophils inhibit seeding in the premetastatic lung**. *Cancer cell* 2011, **20**(3):300-314.

57. Tabariès S, Ouellet V, Hsu BE, Annis MG, Rose AA, Meunier L, Carmona E, Tam CE, Mes-Masson A-MM, Siegel PM: **Granulocytic immune infiltrates are essential for the efficient formation of breast cancer liver metastases**. *Breast cancer research : BCR* 2015, **17**:45.
58. Coffelt SB, Kersten K, Doornebal CW, Weiden J, Vrijland K, Hau C-SS, Verstegen NJ, Ciampricotti M, Hawinkels LJ, Jonkers J *et al*: **IL-17-producing γδ T cells and neutrophils conspire to promote breast cancer metastasis**. *Nature* 2015, **522**(7556):345-348.
59. Noël A, Foidart JM: **The role of stroma in breast carcinoma growth in vivo**. *Journal of mammary gland biology and neoplasia* 1998, **3**(2):215-225.
60. Emeline Van Goethem RP, Fabienne Gauffre, Isabelle Maridonneau-Parini and Véronique Le Cabec: **Matrix Architecture Dictates Three-Dimensional Migration Modes of Human Macrophages: Differential Involvement of Proteases and Podosome-Like Structures**. *Journal of Immunology* 2010, **184**:1049-1061.
61. Laskin DL, Soltys RA, Berg RA, Riley DJ: **Activation of alveolar macrophages by native and synthetic collagen-like polypeptides**. *American journal of respiratory cell and molecular biology* 1994, **10**(1):58-64.
62. Obeid E, Nanda R, Fu YX, Olopade OI: **The role of tumor-associated macrophages in breast cancer progression (Review)**. *International journal of oncology* 2013, **43**:5-12.
63. Ulisse S, Baldini E, Sorrenti S, D'Armiento M: **The urokinase plasminogen activator system: a target for anti-cancer therapy**. *Current cancer drug targets* 2009, **9**(1):32-71.
64. Madsen DH, Leonard D, Masedunskas A, Moyer A, Jurgensen HJ, Peters DE, Amornphimoltham P, Selvaraj A, Yamada SS, Brenner DA *et al*: **M2-like macrophages are responsible for collagen degradation through a mannose receptor-mediated pathway**. *J Cell Biol* 2013, **202**(6):951-966.
65. Burke RM, Madden KS, Perry SW, Zettel ML, Brown EB, 3rd: **Tumor-associated macrophages and stromal TNF-alpha regulate collagen structure in a breast tumor model as visualized by second harmonic generation**. *J Biomed Opt* 2013, **18**(8):86003.
66. Grinnell F: **Migration of human neutrophils in hydrated collagen lattices**. *Journal of cell science* 1982, **58**:95-108.
67. Monboisse JC, Garnotel R, Randoux A: **Adhesion of human neutrophils to and activation by type-I collagen involving a beta 2 integrin**. *Journal of Leukocyte Biology* 1991, **50**:373-389.
68. Werr J, Johansson J, Eriksson EE, Hedqvist P: **Integrin α2β1 (VLA-2) is a principal receptor used by neutrophils for locomotion in extravascular tissue**. *Blood* 2000, **95**(5):1804-1809.
69. Ridger VC, Wagner BE, Wallace WAH: **Differential effects of CD18, CD29, and CD49 integrin subunit inhibition on neutrophil migration in pulmonary inflammation**. *The Journal of Immunology* 2001, **166**:3484-3490.

70. Lämmermann T, Bader BL, Monkley SJ, Worbs T, Wedlich-Söldner R, Hirsch K, Keller M, Förster R, Critchley DR, Fässler R *et al*: **Rapid leukocyte migration by integrin-independent flowing and squeezing**. *Nature* 2008, **453**(7191):51-55.
71. Afonso PV, McCann CP, Kapnick SM, Parent CA: **Discoidin domain receptor 2 regulates neutrophil chemotaxis in 3D collagen matrices**. *Blood* 2013, **121**(9).
72. Houghton AM: **The paradox of tumor-associated neutrophils: fueling tumor growth with cytotoxic substances**. *Cell cycle* 2010, **9**(9):1732-1737.
73. Boyd NF, Guo H, Martin LJ, Sun L, Stone J, Fishell E, Jong RA, Hislop G, Chiarelli A, Minkin S *et al*: **Mammographic density and the risk and detection of breast cancer**. *The New England journal of medicine* 2007, **356**(3):227-236.
74. Conklin MW, Eickhoff JC, Riching KM, Pehlke CA, Eliceiri KW, Provenzano PP, Friedl A, Keely PJ: **Aligned collagen is a prognostic signature for survival in human breast carcinoma**. *The American journal of pathology* 2011, **178**(3):1221-1232.
75. Provenzano PP, Inman DR, Eliceiri KW, Keely PJ: **Matrix density-induced mechanoregulation of breast cell phenotype, signaling and gene expression through a FAK-ERK linkage**. *Oncogene* 2009, **28**(49):4326-4343.
76. Zhang K, Corsa CA, Ponik SM, Prior JL, Piwnica-Worms D, Eliceiri KW, Keely PJ, Longmore GD: **The collagen receptor discoidin domain receptor 2 stabilizes SNAIL1 to facilitate breast cancer metastasis**. *Nature cell biology* 2013, **15**(6):677-687.
77. Lin EY, Jones JG, Li P, Zhu L, Whitney KD, Muller WJ, Pollard J: **Progression to Malignancy in the Polyoma Middle T Oncoprotein Mouse Breast Cancer Model Provides a Reliable Model for Human Diseases**. *The American Journal of Pathology* 2003, **163**(5):21132126.
78. Guy CT, Cardiff RD, Muller WJ: **Induction of mammary tumors by expression of polyomavirus middle T oncogene: a transgenic mouse model for metastatic disease**. *Molecular and cellular biology* 1992, **12**(3):954-961.
79. DeNardo DG, Coussens LM: **Inflammation and breast cancer. Balancing immune response: crosstalk between adaptive and innate immune cells during breast cancer progression**. *Breast Cancer Res* 2007, **9**(4):212.
80. Condeelis J, Pollard JW: **Macrophages: obligate partners for tumor cell migration, invasion, and metastasis**. *Cell* 2006, **124**:263-266.
81. Pollard JW: **Macrophages define the invasive microenvironment in breast cancer**. *Journal of Leukocyte Biology* 2008, **84**(3):623-630.
82. Yan HH, Pickup M, Pang Y, Gorska AE, Li Z, Chytil A, Geng Y, Gray JW, Moses HL, Yang L: **Gr-1+ CD11b+ myeloid cells tip the balance of immune protection to tumor promotion in the premetastatic lung**. *Cancer research* 2010, **70**(15):6139-6149.
83. Fridlender ZG, Albelda SM, Granot Z: **Promoting metastasis: neutrophils and T cells join forces**. *Cell research* 2015, **25**(7):765-766.
84. Bekes EM, Schweighofer B, Kupriyanova TA, Zajac E, Ardi VC, Quigley JP, Deryugina EI: **Tumor-recruited neutrophils and neutrophil TIMP-free MMP-9 regulate coordinately the levels of tumor angiogenesis and efficiency of**

malignant cell intravasation. *The American journal of pathology* 2011, **179**(3):1455-1470.

85. Kitamura T, Qian B-ZZ, Pollard JW: **Immune cell promotion of metastasis**. *Nature reviews Immunology* 2015, **15**(2):73-86.
86. Liu X, Wu H, Byrne M, Jeffrey J, Krane S, Jaenisch R: **A targeted mutation at the known collagenase cleavage site in mouse type I collagen impairs tissue remodeling**. *The Journal of cell biology* 1995, **130**(1):227-237.
87. Schindelin J, Arganda-Carreras I, Frise E, Kaynig V, Longair M, Pietzsch T, Preibisch S, Rueden C, Saalfeld S, Schmid B: **Fiji: an open-source platform for biological-image analysis**. *Nature methods* 2012, **9**(7):676-682.
88. Sven B, Katrin M, Stephan L: **The kinship of neutrophils and granulocytic myeloid-derived suppressor cells in cancer: Cousins, siblings or twins?** *Seminars in Cancer Biology* 2013, **23**(3).
89. Chen J, Deng Q, Pan Y, He B, Ying H, Sun H, Liu X, Wang S: **Prognostic value of neutrophil-to-lymphocyte ratio in breast cancer**. *FEBS open bio* 2015, **5**:502-507.
90. Abbey CK, Borowsky AD, Gregg JP, Cardiff RD, Cherry SR: **Preclinical imaging of mammary intraepithelial neoplasia with positron emission tomography**. *Journal of mammary gland biology and neoplasia* 2006, **11**(2):137-149.
91. Brown RS, Leung JY, Fisher SJ, Frey KA, Ethier SP, Wahl RL: **Intratumoral distribution of tritiated-FDG in breast carcinoma: correlation between Glut-1 expression and FDG uptake**. *Journal of nuclear medicine : official publication, Society of Nuclear Medicine* 1996, **37**(6):1042-1047.
92. Lin EY, Li JF, Gnatovskiy L, Deng Y, Zhu L, Grzesik DA: **Macrophages regulate the angiogenic switch in a mouse model of breast cancer**. *Cancer research* 2006.
93. DeNardo DG, Barreto JB, Andreu P, Vasquez L, Tawfik D, Kolhatkar N, Coussens LM: **CD4(+) T cells regulate pulmonary metastasis of mammary carcinomas by enhancing protumor properties of macrophages**. *Cancer cell* 2009, **16**(2):91-102.
94. Shishido S, Delahaye A, Beck A, Nguyen TA: **The MMTV-PyVT Transgenic Mouse as a Multistage Model for Mammary Carcinoma and the Efficacy of Antineoplastic Treatment**. *The MMTV-PyVT Transgenic Mouse as a Multistage Model for Mammary Carcinoma and the Efficacy of Antineoplastic Treatment* 2013, **4**:1187-1197.
95. Qian B-ZZ, Pollard JW: **Macrophage diversity enhances tumor progression and metastasis**. *Cell* 2010, **141**(1):39-51.
96. Weathington NM, van Houwelingen AH, Noerage BD, Jackson PL, Kraneveld AD, Galin FS, Folkerts G, Nijkamp FP, Blalock JE: **A novel peptide CXCR ligand derived from extracellular matrix degradation during airway inflammation**. *Nature medicine* 2006, **12**(3):317-323.
97. Gomez-Cambronero J, Horn J, Paul CC: **Granulocyte-macrophage colony-stimulating factor is a chemoattractant cytokine for human neutrophils: involvement of the ribosomal p70 S6 kinase signaling pathway**. *The Journal of Immunology* 2003, **171**:6846-6855.

98. Khajah M, Millen B, Cara DC: **Granulocyte-macrophage colony-stimulating factor (GM-CSF): a chemoattractive agent for murine leukocytes in vivo**. *Journal of Leukocyte Biology* 2011, **89**:945-953.
99. Ferlazzo G, Klein J, Paliard X, Wei WZ: **Dendritic cells generated from CD34+ progenitor cells with flt3 ligand, c-kit ligand, GM-CSF, IL-4, and TNF-α are functional antigen-presenting cells resembling mature monocyte-derived dendritic cells**. *Journal of Immunotherapy* 2000, **23**(1):48-58.
100. Dranoff G, Jaffee E, Lazenby A: **Vaccination with irradiated tumor cells engineered to secrete murine granulocyte-macrophage colony-stimulating factor stimulates potent, specific, and long-lasting anti-tumor immunity**. *Proceedings of the National Academy of Sciences* 1993, **90**:3539-3543.
101. Eubank TD, Roberts RD, Khan M, Curry JM, Nuovo GJ, Kuppusamy P, Marsh CB: **Granulocyte macrophage colony-stimulating factor inhibits breast cancer growth and metastasis by invoking an anti-angiogenic program in tumor-educated macrophages**. *Cancer research* 2009, **69**(5):2133-2140.
102. Ghirelli C, Reyal F, Jeanmougin M, Zollinger R, Sirven P, Michea P, Caux C, Bendriss-Vermare N, Donnadieu M-HH, Caly M *et al*: **Breast Cancer Cell-Derived GM-CSF Licenses Regulatory Th2 Induction by Plasmacytoid Predendritic Cells in Aggressive Disease Subtypes**. *Cancer research* 2015, **75**(14):2775-2787.
103. Carl-Henrik H: **Targeting the PDGF signaling pathway in tumor treatment**. *Cell Communication and Signaling* 2013, **11**:97.
104. Shao ZM, Nguyen M, Barsky SH: **Human breast carcinoma desmoplasia is PDGF initiated**. *Oncogene* 2000, **19**(38):4337-4345.
105. Deuel TF, Senior RM, Huang JS, Griffin GL: **Chemotaxis of monocytes and neutrophils to platelet-derived growth factor**. *Journal of Clinical Investigation* 1982, **69**:1046-1049.
106. Tzeng DY, Deuel TF, Huang JS, Senior RM, Boxer LA, Baehner RL: **Platelet-derived growth factor promotes polymorphonuclear leukocyte activation**. *Blood* 1984, **64**(5):1123-1128.
107. Nozaki S, Sledge GW, Nakshatri H: **Cancer cell-derived interleukin 1alpha contributes to autocrine and paracrine induction of pro-metastatic genes in breast cancer**. *Biochemical and biophysical research communications* 2000, **275**(1):60-62.
108. Ji H, Houghton AM, Mariani TJ, Perera S, Kim CB, Padera R, Tonon G, McNamara K, Marconcini LA, Hezel A *et al*: **K-ras activation generates an inflammatory response in lung tumors**. *Oncogene* 2006, **25**(14):2105-2112.
109. Sparmann A, Bar-Sagi D: **Ras-induced interleukin-8 expression plays a critical role in tumor growth and angiogenesis**. *Cancer cell* 2004, **6**(5):447-458.
110. Luboshits G, Shina S, Kaplan O, Engelberg S, Nass D, Lifshitz-Mercer B, Chaitchik S, Keydar I, Ben-Baruch A: **Elevated expression of the CC chemokine regulated on activation, normal T cell expressed and secreted (RANTES) in advanced breast carcinoma**. *Cancer research* 1999, **59**(18):4681-4687.
111. Adler EP, Lemken CA, Katchen NS, Kurt RA: **A dual role for tumor-derived chemokine RANTES (CCL5)**. *Immunology Letters* 2003, **90**(2-3):187-194.

112. Stormes KA, Lemken CA, Lepre JV, Marinucci MN, Kurt RA: **Inhibition of metastasis by inhibition of tumor-derived CCL5**. *Breast cancer research and treatment* 2005, **89**(2):209-212.
113. Zhang Y, Lv D, Kim H-JJ, Kurt RA, Bu W, Li Y, Ma X: **A novel role of hematopoietic CCL5 in promoting triple-negative mammary tumor progression by regulating generation of myeloid-derived suppressor cells**. *Cell research* 2013, **23**(3):394-408.
114. Venmar KT, Fingleton B: **Lessons from immunology: IL4R directly promotes mammary tumor metastasis**. *Oncoimmunology* 2014, **3**(9).
115. Venmar KT, Carter KJ, Hwang DG, Dozier EA, Fingleton B: **IL4 receptor ILR4α regulates metastatic colonization by mammary tumors through multiple signaling pathways**. *Cancer research* 2014, **74**(16):4329-4340.
116. Taub DD, Conlon K, Lloyd AR, Oppenheim JJ: **Preferential migration of activated CD4+ and CD8+ T cells in response to MIP-1 alpha and MIP-1 beta**. *Science* 1993, **260**:355-358.
117. Nath A, Chattopadhya S, Chattopadhyay U, Sharma NK: **Macrophage inflammatory protein (MIP)1alpha and MIP1beta differentially regulate release of inflammatory cytokines and generation of tumoricidal monocytes in malignancy**. *Cancer immunology, immunotherapy : CII* 2006, **55**(12):1534-1541.
118. Kitamura T, Qian B-ZZ, Soong D, Cassetta L, Noy R, Sugano G, Kato Y, Li J, Pollard JW: **CCL2-induced chemokine cascade promotes breast cancer metastasis by enhancing retention of metastasis-associated macrophages**. *The Journal of experimental medicine* 2015, **212**(7):1043-1059.
119. Noel A, Foidart JM: **The role of stroma in breast carcinoma growth in vivo**. *J Mammary Gland Biol Neoplasia* 1998, **3**(2):215-225.
120. Boyd NF, Martin LJ, Stone J, Greenberg C, Minkin S, Yaffe MJ: **Mammographic densities as a marker of human breast cancer risk and their use in chemoprevention**. *Curr Oncol Rep* 2001, **3**(4):314-321.
121. Bingle L, Brown NJ, Lewis CE: **The role of tumour-associated macrophages in tumour progression: implications for new anticancer therapies**. *The Journal of Pathology* 2002, **196**(3):254-265.
122. Harris RE, Chlebowski RT, Jackson RD, Frid DJ, Ascenseo JL, Anderson G, Loar A, Rodabough RJ, White E, McTiernan A: **Breast cancer and nonsteroidal anti-inflammatory drugs: prospective results from the Women's Health Initiative**. *Cancer Res* 2003, **63**(18):6096-6101.
123. Wozniak MA, Keely PJ: **Use of three-dimensional collagen gels to study mechanotransduction in T47D breast epithelial cells**. *Biological Procedures Online* 2005, **7**(1):144-161.
124. Ralph P, Nakoinz I: **Phagocytosis and cytolysis by a macrophage tumour and its cloned cell line**. *Nature* 1975, **257**(5525):393-394.
125. Raschke WC, Baird S, Ralph P, Nakoinz I: **Functional macrophage cell lines transformed by Abelson leukemia virus**. *Cell* 1978, **15**:261-267.
126. Theocharis AD, Skandalis SS, Gialeli C, Karamanos NK: **Extracellular matrix structure**. *Adv Drug Deliv Rev* 2015.

127. McWhorter FY, Davis CT, Liu WF: **Physical and mechanical regulation of macrophage phenotype and function**. *Cellular and Molecular Life Sciences* 2015, **72**:1303-1316.
128. Parihar A, Eubank TD, Doseff AI: **Monocytes and macrophages regulate immunity through dynamic networks of survival and cell death**. *Journal of innate immunity* 2010, **2**(3):204-215.
129. Creagh EM, Conroy H, Martin SJ: **Caspase - activation pathways in apoptosis and immunity**. *Immunological reviews* 2003, **193**:10-21.
130. Jun-Lin G: **Integrin signaling through FAK in the regulation of mammary stem cells and breast cancer**. *IUBMB Life* 2010, **62**(4):268-276.
131. Marks F, Klingmüller U, Müllar-Decker K: **Cellular Signal Transduction: an introduction to the molecular mechanisms of signal transduction**, vol. 1, 1 edn. New York, NY: Garland Science, Taylor and Francis Group; 2009.
132. Provenzano PP, Eliceiri KW, Campbell JM, Inman DR, White JG, Keely PJ: **Collagen reorganization at the tumor-stromal interface facilitates local invasion**. *BMC medicine* 2006, **4**(1):38.
133. Adams JM: **Ways of dying: multiple pathways to apoptosis**. *Genes & Development* 2003, **17**:2481-2495.
134. Taylor RC, Cullen SP, Martin SJ: **Apoptosis: controlled demolition at the cellular level**. *Nature reviews Molecular cell biology* 2008, **8**:231-241.
135. McNamara CR, Ahuja R, Osafo-Addo AD, Barrows D, Kettenbach A, Skidan I, Teng X, Cuny G, Gerber S, Degterev A: **Akt regulates TNFalpha synthesis downstream of RIP1 kinase activation during necroptosis**. *PloS one* 2013, **8**(3):e56576.
136. Pan YR, Chen CL, Chen HC: **FAK is required for the assembly of podosome rosettes**. *The Journal of cell biology* 2011, **195**(1):113-129.
137. Duong LT, Rodan GA: **PYK2 is an adhesion kinase in macrophages, localized in podosomes and activated by β 2 - integrin ligation**. *Cell motility and the cytoskeleton* 2000, **47**(174-188).
138. Gowen BB, Borg TK, Ghaffar A, Mayer EP: **Selective adhesion of macrophages to denatured forms of type I collagen is mediated by scavenger receptors**. *Matrix Biology* 2000, **19**:61-71.
139. Kim S-HH, Lee S, Suk K, Bark H, Jun C-DD, Kim D-KK, Choi C-HH, Yoshimura T: **Discoidin domain receptor 1 mediates collagen-induced nitric oxide production in J774A.1 murine macrophages**. *Free radical biology & medicine* 2007, **42**(3):343-352.
140. Erez N, Glanz S, Raz Y, Avivi C, Barshack I: **Cancer associated fibroblasts express pro-inflammatory factors in human breast and ovarian tumors**. *Biochemical and biophysical research communications* 2013, **437**(3):397-402.
141. Erez N, Truitt M, Olson P, Hanahan D: **Cancer-associated fibroblasts are activated in incipient neoplasia to orchestrate tumor-promoting inflammation in an NF-κB-dependent manner**. *Cancer cell* 2010, **17**:135-147.
142. Condeelis J, Segall JE: **Intravital imaging of cell movement in tumours**. *Nature Reviews Cancer* 2003, **3**(12):921-930.

143. Ingman WV, Wyckoff J, Gouon-Evans V, Condeelis J, Pollard JW: **Macrophages promote collagen fibrillogenesis around terminal end buds of the developing mammary gland**. *Developmental Dynamics* 2006, **235**(12):3222-3229.
144. Baba F, Swartz K, Buren R, Eickhoff J, Zhang Y, Wolberg W, Friedl A: **Syndecan-1 and syndecan-4 are overexpressed in an estrogen receptor-negative, highly proliferative breast carcinoma subtype**. *Breast Cancer Research and Treatment* 2006, **98**:91-98.
145. Angsana J, Chen J, Smith S, Xiao J, Wen J, Liu L, Haller CA, Chaikof EL: **Syndecan-1 modulates the motility and resolution responses of macrophages**. *Arteriosclerosis, thrombosis, and vascular biology* 2015, **35**(2):332-340.
146. Orimo A, Gupta PB, Sgroi DC, Arenzana-Seisdedos F, Delaunay T, Naeem R, Carey VJ, Richardson AL, Weinberg RA: **Stromal fibroblasts present in invasive human breast carcinomas promote tumor growth and angiogenesis through elevated SDF-1/CXCL12 secretion**. *Cell* 2005, **121**(3):335-348.